Stony Brook University

Novel Carbon Nanomaterial Coating for Dispersibility, Delivery and Sensing

A Dissertation Presented

by

Magdalena Swierczewska

to

The Graduate School

in Partial Fulfillment of the

Requirements

for the Degree of

Doctor of Philosophy

in

Biomedical Engineering

Stony Brook University

December 2012

Stony Brook University

The Graduate School

Magdalena Swierczewska

We, the dissertation committee for the above candidate for the

Doctor of Philosophy degree, hereby recommend

acceptance of this dissertation.

Dr. Mary D. Frame – Dissertation Advisor
Associate Professor
Department of Biomedical Engineering

Dr. Jonathan T. C. Liu - Chairperson of Defense
Assistant Professor
Department of Biomedical Engineering

Dr. Helmut H. Strey
Associate Professor
Department of Biomedical Engineering

Dr. Xiaoyuan Chen
Chief and Senior Investigator
National Institute of Biomedical Imaging and Bioengineering
National Institutes of Health

This dissertation is accepted by the Graduate School

Charles Taber
Interim Dean of the Graduate School

Abstract of the Dissertation

Novel Carbon Nanomaterial Coating for Dispersibility, Delivery and Sensing

by

Magdalena Swierczewska

Doctor of Philosophy

in

Biomedical Engineering

Stony Brook University

2012

Carbon nanomaterials have been cited to provide great potential in biomedical applications such as *in vivo* imaging, drug delivery, and biomarker detection. Yet poor dispersibility in physiological conditions greatly limits their biomedical promise. As with most nanoparticles, the surface interaction with biological systems is the driving force towards effective activity *in vivo*, namely exhibiting dispersion, low cytotoxicity, and molecular targetability. Therefore, by surface engineering carbon nanomaterials with a distinct biocompatible coating, their applications in imaging, drug delivery, biomarker detection, and therapy can be empowered.

We render carbon nanomaterials useful for such *in vivo* biomedical applications by providing dispersibility, delivery and sensing capabilities with a facile surface coating method. A single, yet multifunctional, hyaluronic acid-based biosurfactant was strategically chosen to meet the design criteria. The amphiphilic material, hyaluronic acid-5β-cholanic acid (HACA), is an **efficient dispersing agent** for carbon nanomaterials, including single-walled carbon nanotubes (SWCNTs), in physiological conditions for a sustained period of time. Furthermore, the biological activity and **cancer cell targeting** of HACA wrapped SWCNTs (HACA-SWCNTs) were evaluated *in vitro* and *in vivo* utilizing imaging techniques intrinsic to SWCNTs, HACA, and HACA-SWCNTs. Fluorescent dye-labeled HACA-SWCNTs were designed to **activate fluorescence signals** intracelluarly, not only serving as an approach to image cellular uptake but also to determine the coating efficacy of HACA onto SWCNTs. SWCNT localization within cells was also confirmed by tracking the intrinsic Raman signals of carbon nanomaterials. *In vivo* photoacoustic, fluorescence, and positron emission tomography imaging display **high tumor targeting capability** of HACA-SWCNTs in a murine tumor model. Once targeted, HACA-SWCNTs have potential to serve as **photothermal tumor ablation agents** after laser activation.

HACA coating of carbon nanomaterials creates a system to **simultaneously 1) disperse** insoluble carbon-based materials, **2) target** these coated materials to cancer cells, **3) image** intracellular uptake of the platform *in vitro* and *in vivo* and, after integrating these properties, **4)** serve as therapeutics. This work brings carbon nanomaterials closer to their biomedical potential.

To my parents, Maria and Richard, for their sacrifices that made this possible.

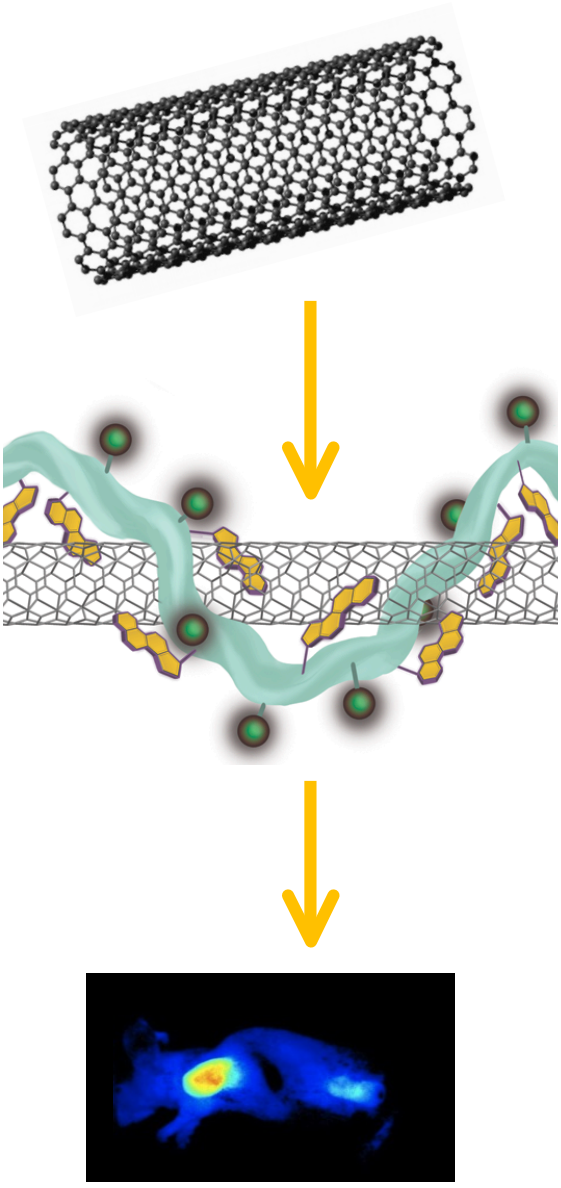

Table of Contents

List of Figures

List of Tables

List of Abbreviations

AUC: Area under curve

CA: cholanic acid

DOC: Deoxycholate

EDC: 1-Ethyl-3-(3-dimethylaminopropyl)carbodiimide

EPR: Enhanced permeation and retention

FACS: Fluorescence activated cell sorting

HA: Hyaluronic acid

HACA: Hyaluronic acid-5β-cholanic acid

HACA-SWCNT: Hyaluronic acid-5β-cholanic acid coated single-walled carbon nanotubes

$HACA_{Cy5.5}$: Cy5.5 labeled HACA

$HACA_{dye}$: Fluorescently labeled HACA

$HACA_{FA}$: Fluorescein amine labeled HACA

Hyal: Hyaluronidase

mLDH: modified lactate dehydrogenase

NHS: N-Hydroxysuccinimide

NIR: Near infrared

OCT: Optimal cutting temperature compound

PA: Photoacoustic imaging

PET: Positron emission tomography

PI: Propidium iodide

PL-PEG: phospholipid–polyethylene glycol

PL: Photoluminescence

PTT: Photothermal therapy

RGD: Arginine–glycine–aspartic acid peptide

SWCNT: Single-walled carbon nanotube

UV-vis: Ultraviolet-visible light

Acknowledgments

I am very blessed and lucky to have been and continue to be around tremendous people in my life. Thank you to my parents for inspiring me to do my best at all times. Growing up, they have cultivated all my interests in school and beyond. Their love and endless sacrifices have given me the strength and persistence to make this possible. I have always looked up to my sister, Katherine. She is an inspirational teacher, mother, daughter and sister. Thank you to Chris Scully for supporting me on this path, especially during some difficult times, and inspiring many smiles. To my high school biology teacher, Ms. Cecilia Penna, for opening my eyes to the amazing world of biology and the awesome engineering principles we can learn from it. Dr. Shawn Chen, I would like to express my immense gratitude for taking a chance on me as a researcher in LOMIN and for continually expanding my learning experiences. Thank you Dr. Molly Frame for your amazing support, trust and loyalty as my mentor. There are no words to express how thankful I am for the opportunities I have had during my graduate studies because of my mentors, Molly and Shawn. During my research experience at NIH, I would like to thank all of my LOMIN labmates, especially Dr. Ki Young Choi, and collaborators, especially Dr. Edward Mertz. Dr. Seulki Lee has made an amazing impact on my graduate studies as my supervisor of the Theranostics Nanomedicine group at LOMIN. I thank him for allowing me to expand and harness my skills. Acknowledgement must go out to the Department of Biomedical Engineering at Stony Brook University, the Office of Intramural Training and Education of the NIH, and NIBIB for making my individual partnership with the NIH possible. Thank you to my committee members, Dr. Liu, Dr. Strey, Dr. Frame, and Dr. Chen, for giving me the opportunity to defend this work.

Google Scholar Citations Page:
http://scholar.google.com/citations?hl=en&user=lZsA8OoAAAAJ

M. Swierczewska,* K. Y. Choi,* E. L. Mertz, X. Huang, F. Zhang, L. Zhu, H. Y. Youn, J. H. Park, A. Bhirde, S. Lee, X. Chen. A Facile, One-Step Nanocarbon Functionalization for Biomedical Applications. *Nano Letters.* **2012**, 12(7): 3613-3620.

K.Y. Choi,* **M. Swierczewska,*** S. Lee, X. Chen. Protease-activated drug development. *Theranostics*. **2012**, 2 (2): 156-178.

X. Huang, **M. Swierczewska**, K.Y. Choi, L. Zhu, A. Bhirde, J. Park, K. Kim, J. Xie, G. Niu, K. C. Lee. Multiplex Imaging of an Intracellular Proteolytic Cascade by using a Broad-Spectrum Nanoquencher. *Angewandte Chemie International Edition*. **2012,** 51(7): 1625-1630.

M. Swierczewska, G. Liu, S. Lee, X. Chen. High-Sensitivity Nanosensors for Biomarker Detection. *Chemical Society Reviews*. **2011**, 41(7): 2641-2655.

G. Liu, K.Y. Choi, A. Bhirde, **M. Swierczewska**, J. Yin, S. W. Lee, J. H. Park, J. I. Hong, J. Xie, G. Niu, D. O. Kiesewetter, S. Lee, X. Chen. Sticky Nanoparticles: A New Platform for siRNA Delivery by Bis(Zinc(II)-Dipicolyamine)-Functionalized, Self-Assembled Nanoconjugate. *Angewandte Chemie International Edition*. **2012**, 124(2): 460-464.

M. Swierczewska, S. Lee, X. Chen. Moving Theranostics from Bench to Bedside in an Interdisciplinary Research Team. *Therapeutic Delivery*. **2011**, 2(2): 165-170.

M. Swierczewska, S. Lee, X. Chen. Inorganic Nanoparticles for Multimodal Molecular Imaging. *Molecular Imaging*. **2011**, 10(1): 3-16.

M. Swierczewska, S. Lee, X. Chen. The Design and Application of Fluorophore-Gold Nanoparticle Activatable Probes. *Physical Chemistry Chemical Physics.* **2011**, 13(21): 9929-9941.

G. Liu*, **M. Swierczewska***, S. Lee, X. Chen. Functional Nanoparticles for Molecular Imaging Guided Gene Delivery. *Nano Today*. **2010**, 5(6): 524-539.

M. Swierczewska, I. Rusakova, and B. Sitharaman. Gadolinium and Europium Catalyzed Growth of Single-Walled Carbon Nanotubes. *Carbon*. **2009**. 47(13): 3139-3142.

M. Pramanik, **M. Swierczewska**, D. Green, B. Sitharaman, L. V. Wang. Single-Walled Carbon Nanotubes as a Multimodal-Thermoacoustic and Photoacoustic-Contrast Agent. *Journal of Biomedical Optics*. **2009**, 14(3): 034018.

M. Pramanik, K. H. Song, **M. Swierczewska**, D. Green, B. Sitharaman, L. V. Wang. In Vivo Carbon Nanotube-Enhanced Non-Invasive Photoacoustic Mapping of the Sentinel Lymph Node. *Physics in Medicine and Biology*. **2009**. 54(11): 3291–3301.

M. Swierczewska, C. S. Hajicharalambous, A. V. Janorkar, Z. Megeed, M. L. Yarmush, and P. Rajagopalan. Cellular Response to Nanoscale Elastin Like Polypeptide Polyelectrolyte Multilayers. *Acta Biomaterialia*, **2008**. 4(4): 827-837.

BOOK CHAPTER

D. Green, **M. Swierczewska**, B. Sitharaman (**2010**). Carbon Nanotubes: Prospects for Tissue Engineering, Therapeutics, and Medical Diagnostics. In R.S. Chaughule and R.V. Ramanujan (Ed.), *Nanoparticles: Synthesis, Characterization, and Application*. India: American Scientific Publishers.

Chapter 1:

Introduction and Specific Aims

A. Introduction

Carbon nanomaterials, especially single-walled carbon nanotubes (SWCNTs), have enormous potential in cancer therapy.[1, 2] For example, they can be utilized for drug delivery[3] due to their high surface area to volume ratio, tumor imaging[4-6] due to their intrinsic optical signals and targeting efficacy by the enhanced permeation and retention (EPR) effect, and cancer biomarker sensing[7-9] as *ex vivo* and *in vivo* nanosensors based on their sensitive electron conductance. In addition, when SWCNTs are properly dispersed and targeted *in vivo*, they can be utilized as photothermal therapeutics for cancerous tumors because of their ability to absorb energy and transfer that energy into heat.[10] Yet for *in vivo* applications, carbon nanotubes still lack effective dispersibility in order to achieve their designated role. Therefore, to maintain the unique carbon nanomaterial properties in physiological conditions, surface engineering with biomolecules and targeting ligands is required to bestow improved dispersibility, reduced toxicity, and cellular targetability.[11] Existing coating materials, specifically for SWCNTs, have been demonstrateed in proof-of-concept, *in vivo* applications; yet, time-consuming synthetic processes, high concentrations of coating material, time-consuming purification steps and low recovery amounts hamper translation toward multifunctional and innovative products.[12] Therefore, to harness the potential of carbon nanomaterials for real biomedical applications, a facile surface coating is required to equip nanocarbons with dispersibility and multifunctionality for imaging, delivery and therapy.

B. Specific Aims

In this study, a multifunctional biosurfactant, hyaluronic acid-5β-cholanic acid (HACA), coated onto carbon nanomaterials will be examined for dispersibility, cancer cell targetability

and receptor-mediated uptake *in vitro* and *in vivo*. With the interaction between the amphiphilic HACA conjugate and SWCNTs, the one-dimensional SWCNT can efficiently bind with the hydrophobic cholanic acid, leaving the highly hydrophilic hyaluronic acid on the surface of the tube. This helps to solubilize the SWCNTs and is useful for incorporating specific cell targeting and uptake properties. With this type of enhanced dispersibility, uptake and efficiency, SWCNTs are expected to reach their potential as imaging, delivery, and therapeutic agents *in vivo*. Therefore, the overall objective of this work is to render carbon nanomaterials useful for *in vivo* biomedical applications by providing dispersibility, delivery, sensing and therapy capabilities with a facile biomaterial surface coating. With this type of material coating, researchers can go beyond *in vitro* experiments and into a more realistic tumor model for *in vivo* study of cancer therapy using carbon nanomaterials. Accordingly, the specific aims of this research proposal are:

Specific Aim 1: Design a hyaluronic acid based, non-covalent coating method for carbon nanomaterials and characterize the physicochemical properties of coated single-walled carbon nanotubes.

Specific Aim 2: Characterize the biological activity of hyaluronic acid wrapped single-walled carbon nanotubes *in vitro*.

Specific Aim 3: Demonstrate application of hyaluronic acid wrapped single-walled carbon nanotubes *in vivo*.

Specific Aim 4: Utilize the targeting of hyaluronic acid wrapped single-walled carbon nanotubes for photothermal therapy.

In other words, the use of HACA as a coating material for SWCNTs will be tested for dispersibility (Specific Aim 1), *in vitro* cellular uptake as well as fluorescence activation (Specific Aim 2), *in vivo* delivery to tumors (Specific Aim 3), and targeted tumor destruction by photothermal therapy and treatment monitoring (Specific Aim 4). Each aim will correspond to the consecutive chapters.

C. Significance

With the development of a new SWCNT coating, this study can provide researchers in the nanomedicine field with a facile and single material that can simultaneously disperse and allow tumor specific targeting and uptake of carbon nanomaterials. This tool could then be used to further the design elements for carbon nanomaterials in cancer therapy. For example, HACA-coated SWCNTs can be utilized as optical probes for Raman microscopy or MRI or PARACEST imaging agents when loaded with unique metals. The targeted SWCNTs can also be used as drug delivery vectors or prodrugs, where the conjugated anti-cancer drug on the HACA is released by the hyaluronidase degradation of the HA backbone during cellular uptake. Additionally, the use of SWCNTs as activatable probes can open the door towards the design of SWCNTs as quenchers; additional fluorophore-substrate pairs can be designed for similar systems such as molecular beacons. With an effective biomaterial coating, as engineered in this proposal, further work on the sensing, drug delivery, and imaging capabilities of carbon nanomaterials can be pursued.

D. References

1. R. H. Baughman, A. A. Zakhidov and W. A. de Heer, *Science*, 2002, **297**, 787-792.
2. Z. Liu, S. Tabakman, K. Welsher and H. Dai, *Nano Res.*, 2009, **2**, 85-120.
3. Z. Liu, K. Chen, C. Davis, S. Sherlock, Q. Cao, X. Chen and H. Dai, *Cancer Res.*, 2008, **68**, 6652-6660.
4. A. De La Zerda, C. Zavaleta, S. Keren, S. Vaithilingam, S. Bodapati, Z. Liu, J. Levi, B. R. Smith, T.-J. Ma, O. Oralkan, Z. Cheng, X. Chen, H. Dai, B. T. Khuri-Yakub and S. S. Gambhir, *Nat. Nanotechnol.*, 2008, **3**, 557-562.
5. S. Keren, C. Zavaleta, Z. Cheng, A. de la Zerda, O. Gheysens and S. S. Gambhir, *Proc. Natl. Acad. Sci. U. S. A.*, 2008, **105**, 5844-5849.
6. J. Lefebvre, D. G. Austing, J. Bond and P. Finnie, *Nano Lett.*, 2006, **6**, 1603-1608.
7. K. Besteman, J. O. Lee, F. G. M. Wiertz, H. A. Heering and C. Dekker, *Nano Lett.*, 2003, **3**, 727-730.
8. R. J. Chen, S. Bangsaruntip, K. A. Drouvalakis, N. W. S. Kam, M. Shim, Y. M. Li, W. Kim, P. J. Utz and H. J. Dai, *Proc. Natl. Acad. Sci. U. S. A.*, 2003, **100**, 4984-4989.
9. A. Javey, J. Guo, Q. Wang, M. Lundstrom and H. J. Dai, *Nature*, 2003, **424**, 654-657.
10. H. K. Moon, S. H. Lee and H. C. Choi, *ACS Nano*, 2009, **3**, 3707-3713.
11. Y.-L. Zhao and J. F. Stoddart, *Acc. Chem. Res.*, 2009, **42**, 1161-1171.
12. Z. Liu, S. M. Tabakman, Z. Chen and H. Dai, *Nat. Protoc.*, 2009, **4**, 1372-1381.

Chapter 2:

Design of a Hyaluronic Acid Based, Non-Covalent Coating Method for Carbon Nanomaterials

A. Abstract

Design criteria for a carbon nanomaterial functionalization technique were addressed and evaluated to identify HACA as an exemplary amphiphilic biomaterial coating. Three significant coating characteristics for biomedical applications were acknowledged: 1) non-covalent interaction with the carbon nanomaterial, 2) amphiphilic nature and 3) biocompatibility. Previously used for tumor targeted drug delivery,[1-3] HACA is a promising carbon nanomaterial coating according to the key design criteria. For further in vitro and in vivo analysis, HACA functionalization methods were optimized to efficiently and effectively disperse carbon nanomaterials in physiological conditions. Within this study, the model carbon nanomaterial, SWCNTs, were evaluated in further detail. Physicochemical properties of coated SWCNTs were characterized to determine proper dispersion and feasibility for in vitro and in vivo use. In conclusion, an effective HACA coating method for carbon nanomaterials was developed.

B. Introduction

Various coating techniques for carbon nanomaterials, namely carbon nanotubes, have been utilized to achieve effective dispersion;[4, 5] but, few have been optimized for proper *in vivo* activity, where the nanotube remains soluble in physiological conditions. Without any processing after synthesis, SWCNTs are insoluble in both organic solvents and aqueous solutions. Three approaches can be utilized to functionalize CNTs, with the first two playing an essential role in dispersion: 1) covalent bonding onto the graphene structure of the CNT, 2) non-covalent techniques, which maintain the graphene structure, and 3) endohedral filling of the inner nanotube cavity.

Covalent techniques require functional groups to coordinate on the surface of the graphene structure to adopt a tetrahederal coordination and an sp3 hybridization, destroying the

electronic band structure of CNTs (Figure 1). For example, CNTs can undergo fluorination reactions and then undergo substitution to other functional groups, such as alkyls for dispersion in organic solvents or diamines (Figure 1A).[5] For biomedical applications, amino-functionalized CNTs have been especially useful to further covalently attach different biomolecules, like amino acids, peptides, and nucleic acids.[6] CNTs can be directly functionalized with amino groups (Figure 1B). Additionally, polymers can be grafted onto SWCNTs using various chemical reactions (nucleophilic, cycloaddition or free radical polymerization)[7] or by an in situ radical polymerization process,[8] where the nanotube carbanions themselves can initiate polymerization. Another technique is to utilize the defect sites of CNTs, which become present after production of CNTs and during acid purification (Figure 1C). The defect sites, made up of mainly carbonyl and carboxylic groups, can undergo amidation or esterifications to attach biomaterials or hydrophilic materials as well. [6]

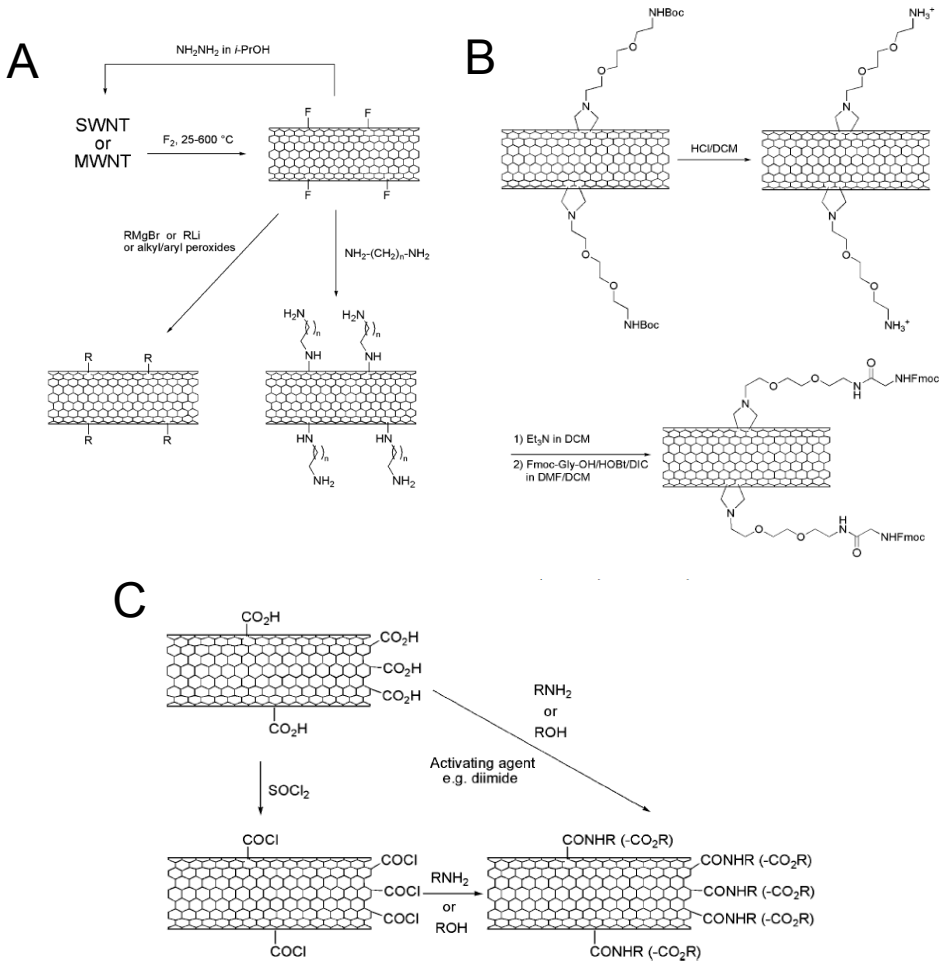

Figure 1: Examples of Covalent Carbon Nanomaterial Functionalization Techniques. A) Fluorination reaction, where the graphene structure decomposes to form C_2F binds. Fluorination allows for further substitution, like alkyl groups, diamines or diol. B) Ammonium groups provide water solubility and covalent attachment of other biomolecules. C) Defect site reaction utilizing the oxidized locations on the CNTs for amidification or esterification. Figures adapted with pemission from ref [5].

Although carbon nanotubes can be coated by covalent techniques, non-covalent functionalization has been the overwhelmingly preferred technique as it does not destroy the ordered structure of the graphene surface and in turn does not disrupt important intrinsic properties of carbon nanomaterials. [9] In non-covalent functionalization, SWCNTs, with surface areas over 2500 m^2/g when on the micrometer length[10], can be modified with aromatic compounds, surfactants, polymers or biomolecules via van der Waals forces, pi-pi interactions or

by adsorption (references within [4]) via sonication (Figure 2). For example, the aromatic molecule, pyrene, is extensively used to interact with the CNT surface by pi-stacking. Furthermore, pyrenes can be modified with different types of functional groups to serve as a chemical linker between the nanotube surface and the additional molecule (Figure 2A).[11, 12] But this system was not efficient for in vitro use because serum proteins were able to displace pyrene. Since the first example of water-soluble SWCNTs,[5] carbon nanomaterials were examined *in vitro*. Yet, it became evident that a balance between robustness and biocompatibility were required to maintain solubility in high salt and serum conditions. Low concentrations of non-covalent coatings are required to reduce cytotoxicity. Charged surfactants like sodium dodecyl sulfate or cetyltrimethyl ammonium bromide are shown to disperse CNTs non-covalently.[15] Although these positively charged surfactants in excess amounts show improvement in solubility and cellular uptake of CNTs, such surplus can also lead to cell membrane lysis or protein denaturation. Other amphiphiles, such as Tween-20 and Pluronic triblock copolymers, have utilized their hydrophobic domains to attach to the nanotube surface through hydrophobic effects while exposing the hydrophilic domain for water solubility.[5] Yet, their application in physiological conditions suffers from non-specific absorption, where serum proteins can efficiently replace the surfactant, and hence lead to poor tissue accumulation. Therefore more sophisticated coating materials are required to achieve carbon nanotubes that are stable in high salt and serum conditions.

Specific sequences of single-stranded DNA molecules can also be utilized to disperse individual nanotubes through pi-pi stacking of the DNA base unit and graphene surface (Figure 2B).[13-15] This seminal work initiated by Zheng et al. has greatly opened the understanding of specific interactions between carbon nanotubes and additionally for nanotube separation based

on chirality and length.[15] Yet for biomedical applications, DNA-wrapped carbon nanotubes are not stable in physiological conditions that contain nucleases and are limited in their coating efficacy because high concentrations of DNA are required for low concentration of CNT dispersion.

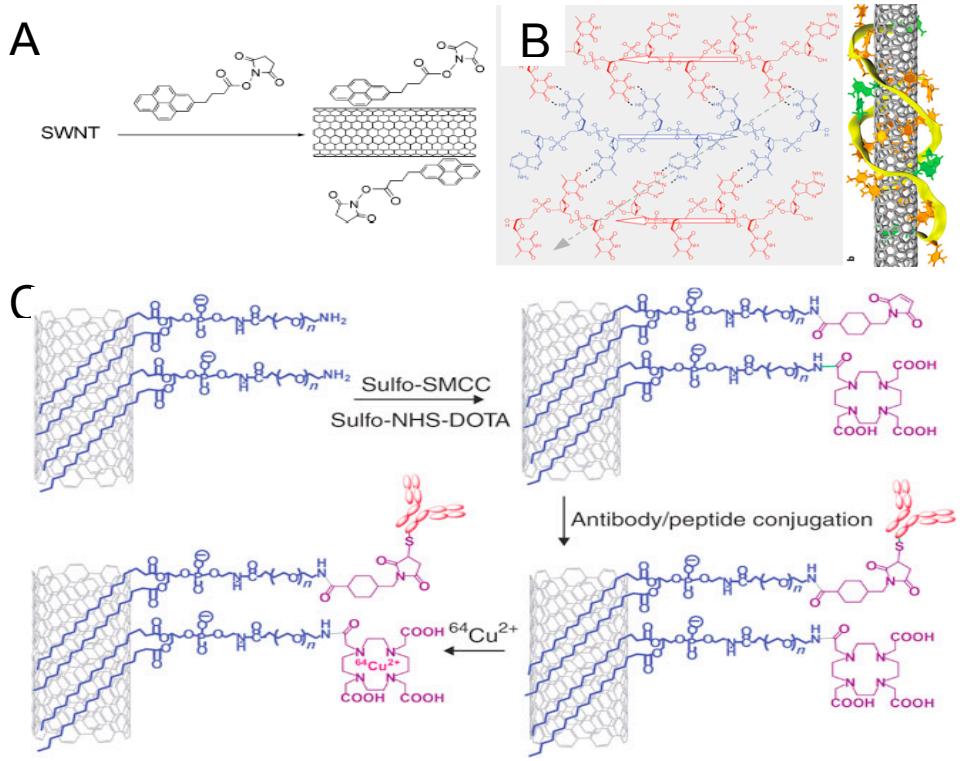

Figure 2: Examples of Non-Covalent Carbon Nanomaterial Functionalization Techniques. 1) Pyrene derivatives pi-stack with the graphene and are used as linkers. 2) DNA selectively binds to SWCNTs based on chirality. Figure adapted with permission from ref [14]. 3) PEGylated phospholipids interacts with SWCNTs by hydrophobic interactions. Figure adapted with permission from ref [16].

An important coating material that has made considerable advancement in the carbon nanomaterial field is PEGylated phospholipids (PL-PEG) pioneered by Dai and colleagues (Figure 2C).[17] SWCNTs non-covalently modified with PL-PEG exhibit high stability *in vivo* and notably can be subjected to chemical modification, such as with arginine–glycine–aspartic acid (RGD) peptide, to target integrin receptors for high tumor accumulation.[17] RGD recognizes the

$\alpha_v\beta_3$ integrin, which is known to be upregulated on solid tumor cells and tumor vasculature. Targeting capabilities imposed on coating materials, although not essential for dispersion, give potential use for targeted imaging and therapy. For example, Using the targeted PL-PEG SWCNTs, a tumor uptake of about 13% injected dose per gram tissue (% ID/g) was exhibited, about three times more than non-targeted PEGylated SWCNTs.[17] This pertinent technique has opened up the use of CNTs in biomedical applications for high sensitivity tumor imaging and delivery of abundant therapeutic pay-loads.[17-22] However, its preparation involves multi-step conjugations totaling up to ten days of functionalization and conjugation and leads to low concentrations of recovered materials (20% recovery of the initial SWCNT concentration).[16] For effective SWCNT use in future biomedical applications, sophisticated surface coatings are required to confer biocompatibility and multifunctionality. Although the existing coating methods demonstrate great potential and have been studied for proof-of-concept *in vivo* applications,[17-22] complicated synthetic processes and time-consuming purification steps hamper translation toward multifunctional and innovative products.

Therefore, to harness the potential of nanocarbons for real biomedical applications in the clinic, a facile surface coating is required to equip nanocarbons with solubility and multifunctionality, from imaging, delivery and therapy. Design criteria for such a material were developed and compared in Table 1. First the coating efficiency was examined based on: 1) efficient coating based on the maximum concentration achieved after solubility (Max. Dispersibility Concentration), 2) required amount of coating material for dispersion based on the mass ratio between SWCNTs and the material (SWCNT:Coating Material), and 3) stability in salt and serum conditions without excessive use of materials (Stable Without Excess?). Next the required characteristics for biomedical applications were compared based on: 1) the use of

materials that exhibit low cytotoxicity, ideally a biomaterial (Low Cytotoxicity?), and 2) a material that can target cell surface ligands or be easily conjugated with antibodies or other molecules for targeted delivery (Targetable to Biomolecules?). Based on Table 1, an approach that utilizes the conjugation of two materials shows promise because the final material can be strategically developed to bind strongly to the SWCNT surface while exhibiting hydrophilic properties. In this way, an amphiphilic material would be a model choice. Furthermore, since CNTs can be loaded with extremely high concentrations of coating, the use of biomaterials or biomimetic materials represents an ideal CNT coating choice to prevent cytotoxicity. Based on the criteria chart, the combination of two biomaterials was chosen based on their reported efficiency: hyaluronic acid (HA) and a bile acid, cholanic acid (CA). HACA is an amphiphilic material that is made up of HA and CA biomaterials;[2] each contributing to the unique interactions with carbon nanomaterials. HA is a straight, anionic polysaccharide that is a major component of the extracellular matrix and is therefore found in the connective, epithelial, and neural tissue.[23] It has an exceptional hydrodynamic character[24] and can maintain proper dispersion of nanomaterials by its strong Coulomb repulsion. As reported by Wallace and colleagues, SWCNTs can be stabilized in aqueous biological HA solutions just by sonicating the two materials, forming a well-dispersed, single-phase isotropic dispersion. Based on the phase diagram, only about a 0.1 wt % of HA is required to properly disperse SWCNTs, owing to the efficient dispersive properties of this biomaterial. Yet Wallace and colleagues surmise that these HA dispersed SWCNTs can form SWCNT bundles overtime. Therefore, an additional material is required to interrupt the strong van der Waals interactions among the tubes even with HA coating.

Design Criteria			CNT Coating Material					
			Aromatic Compounds	Amphiphiles				
					Charged		Neutral	Dyes
			Pyrene	**SDS**	**CTAB**	**Imidazolium salts**	**Triton-X**	**Congo red**
	Coating Efficiency*	Max. Solubility Concentration	N/A	0.01 mg/mL	0.02 mg/mL		0.02 mg/mL	>3.5 mg/mL
		SWCNT:Coating Material		1:1.7				1:5
		Stable Without Excess?	Y	N	N	N	N	N
	Biomedical Requirements*	Material Properties	Organic solvent	Cationic	Cationic	Cationic	Detergent	Diazo dye
		Low Cytotoxicty?	N	N	N	N	N	N
		Targetable to Biomolecules?	N	N	N	N	N	Y
	Total (Y)		1	0	0	0	0	1
		Interaction	pi-pi	hydrophobic	hydrophobic	hydrophobic	hydrophobic	pi-pi
		References	A	B	C	D	E	F

Design Criteria			CNT Coating Material							
			Biomolecules							
			High Molecular Weight Proteins				Polysaccharides		DNA	Bile Salts
			Lysozyme	**BSA**	**Hydrophobins**	**Oligopeptides**	**Chitosan**	**HA**		**SDOC**
	Coating Efficiency*	Max. Solubility Concentration	0.3 mg/mL						<0.1 mg/mL	0.3 mg/mL
		SWCNT:Coating Material	3:10	1:200	4:5	1:200	1:10	2.1:1	1:2	1:10
		Stable Without Excess?	Y	Y	Y	Y	Y	Y	Y	Y
	Biomedical Requirements*	Material Properties	pH sensitive	Biomaterial	From Fungi	Chiral specific	Biomaterial	Biomaterial	Biomaterial	Biomateial
		Low Cytotoxicty?	N	y	Y	Y	Y	Y	Y	Y
		Targetable to Biomolecules?	N	N	N	N	N	Y, CD44	N	N
	Total (Y)		2	2	2	2	2	3	2	2
		Interaction	hydrophobic, pi-pi, amine adsorption	adsorption	adsorption	pi-pi	adsorption	adsorption	pi-pi	hydrophobic
		References	G	H	I	J	K	L	M	N

Design Criteria			CNT Coating Material		
			Combinatorial Approach**		Proposed Approach
			Mucin Analogs	**PL-PEG**	**HACA**
	Coating Efficiency*	Max. Solubility Concentration		<0.1 mg/mL	>5 mg/mL
		SWCNT:Coating Material	1:40	1:5	1:2
		Stable Without Excess?	Y	Y	Y
	Biomedical Requirements*	Material Properties	Biomimetic	In vivo tested	Biomaterial
		Low Cytotoxicty?	Y	Y	Y
		Targetable to Biomolecules?	Y, carbohydrates	Y, versatile bioconjugation	Y, CD44
	Total (Y)		3	3	3
		Interaction	adsorption	adsorption	adsorption
		References	O	P	Section E

Table 1: Design Criteria of Nanocarbon Coating Material.

Abbreviations: SDS, sodium dodecyl sulfate; CTAB, cetyltrimethyl ammonium bromide; BSA, bovine serum albumin; HA, hyaluronic acid; PL, phospholipid; SDOC, sodium deoxycholate; Mucin Analogs, mucin Analogs with octadecyl C18 aliphatic chain; PL-PEG, polar phospholipid with polyethyleneglycol

Notations: *Y – Yes, N – No, ** The use of two materials that were strategically chosen to interact with SWCNTs.

References: A: [4] B: [4, 25, 26] C: [25, 26] D: [27] E: [25, 26] F: [28] G: [29] H: [30] I: [31] J: [32] K: [27, 33] L: [34, 35] M: [15] N: [27] O: [36] P: [16]

The bile acid, CA, can be used to directly interact with the SWCNT wall. CA is a direct analog of an efficient SWCNT dispersing agent, deoxycholate (DOC).[27, 37, 38] Hydrophobic forces between SWCNTs and DOC, although non-specific, have shown superior stability over specific, pi-stacking interactions. A comprehensive study of aqueous dispersions for single walled carbon nanotubes compared various polymers such as oligonucleotides, peptides, chitosan and cellulose along with surfactants like cholates and organsulfates using optical absorption and fluorescence spectroscopy measures.[27] Of these materials, sodium DOC (SDOC) and specific oligonucleotide sequences exhibited the highest dispersion efficacy for nanotubes, overcoming the strong van der Waals forces among tubes. Importantly, the study pointed out that in terms of polymer wrapping, higher molecular weight polymers (chitosan and cellulose were studied) show more effective dispersion than their lower molecular weight analogs. In terms of the bile salts, the loss of one hydroxyl group from sodium cholate to yield DOC resulted in a 17% dispersion efficiency increase. However, by further reducing the hydroxyl groups in cholates, the material can no longer serve as a single dispersing agent in water because it is too hydrophobic. Yet, it is that hydrophobic nature that enhances the interaction with the SWCNT. Therefore we utilize high molecular weight HA (M.W. 234.4 kDa), as opposed to low MW that can induce apoptosis by intracellular signaling pathways,[1-3] along with CA as a surface coating for SWCNTs. The bio-conjugate, HACA, has been previously utilized as a hydrophobic drug delivery carrier with cell targeting in vitro characteristics.[1-3] Here, we utilize this material to synergize with SWCNTs, especially by examining the SWCNT dispersion efficacy of HACA. In additional studies (Chapters 3, 4 and 5), the in vitro and in vivo capabilities will be studied.

C. Research Design and Methods

In this study, the use of HACA as a coating material for SWCNTs was examined for dispersibility. HACA is a biomaterial conjugate consisting of a highly hydrophobic CA, hypothesized to interact with the graphene wall of the SWCNT via hydrophobic interactions, linked to the hydrophilic HA backbone (Figure 3). The lowest required SWCNT:HACA weight ratio and the quality of SWCNT dispersion after HACA coating was characterized and measured. The major variable is the SWCNT to HACA weight ratio. The SWCNT concentration recovered after sonication and centrifugation will be used to determine the dispersion efficiency. Concentration of SWCNTs can be measured by optical absorbance. Efficiency of the coating ratio will be based on the amount of SWCNTs in suspension after centrifugation as a percent from the initial concentration. Once no statistical difference exists among absorbance values above 1, the SWCNT concentration reached a maximum. The lowest weight ratio that reaches the maximum will be considered the optimized SWCNT:HACA ratio. Qualitative measures, like visual inspection and atomic force microscopy (AFM) images, will be used to characterize the dispersion quality of HACA-SWCNTs in different media over time. In addition, HACA will be further modified with fluorophores for future in vitro and in vivo studies, relevant to Chapters 3 and 4.

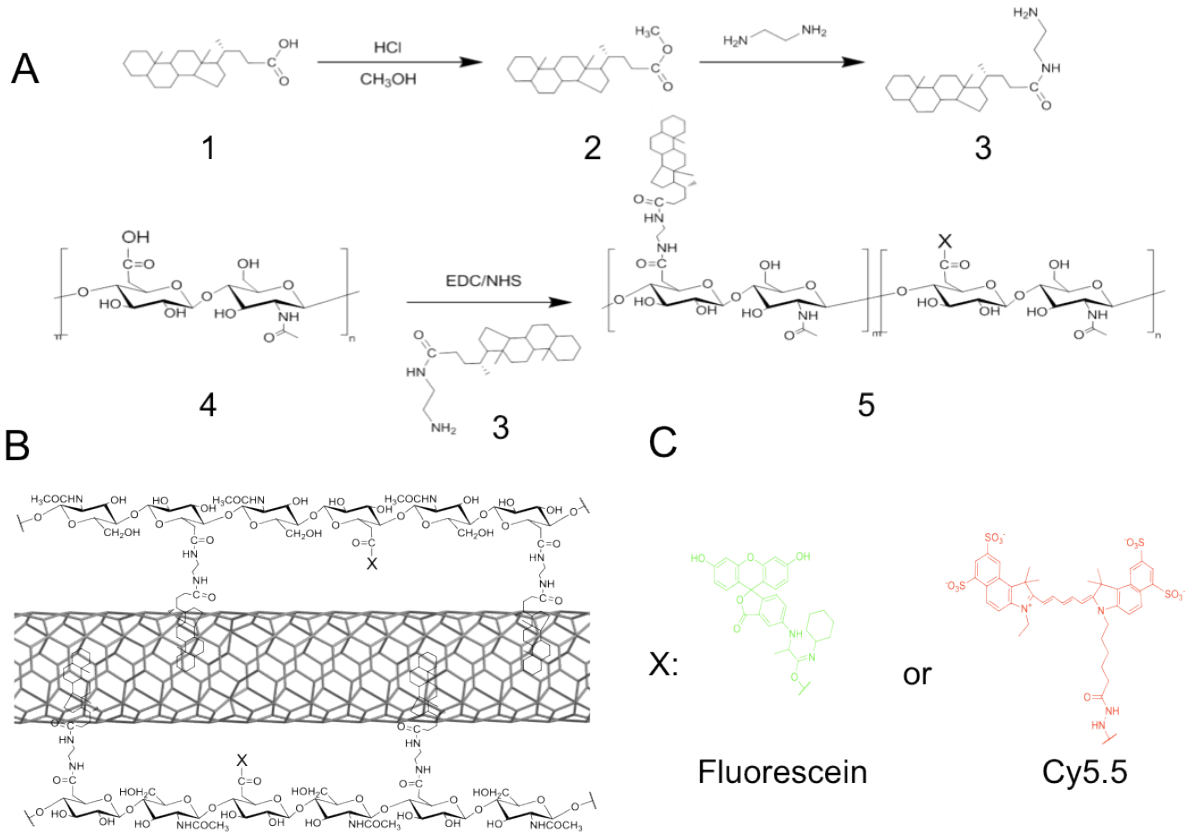

Figure 3: Development of HACA and its proposed interaction with SWCNTs. A) First, 5β-cholanic acid (1) is converted to aminoethyl 5β-cholanoamide (3) via an intermediate state (2). The amine group can then be conjugated onto the carboxylic acid groups of the HA backbone (4) to produce HACA (5). B) The proposed interaction of HACA with SWCNTs involves hydrophobic interactions between the CA and SWCNT, exposing the hydrophilic HA domain to the solvent. C) HACA as seen in B) can be conjugated with fluorophores such as fluorescein amine or Cy5.5. Structures drawn by ChemDraw Std 12.0.

1. Carbon Nanomaterial Coating with HACA

SWCNTs were dispersed via probe sonication for one hour with varying concentrations of HACA (SWCNT:HACA weight ratios of 1:5, 1:2, 1:1, 1:0.5, 1:0.1). The concentration of SWCNTs was kept constant, at approximately 1 mg/mL, while the weight of HACA introduced to the solution was adjusted. Five mg of SWCNTs was added to 5 mL of water along with either 25, 10, 5, 2.5 or 0.5 mg of HACA to make the respective SWCNT:HACA ratios of 1:5, 1:2, 1:1,

1:0.5, 1:0.1. Sonication was performed on a VCX-750 ultrasonic processor (Sonics & Materials, Newtown, CT). The ultrasonic probe (6 mm microtip extension, Sonics & Materials) was immersed into the mixture with a volume ranging from 5 - 10 mL. The probe was driven at 60% of the instrument's maximum amplitude at ~ 20 kHz with a 10 sec on / 1 sec off pulse sequence. To avoid heating, the solution was immersed in an ice-bath during sonication. Probe sonication position and height was adjusted every 20 minutes in order to induce a uniform dispersion of the SWCNTs.

In addition to testing the solubility of SWCNTs among different weight ratios, other carbon nanomaterials were qualitatively compared for solubility after HACA sonication. Carbon nanomaterials included: short single walled carbon nanotubes with an outer diameter of 1-2 nm and a quoted purity of > 90 wt% (CheapTubes, Inc., Brattleboro, VT), short multi-walled carbon nanotubes with an outer diameter > 50 nm and a stated purity of > 95 wt% (CheapTubes, Inc.) and fullerenes with a purity of 99.9% (Sigma). The nanomaterials were directly used without additional processing. Visual inspection for any carbon nanomaterial settling was monitored for HACA-SWCNTs in water, 10 mM phosphate buffered saline solution (pH 7.4), cell culture media RPMI 1640 (Cellgro, Manassas, VA), and cell culture media supplemented with 10% fetal bovine serum (Invitrogen, Grand Island, NY).

2. SWCNT Characterization Methods

SWCNTs have intrinsic optical properties that can be utilized to characterize individual tubes and measure SWCNT concentration. The sharp densities of states at the Van Hove singularities give nanotubes optical transitions that correspond to photon absorption in the near infrared (NIR), visible, and ultraviolet (UV) range.[39] In addition, because all the carbon atoms of SWCNTs are exposed on the surface (1D material) and they have sharp density of states,

SWCNTs have distinctive resonance-enhanced Raman spectra signatures with large scattering cross sections for single tubes. Therefore, NIR absorbance and Raman spectroscopy are use dto characterize SWCNTs. Atomic force microscopy (AFM) was also used to visualize disperse SWCNTs after HACA coating.

a. Absorbance

Because of the $E_{1,1}$ optical transition, SWCNTs are highly absorbing materials in the NIR range. NIR absorbance, therefore, has traditionally been used to measure SWCNT concentration. To measure concentration, the extinction coefficient needs to be established using the Beer-Lambert law. Absorbance spectra were measured by a Genesys 10S UV-Vis Spectrophotometer (Thermo Scientific, Waltham, MA). Absorbance spectra were collected directly after sonicating SWCNTs with HACA (at a weight ratio of 1:10) at different SWCNT concentrations (0.03-1 mg/mL) and were assumed to be 100% dispersed. Based on well-established methods,[18] the absorbance peak at 808 nm was used as a marker for SWCNT concentrations. A calibration curve of absorbance at 808 nm versus the known SWCNT concentration was created (Figure 4A).The average of at least three measurements was tested. The slope of the linear least-square fit of the absorbance vs. SWCNT concentration is the extinction coefficient and can be used for all further studies to determine SWCNT concentration. Absorbance of HACA conjugated with fluorescein, the visible light fluorophore, or Cy5.5, the near infrared dye, and coated onto SWCNTs was also collected using the Genesys 10S system. The spectra were normalized using Prism Version 4 for Windows (Graphpad, La Jolla, CA) and verified to include their respective dyes.

b. Raman spectroscopy and Microscopy

A typical Raman spectrum of SWCNTs includes three distinct regions: radial breathing modes in the 100-300 cm^{-1} range, D-band in the 1400-1500 cm^{-1} range, and G-band in the 1550-1650 cm^{-1}

range.[40] The G-band, which correlates to the resonance of ordered graphene, is a Lorentzian type peak with little overlapping signals in biological samples and distinguishable from fluorescence backgrounds.[22, 41] The G-band is also dependent on SWCNT concentration, and the area under the curve at the 1550-1650 cm^{-1} range was therefore used for concentration verification of absorbance readings (Figure 4B). Known concentrations of HACA-SWCNTs at 0.03 – 1 mg/mL were measured in cuvettes. Raman spectra were recorded on an iRaman 785 spectrometer with a BCF100A cuvette holder (B&W Tek, Inc, DE). The power output was 35 mW, and the excitation source was an argon ion laser at 785 nm.

c. Atomic Force Microscopy imaging of HACA-SWCNTs

After being diluted in DW at 100 µg/mL, HACA coated SWCNTs were examined under a PicoForce Multimode AFM (Bruker, CA) consisting of a Nanoscope® V controller, a type E scanner head, and a sharpened TESP-SS (Bruker, CA), OMCL (Bruker, CA).

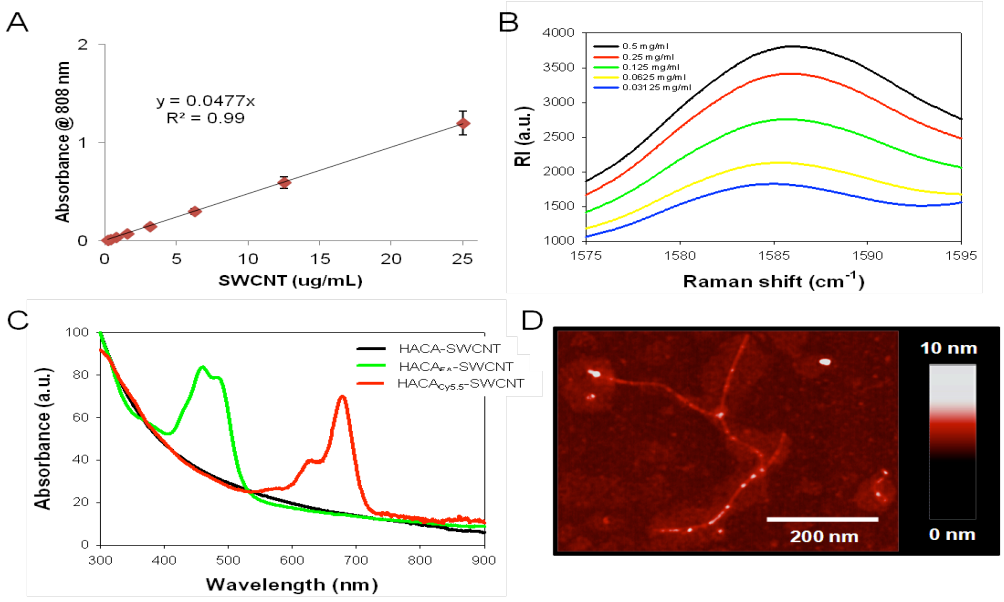

Figure 4: Tools for SWCNT Characterization. A) Calibration curve of SWCNT absorbance intensity at 808 nm versus a known SWCNT concentration. B) Concentration dependent Raman G-band for concentration verification of absorbance readings. C) UV/Vis spectra of HACA-SWCNTs before and after conjugation of Cy5.5 or fluorescein. D) AFM phase image of HACA-SWCNTs dispersed in water.

3. Percent Efficiency of Coating

Efficiency of coating at different SWCNT: HACA weight ratios will be examined by the concentration of SWCNTs recovered after centrifugation. The initial SWCNT concentration, based on the absorbance vs. concentration curve above, will correlate to 100% SWCNT dispersion. After 1 hour centrifugation of 15 000g, the concentration will be measured again. The percent of recovered concentration will be known as the efficiency value. Once no statistical difference exists of the weight ratios, the SWCNT concentration recovered reached a maximum. The lowest weight ratio that reaches the maximum will be considered the optimized SWCNT:HACA ratio.

4. Dye-labeling of HACA Coating

The same HACA synthesis method was used as previously reported.[42] The hydrophobic bile acid, 5β-cholanic acid, (Sigma-Aldrich, St. Louis, MO) is conjugated onto the water soluble HA polymer (Lifecore Biomedical, Chaska, MN) via amide formation to develop an amphiphilic material composed entirely of biomaterials. To initiate conjugation, 5β-cholanic acid is converted to aminoethyl 5β-cholanoamide and then reacted via EDC and NHS chemistry with the carboxylic acids of HA. In this way, CA is chemically conjugated onto HA to form HACA (Fig. X). ^{1}H NMR (UnityPlus 300, Varian, CA) was used to measure the amount of CA conjugated onto the HA backbone.

Two fluorescent dyes, fluorescein (Sigma) that emits in the visible and Cy5.5 (GE Healthcare, Piscataway, NJ) that emits in the near-infrared region, were chosen as labels for optical tracking of HACA-SWCNTs in cells and *in vivo*, respectively. The labeling techniques of HACA with fluorescein amine and Cy5.5-hydrazide were previously reported and were followed in this study .[43,44] Just as CA was conjugated to HA, EDC and NHS chemistry is utilized to bind

the amine form of fluorescein onto the HA backbone. Cy5.5-hydrazide is chemically conjugated through amide formation with EDC and HOBt. To determine the labeling efficacy, the amount of fluorescein amine and Cy5.5 conjugated onto HACA was calculated using an absorbance vs. fluorescence dye concentration curve, obtained by UV/Vis spectrophotometery (Genesys 10s, Thermo Scientific, Waltham, MA) at 675 nm and 450 nm for Cy5.5 and fluorescein, respectively (Figure 4C).

5. Statistical Analysis

At least three different rounds of HACA-SWCNT dispersions were performed for each weight ratio. Each round of HACA dispersed SWCNTs was tested for the percent efficiency. For each response measure, a one-way ANOVA with Tukey's *post hoc* test was performed to compare differences among each weight ratio. Without statistical significance among different responses, the smallest weight ratio was chosen for further studies.

D. Results

To design a hyaluronic acid based, non-covalent coating method for carbon nanomaterials, a proper coating method was developed. A non-covalent technique was utilized and based on sonication because it is the ideal energy input needed to break apart the strong van der Waals forces across the length of the carbon nanotubes.[45] Once the forces are overcome, HACA can interact with the individual SWCNT surface. For an efficient coating system, the minimum amount of HACA needed to disperse SWCNTs was found to be a weight ratio of 2:1, a much smaller amount of dispersing agents previously reported.[21-23] Additionally, carbon nanomaterials like SWCNT, MWCNTs and fullerenes, were sonicated with HACA at the optimized weight ratio and exhibited effective dispersion in distilled water (DW). Once in DW, these HACA coated materials could be further transferred into PBS, cell culture medium, and medium with

10% serum with continued dispersion (Figure 5). The HACA-carbon nanomaterials maintained their dispersibility in these conditions when stored in 4°C for over five months (Figure 5).

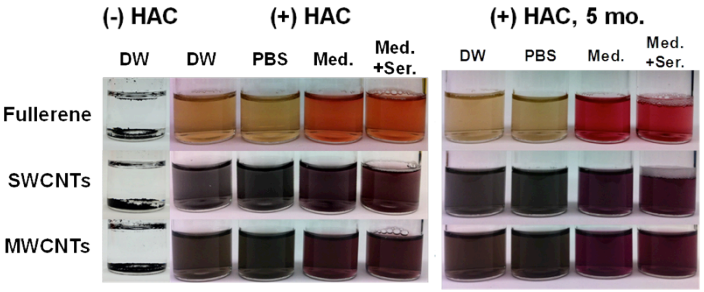

Figure 5: Photographs of dispersed nanocarbons with and without HACA in distilled water (DW), phosphate buffer saline solution (PBS), cell culture media (Med.) , and media with 10% serum. Right image shows the same nanocarbons after 5 months. Each solution is over 5 mg/mL.

Coating of HACA onto SWCNTs was verified by AFM images and zeta potential measurements (Figure 4D). AFM phase image displays individualized HACA-SWCNTs when dried on a substrate with little excess of HACA. Zeta-potential measurements of centrifuged HACA-SWCNTs exhibited a negative charge at -62.7 ± 5 mV, a similar value to previous reported data for HACA,[21] implying the coated HACA contribution on SWCNTs.

For future in vitro and in vivo tracking studies, HACA was conjugated with fluorophores, fluoresceinamine and Cy5.5, respectively. The conjugation, as described in Figure 3, was characterized for its degree of substitution with the dyes. Analysis by UV-Vis spectroscopy showed that about 130 FA molecules and 7 Cy5.5 molecules were conjugated per HAC chain. This material will be used in all future studies (Chapter 3 and 4).

E. Discussion

SWCNTs contain properties useful for biomedical imaging and therapy, but are inherently insoluble in organic solvents and aqueous solutions and, needless to say, physiological relevant conditions. Without dispersion, bundled SWCNTs resemble macroscopic carbon soot, which cannot have semiconducting properties to serve as nano-biosensors or cannot be

controlled as mechanical strength fillers in medical implants, to name a few examples of their biomedical applications. Therefore, coating methods to disperse SWCNTs have been extensively studied. In this study, analysis was performed to identify the relevant properties for a carbon nanomaterial coating useful for biomedical applications: non-covalent interaction with the carbon nanomaterial, amphiphilic, and biocompatible. HACA was identified to be that effective biomaterial coating. Coating techniques with HACA were optimized for efficiency in dispersing the model carbon nanomaterial, SWCNTs.Optimization was based on the amount of dispersing agent required to disperse the maximum amount of SWCNTs. For non-covalent coating, sonication is the predominant method to disperse SWCNTs.[4, 5, 16] The optimized weight ratio of HACA:SWCNT was measured to be 2:1. Above this ratio, no significant increase in dispersion concentration was detected; while below this ratio, not all the SWCNTs could be dispersed.

Dispersion quality was qualitatively monitored by visual inspection, AFM images and dispersion efficacy as a percent of the total SWCNT concentration recovered after centrifugation. Previously proposed methods for quality included using optical detection methods, such as absorption and photoluminescence (PL) measures. Yet these techniques were not sensitive to study the commercially purchased short CNTs with a purity of >90%. Traditionally, absorption studies are robust measures of SWCNT concentration and dispersion (including both metallic and semiconducting tubes) and do not show changes in spectra due to changes in environmental conditions, like PL measurements exhibit. Other issues exist with PL methods. For example, PL intensity can decrease as SWCNT concentrations increase. Since these commercial SWCNTs exhibited a linear concentration relationship with absorbance at the optical transition energy of 808 nm and with the Raman G-band (Figure 4), there is confidence that SWCNTs do exist in an appropriately high amount of the sample. However, purity guidelines for all commercial

SWCNTs need to be set, as chemical grades are set for reagents. Importantly, readily available standards for carbon nanotubes are required, based on size and chirality. The National Institute of Standards and Technology (NIST) released one standard for single-wall carbon nanotubes (SRM 2484) last year.[46]

Another limitation to this study is that a direct molecular interaction between HACA and SWCNTs is not discerned. Molecular modeling would identify thermodynamically favored interactions between the graphene wall of the nanotube and HACA, along with discerning any environmental changes that could affect the dispersion. In future work, the development of such a model should be attempted; but, it is currently beyond the experimental design.

In conclusion, this study led to a facile coating that was completely achieved in about 1.5 h with a low amount of HACA. An observed maximum concentration of soluble SWCNTs could be concentrated to about 5 mg/mL. More importantly, the dispersion was stable for over 5 months not only in distilled water but also in salt and serum conditions. In this way, a practical dispersing and functionalization technique can be utilized for researchers in the study of SWCNTs.

F. References

1. K. Y. Choi, H. Y. Yoon, J.-H. Kim, S. M. Bae, R.-W. Park, Y. M. Kang, I.-S. Kim, I. C. Kwon, K. Choi, S. Y. Jeong, K. Kim and J. H. Park, *ACS Nano*, 2011, **5**, 8591-8599.

2. K. Y. Choi, H. Chung, K. H. Min, H. Y. Yoon, K. Kim, J. H. Park, I. C. Kwon and S. Y. Jeong, *Biomaterials*, 2010, **31**, 106-114.

3. K. Y. Choi, K. H. Min, J. H. Na, K. Choi, K. Kim, J. H. Park, I. C. Kwon and S. Y. Jeong, *J. Mater. Chem.*, 2009, **19**, 4102-4107.

4. N. Karousis, N. Tagmatarchis and D. Tasis, *Chem. Rev.*, 2010, **110**, 5366-5397.

5. D. Tasis, N. Tagmatarchis, A. Bianco and M. Prato, *Chem. Rev.*, 2006, **106**, 1105-1136.

6. A. Bianco, K. Kostarelos, C. D. Partidos and M. Prato, *Chem. Commun.*, 2005, 571-577.

7. W. Wu, S. Zhang, Y. Li, J. Li, L. Liu, Y. Qin, Z.-X. Guo, L. Dai, C. Ye and D. Zhu, *Macromolecules*, 2003, **36**, 6286-6288.

8. G. Viswanathan, N. Chakrapani, H. Yang, B. Wei, H. Chung, K. Cho, C. Y. Ryu and P. M. Ajayan, *J. Am. Chem. Soc.*, 2003, **125**, 9258-9259.

9. Y.-L. Zhao and J. F. Stoddart, *Acc. Chem. Res.*, 2009, **42**, 1161-1171.

10. Z. Liu, X. Sun, N. Nakayama-Ratchford and H. Dai, *ACS Nano*, 2007, **1**, 50-56.

11. N. Nakashima, Y. Tomonari and H. Murakami, *Chem. Lett.*, 2002, **31**, 638-639.

12. K. Yang, L. Zhu and B. Xing, *Environ. Sci. Technol.*, 2006, **40**, 1855-1861.

13. M. S. Strano, M. Zheng, A. Jagota, G. B. Onoa, D. A. Heller, P. W. Barone and M. L. Usrey, *Nano Lett.*, 2004, **4**, 543-550.

14. X. Tu, S. Manohar, A. Jagota and M. Zheng, *Nature*, 2009, **460**, 250-253.

15. M. Zheng, A. Jagota, E. D. Semke, B. A. Diner, R. S. McLean, S. R. Lustig, R. E. Richardson and N. G. Tassi, *Nat. Mater.*, 2003, **2**, 338-342.

16. Z. Liu, S. M. Tabakman, Z. Chen and H. Dai, *Nat. Protoc.*, 2009, **4**, 1372-1381.

17. Z. Liu, W. Cai, L. He, N. Nakayama, K. Chen, X. Sun, X. Chen and H. Dai, *Nat. Nanotechnol.*, 2007, **2**, 47-52.

18. N. W. S. Kam, M. O'Connell, J. A. Wisdom and H. Dai, *Proc. Natl. Acad. Sci. U. S. A.*, 2005, **102**, 11600-11605.

19. A. De La Zerda, C. Zavaleta, S. Keren, S. Vaithilingam, S. Bodapati, Z. Liu, J. Levi, B. R. Smith, T.-J. Ma, O. Oralkan, Z. Cheng, X. Chen, H. Dai, B. T. Khuri-Yakub and S. S. Gambhir, *Nat. Nanotechnol.*, 2008, **3**, 557-562.

20. Z. Liu, K. Chen, C. Davis, S. Sherlock, Q. Cao, X. Chen and H. Dai, *Cancer Res.*, 2008, **68**, 6652-6660.

21. Z. Liu, C. Davis, W. Cai, L. He, X. Chen and H. Dai, *Proc. Natl. Acad. Sci. U. S. A.*, 2008, **105**, 1410-1415.

22. C. Zavaleta, A. de la Zerda, Z. Liu, S. Keren, Z. Cheng, M. Schipper, X. Chen, H. Dai and S. S. Gambhir, *Nano Lett.*, 2008, **8**, 2800-2805.

23. B. P. Toole, *Nat. Rev. Cancer*, 2004, **4**, 528-539.

24. P. Bulpitt and D. Aeschlimann, *J. Biomed. Mater. Res., Part A*, 1999, **47**, 152-169.

25. D. A. Britz and A. N. Khlobystov, *Chem. Soc. Rev.*, 2006, **35**, 637-659.

26. V. C. Moore, M. S. Strano, E. H. Haroz, R. H. Hauge, R. E. Smalley, J. Schmidt and Y. Talmon, *Nano Lett.*, 2003, **3**, 1379-1382.

27. R. Haggenmueller, S. S. Rahatekar, J. A. Fagan, J. Chun, M. L. Becker, R. R. Naik, T. Krauss, L. Carlson, J. F. Kadla, P. C. Trulove, D. F. Fox, H. C. DeLong, Z. Fang, S. O. Kelley and J. W. Gilman, *Langmuir*, 2008, **24**, 5070-5078.

28. C. Hu, Z. Chen, A. Shen, X. Shen, J. Li and S. Hu, *Carbon*, 2006, **44**, 428-434.

29. D. Nepal and K. E. Geckeler, *Small*, 2006, **2**, 406-412.

30. K. Matsuura, T. Saito, T. Okazaki, S. Ohshima, M. Yumura and S. Iijima, *Chem. Phys. Lett.*, 2006, **429**, 497-502.

31. K. Kurppa, H. Jiang, G. R. Szilvay, A. G. Nasibulin, E. I. Kauppinen and M. B. Linder, *Angew. Chem., Int. Ed.*, 2007, **46**, 6446-6449.

32. V. Zorbas, A. L. Smith, H. Xie, A. Ortiz-Acevedo, A. B. Dalton, G. R. Dieckmann, R. K. Draper, R. H. Baughman and I. H. Musselman, *J. Am. Chem. Soc.*, 2005, **127**, 12323-12328.

33. C. Lynam, S. E. Moulton and G. G. Wallace, *Adv. Mater.*, 2007, **19**, 1244-1248.

34. S. E. Moulton, M. Maugey, P. Poulin and G. G. Wallace, *J. Am. Chem. Soc.*, 2007, **129**, 9452-9457.

35. J. M. Razal, K. J. Gilmore and G. G. Wallace, *Adv. Funct. Mater.*, 2008, **18**, 61-66.

36. X. Chen, G. S. Lee, A. Zettl and C. R. Bertozzi, *Angew. Chem., Int. Ed.*, 2004, **43**, 6111-6116.

37. W. Wenseleers, I. I. Vlasov, E. Goovaerts, E. D. Obraztsova, A. S. Lobach and A. Bouwen, *Adv. Funct. Mater.*, 2004, **14**, 1105-1112.

38. J. A. Fagan, J. Y. Huh, J. R. Simpson, J. L. Blackburn, J. M. Holt, B. A. Larsen and A. R. H. Walker, *ACS Nano*, 2011, **5**, 3943-3953.

39. Z. Liu, S. Tabakman, K. Welsher and H. Dai, *Nano Res.*, 2009, **2**, 85-120.

40. M. S. Dresselhaus, G. Dresselhaus, R. Saito and A. Jorio, *Phys. Rep.*, 2005, **409**, 47-99.

41. S. Keren, C. Zavaleta, Z. Cheng, A. de la Zerda, O. Gheysens and S. S. Gambhir, *Proc. Natl. Acad. Sci. U. S. A.*, 2008, **105**, 5844-5849.

42. K. Y. Choi, K. H. Min, J. H. Na, K. Choi, K. Kim, J. H. Park, I. C. Kwon and S. Y. Jeong, *J. Mater. Chem.*, 2009, **19**, 4102-4107.

43. A. N. de Belder and K. O. Wik, *Carbohydr. Res.*, 1975, **44**, 251-257.

44. K. Y. Choi, H. Chung, K. H. Min, H. Y. Yoon, K. Kim, J. H. Park, I. C. Kwon and S. Y. Jeong, *Biomaterials*, 2010, **31**, 106-114.

45. T. Hertel, R. Martel and P. Avouris, *J. Phys. Chem. B*, 1998, **102**, 910-915.

46. in *NIST Tech Beat*, 2011.

Chapter 3:

Biological Activity of Hyaluronic Acid Wrapped Single-Walled Carbon Nanotubes *In Vivo*

A. Abstract

The overall goal of this extensive study is to render carbon nanomaterials useful for biomedical application. In this specific study, the aim is to identify the *in vitro* biological potential of HACA-SWCNTs according to the cytotoxicity, hyaluronidase sensing, and targeting to CD44 receptor expressing cells. Once cell viability was confirmed, HACA-SWCNTs exhibited cellular targeting via the CD44 receptor and uptake via CD44 receptor mediated endocytosis. Uptake was detected in high and low expressing CD44 cells by measuring the SWCNT intrinsic Raman signals as well as a unique fluorescence activation signal based on a system involving the interplay between fluorescently labeled HACA and SWCNTs. The fluorescence quenching system relies on energy transfer between the emitted fluorescence and strong absorbance of SWCNTs which is disrupted in the presence of hyaluronidase. In this study, the HACA coating was tested for two roles: a) its use as a hyaluronidase cleavable substrate between the fluorescent dye and SWCNT and b) its ability to target and induce uptake of HACA-SWCNTs to cells with high CD44 receptor expression.

B. Introduction

HA is a linear, anionic polysaccharide, specifically a glycosaminoglycan, composed of a repeating disaccharide of N-acetyl-D-glucosamine and D-glucuronic acid found ubiquitously throughout vertebrates. Under physiological conditions, the carboxyl groups of the glucuronic acid are ionized, and therefore HA exist in the body as hyaluronan (termed HA as well). It serves diverse biological roles, predominantly serving a vital structural role as a major component of the extracellular matrix (ECM) and forming matrices upon which cells can migrate, divide and activate.[2] HA plays an integral part in connective, epithelial, and neural tissue.[3] In addition, HA

is involved in intracellular signaling by interactions with HA binding proteins, termed hyaladherins.

These hyaladherins are found in the ECM to aid HA in its structural role as well a couple on the cell surface, suggesting that they act as HA receptors. In terms of providing structure, example hyaladherins include proteoglycans, like aggrecan and versican, that form complexes with hyaluronan through the Link protein, made up of two Link modules, allowing elasticity to blood vessels, structural integrity of the skin and brain, and the load-bearing nature of cartilage. The Link module is a structural domain that is about 100 amino acids in length, upon which HA interacts non-covalently [2]. Other members of the Link module family include the hyaluronan receptor, LYVE-1, TSG-6, HARE and CD44. LYVE-1, hyaluronan specific receptor responsible for its degradation, is a cell membrane receptor on the lymph vessel endothelium. Tumor necrosis factor-stimulated gene-6 (TSG-6), a secreted protein, has a single Link module with high affinity to hyaluronan. HA receptor for endocytosis (HARE) is found on the liver sinusoidal endothelial cells[4], responsible for turnover of systemic HA from the blood by binding HA and taking up HA by a clathrin-coated pit pathway.[5, 6] Non-Link module hyaladherins that bind hyaluronan covalently include[2]: inter-α-inhibitor, a serine protease inhibitor expressed predominantly during ovulation; CD38, a type II membrane glycoprotein and enzyme found on white blood cells; two other proteoglycans isolated from the retina; and the receptor for hyaluronan-mediated motility (RHAMM) found intracellularly in various cell types and can infrequently occur on the cell surface as CD168 [7]. But it is the hyaluronan receptor CD44, a Link module superfamily member, that is the only hyaladherin found on the cell membrane of various cell types responsible to maintain the HA tethering on the cell surface for diverse functions.

CD44 is part of the Type B subgroup because of its long chain binding domain with N- and C-terminal extensions. CD44's binding domain for hyaluronan is about 160 amino acids because it extends beyond just the 100 amino acid long Link domain and into the N-terminus as well as in the membrane proximal region, near the C-terminus, that is essential for functional binding. [8] On a molecular basis, the basic amino acids found on CD44 (two arginines Arg-41 and Arg-78 and two tyrosines Tyr-42 and Tyr-79) play a critical role in forming ionic bonds with the carboxylic acid groups of hyaluronan. [8] But because of its unique extended binding domain, other residues and structural elements in CD44 are suggested to play a role in hyaluronan binding, along with the CD44 receptor density on the cell membrane surface and the size of the multivalent HA ligand. [9] Based on important HA to CD44 binding studies, multiple CD44/HA bindings are required to achieve a functional avidity. An HA oligomer size greater than 6 monosaccharides (>1.2 kDa) is needed to efficiently occupy the binding site on CD44, while about 22 monosaccharides (>4.5 kDa) are needed for divalent binding. This value is reinforced with the idea that a single binding site accommodates about 6-10 sugar residues. [9] With increasing molecular weight of HA, the HA/CD44 binding avidity increases because it interacts with multiple CD44 molecules simultaneously.[9]

Once bound, the HA is endocytosed and degraded, important for natural HA homeostasis. Although the specific endocytotic mechanism is not fully understood, many reports imply that HA is taken up into certain types of cells by CD44 receptor-mediated endocytosis.[10] For example, CD44 mediated endocytosis of HA has been demonstrated in chondrocytes[11, 12], macrophages [13]and COS-7 cells [14, 15] by the co-localization of CD44 and HA in intracellular vesicles. Much more reports on HA liposomes and nanoparticles cite CD44 receptor mediated endocytosis for the HA-based particle uptake in cells and tumor models in vitro and in vivo [16, 17].

Based on previous reports of an HACA drug delivery platform, the interaction between HA and its receptor CD44 allowed fast uptake into highly expressing CD44 receptor positive cancer cells.[16] In addition, elevated CD44 expression elevates HA intracellular accumulation.[12, 13] For example, Cutly et al. reported that because of the low CD44 receptor density found on 3T3 cells, endocytosis was reduced.[13] Although, the uptake mechanism is controversial, especially based on inhibition studies. Hua et al. reported that CD44 receptors can be inhibited by anti-CD44 monoclonal antibodies, which in turn blocked HA intracellular concentrations.[11] But more recent reports show that these antibodies fail to block HA uptake, prompting other studies to conclude that HA endocytosis can occur independent of CD44 binding [18, 19]. Despite this controversy, it is clear that hyaluronidase, especially the widely expressed hyaluronidase 1, requires the acidic conditions in intracellular vesicles to degrade and turnover HA in the body.[1, 10, 20] All hyaluronidases cleave the linkage of the disaccharide between N-acetyl-D-glucosamine and D-glucuronic acid.[10] In general, the endocytotic pathway is believed to involve: a) initial degradation by the hyaluronidase 2 into HA fragments of 50-100 saccharides during partial endocytosis, b) endocytosis, receptor mediated or macropinocytosis, c) final degradation of oligosaccharides by hyaluronidase 1 in the endosome d) the final products can be used for future synthesis of HA or the HA fragments can be exocytosed.[10]

During excessive proliferation periods, such as tumor formation and metastasis, CD44 is highly expressed on the cell membrane.[21] It is hypothesized that the excess CD44 plays an important role to degrade the extracellular HA to facilitate tumor cell locomotion for invasion into surrounding tissues.[22] In fact, CD44 is elevated in many malignancies in relation to normal tissues and this increase is related to tumor metastasis in vivo (Table 1). For example, CD44 is

highly expressed in human breast cancer cells, and the highest concentration of CD44 is correlated with the most invasive tumor cells and highest rate of HA degradation.[23] CD44 also plays an important role as a cell marker for human cancer stem cells. Based on recent hypotheses in the cancer field, there exists an extremely small and unique population of cells found in human cancer, identified as cancer stem cells or cancer-initiating cells[24]. This population is said to maintain the tumor during formation and possibly induce metastasis. CD44 has been identified as the surface marker in this unique and important cell population[25-27], implying an important target in cancer. In fact, the CD44 antibody[17, 28-30] and HA[31, 32], like HACA[16], has been used to target drugs to CD44 overexpressing metastatic cancers in vivo, like head and neck squamous cell carcinoma. In summary, HA not only targets CD44 but also has enhanced cellular uptake in CD44 overexpressing cells, i.e. cancer cells. These properties are hypothesized to be imparted on HACA-SWCNTs and are examined in this study.

Malignancy
Non-Hodgkin's lymphoma
Colorectal
Gastric
Pancreatic
Renal
Hepatocellular
Cervical
Ovarian
Non-small lung
Breast carcinoma
Melanoma

Table 1: Malignancies associated with CD44 over- expression as reviewed in [1].

Fluorescence imaging and measurements are common techniques to detect intra- and extracellular mechanisms, such as for cellular uptake of SWNCTs. In this study, the fluorescent dye labeled HACA ($HACA_{dye}$), either with fluorescein ($HACA_{FA}$) or Cy5.5 ($HACA_{Cy5.5}$), from Chapter 2, will be utilized to track HACA-SWCNT cellular uptake. Once coated onto the CNTs, the $HACA_{dye}$-SWCNTs are hypothesized to serve as activatable probes because of the broad absorbance of SWCNTs (Figure 1).

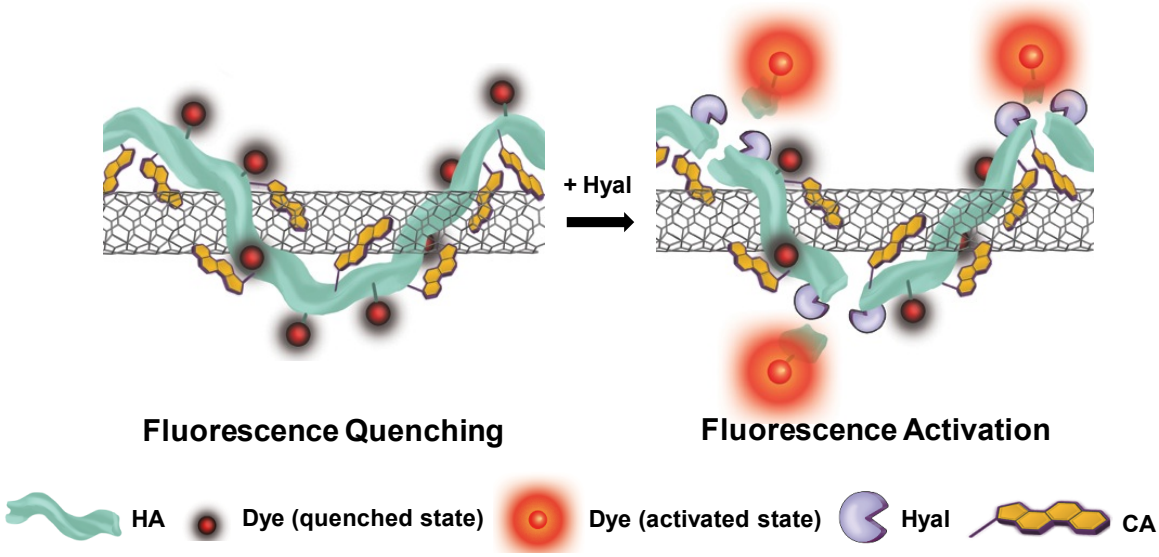

Figure 1: Schematic of dye-labeled HACA wrapped on SWCNTs ($HACA_{dye}$-SWCNT) and its fluorescence activation properties. HACA coating on SWCNTs render the fluorescent dye-labeled material quenched. In the presence of hyaluronidase (HYAL), an enzyme that specifically cleaves HA, the dye molecules are released from the SWCNT and fluorescence is recovered. Image drawn by Ms. Myung Sung Lee.

These probes are more sophisticated fluorescence detection systems because of their improved sensitivity and high signal-to-background ratios[33-35]. Fluorescence signal intensities are detectable only in response to a specific target, like a particular protein or environmental change. At its minimum, the probe consists of two components: the fluorescence donor, such as an organic dye, and the quencher that absorbs the fluorescence emission from the donor. In the HACA-SWCNT system, it is hypothesized that the SWCNT serves as the quencher. The general activatable probe in a native state, usually when the two components are in close vicinity, is fluorescently quenched by various energy transfer mechanisms.[35] Once the interaction between the two components is disrupted by a specific stimuli/target, the fluorescence is restored. In other words, the fluorescence activatable probe releases a fluorescence signal in response to a specific target but maintains a minimal signal in its native state. In this specific study, $HACA_{dye}$-

SWCNTs were studied for their quenching and activation properties in the presence of hyaluronidase (hyal), an enzyme that specifically degrades HA where the dyes are conjugated. This type of fluorescence activation can then signify if HACA-SWCNTs enter the cell when it interacts with the intracellular concentrations of hyal. My previous work involving the design and application of various activatable probes include: imaging the proteolytic cascade (caspase-3, caspase-8, caspase-9) in vitro after apoptosis is induced[36] and detecting the expression of extracellular matrix metalloproteinases in vivo[37] and in real-time[38].

In addition to fluorescence, SWCNTs can be directly detected by Raman spectroscopy (see Chapter 2) and microscopy in vitro and in vivo.[39] Previously, Raman mapping of the G-band intensity was used to directly image the uptake of SWCNTs in murine macrophage cells.[40] Intravenously injected SWCNTs were also monitored by G-band Raman counts collected in the blood to determine the circulation time. [41] Raman spectroscopy has become the gold standard to directly image SWCNTs in biological samples and is therefore utilized in this study to compare SWCNT uptake among cell types.

Since the HACA-SWCNT coating method is established (Chapter 2), the biomaterial coated SWCNTs will be studied for in vitro applications. First cell viability after HACA-SWCNT treatment at different SWCNT concentrations is examined. Next, $HACA_{dye}$-SWCNTs are investigated for fluorescence activation under hyal, both quenching and activation properties. Finally, fluorescence imaging and Raman microspectroscopy are used to monitor HACA-SWCNT uptake into cells. The tracking methods in cells with varying CD44 receptor expression determine if: a) HACA-SWCNTs enter cells, b) SWCNTs enter cells, and c) HACA-SWCNTs enter cells by a specific mechanism.

C. Research Design and Methods

To study the biological activity of HACA-SWCNTs, two distinct experimental directions were taken – I) fluorescence quenching/recovery of dye-labeled HACA coated SWCNTs and II) CD44 receptor cell targeting and uptake of HACA-SWCNTs. Two murine cell lines based on their varying CD44 expression levels were utilized in this study: squamous cell carcinoma (SCC7) and fibroblasts (3T3). SCC7 cells overexpress CD44[16, 42] and 3T3 cells have a low expression of the CD44 receptor.[13]

Before studying the cell uptake of HACA-SWCNTs, cytotoxicity studies are required to determine if HACA-SWCNTs affect cell viability at different SWCNT concentrations. Previous reports have shown that many commonly used cytotoxicity assays give false positive results, because assay chemicals absorb on the SWCNTs and cannot perform their necessary enzymatic reaction to measure cell viability.[43] In addition, the presence of CNTs within the solution can interfere with the signal readout, such as colorimetric or fluorometric signals, because of the broad absorbance of SWCNTs within the entire visible and NIR electromagnetic spectrum. Therefore, a modified assay of lactate dehydrogenase was chosen to reduce interference and reduce false positive and negative results.[44] HACA-SWCNT concentrations were varied and the percentage of viable cells compared to the untreated group was measured.

HACA was labeled with fluorescein amine (FA) (emission in the visible region for *in vitro* studies) or Cy5.5 (emission in the NIR for *in vivo* studies) and then coated onto SWCNTs, known as $HACA_{Cy5.5}$-SWCNT and $HACA_{FA}$-SWCNT, respectively, or jointly as $HACA_{dye}$-SWCNT (see Chapter 2). Fluorescence activation experiments were performed to determine if $HACA_{dye}$-SWCNTs can be used as activatable probes that are fluorescently activated by hyal when endocytosed inside the cell. $HACA_{dye}$ and $HACA_{dye}$-SWCNTs were varied based on

concentration. The response measure was the fluorescence intensity at the dye-specific emission wavelength. In fluorescence recovery studies, $HACA_{dye}$-SWCNTs with and without hyal were compared. The response measure is the ratio of fluorescence intensity with hyal over the fluorescence intensity without hyal (F_{Hyal}/F_0). Then, $HACA_{dye}$-SWCNT cell uptake studies were measured by fluorescence and Raman intensity, separately. SWCNT cellular uptake was measured in cells with low and high expression of CD44 receptors as well in cells where CD44 receptors were inhibited by excess HA to examine if CD44 receptors play a role. The response measure is the fluorescence activated cell sorting (FACS) acquired mean fluorescence intensity and a normalized Raman G-band area under the curve (AUC).

1. Purification of HACA-SWCNTs

For cellular studies, HACA-SWCNTs were divided into 500 μL aliquots and added into disposable PD-10 desalting column (GE Healthcare, Piscataway, NJ) to remove any possible SWCNT agglomerates in solution. SWCNT collection through the column was collected after ~3.5 mL, where a visible dark band of SWCNT solution was seen. Immediately before cell studies, samples in Eppendorf tubes were exposed to UV irradiation for ~ 20 minutes.

2. Cellular Studies

Two murine cells lines with varying CD44 expression levels were compared: SCC7 (squamous cell carcinoma) and 3T3 (fibroblast) cells lines. Cell viability assays and uptake studies were performed on cells plated for over 24 hours after reaching 60-80% confluency and then incubated with a specified concentration of HACA-SWCNT in serum free RPMI media.

3. Cytotoxicity Assay

A modified lactate dehydrogenase (mLDH) assay was performed on cells treated with different concentrations of HACA-SWCNTs from 100-12.5 ug/mL. The control group was untreated cells. The mLDH cytotoxicity assay was performed using a commercial kit – CytoTox 96 Non-Radioactive Cytotoxicity Assay (Promega, Madison, WI) with the adjusted procedure reported by Ali-Boucetta, et al. to eliminate the interaction between the enzymatic reaction required for LDH detection and SWCNTs.[44] The activity of intracellular LDH was correlated with the concentration of live cells.

4. Fluorescence quenching/recovery of dye-labeled HACA coated SWCNTs

All fluorescence measurements were collected on a F-7000 Fluorescence Spectrophotometer (Hitachi, Tokyo, Japan) at scan speed of 240 nm/min, with the PMT voltage set at 950 V. Fluorescence intensity measurements were collected for $HACA_{FA}$, and $HACA_{Cy5.5}$ before and after SWCNT wrapping over a $HACA_{dye}$ molar concentration range of 3.33–213 nM. $HACA_{FA}$ and $HACA_{Cy5.5}$ was measured at their respective excitation/emission wavelengths: 490/525 nm and 675/695 nm. The value recorded was the emission fluorescence value (F) over the initial emission fluorescence (F_0) value at 3.3 nM as F/F_0. Statistical significance was calculated between the two groups (before and after coating) at each HACA concentration. Furthermore, fluorescence intensity recovery was measured by fluorescence spectroscopy on 213 nM $HACA_{dye}$-SWCNT (concentration based on the content of $HACA_{dye}$) before and after the addition of hyal. A high activity of the enzyme (400 units/mL) was added to the solution, and fluorescence measurements were taken at various time points, from 0 to 1 hour, to account for enzyme kinetics. The fluorescence fold change (F_{Hyal}/F_0) before and after addition of the hyal enzyme was calculated. Next, the Maestro all-optical imaging system (Caliper Life Sciences,

Hopkinton, MA) was used to image fluorescence recovery at broader hyal enzyme concentrations (0-400 units/mL) at different time points in clear 96-well plate. Proper hyal activity conditions were maintained for fluorescence recovery studies – 4.5 pH PBS.

5. CD44 Labeling and Fluorescence Activated Cell Sorting (FACS) for CD44 Expression

FACS using an Accuir C6 flow cytometer (BD, Ann Arbor, MI) was used to first determine CD44 expression differences between SCC7 and the negative control 3T3 cells. CD44 labeling for FACS analysis was performed following the manufacturer's instructions. Specifically, rat anti-mouse CD44 primary antibody diluent (1:50) was applied to both cell lines with an incubation in 2-8 °C for 30 min. Excess antibody was washed twice with the company supplied Flow Cytometry Staining Buffer and a fluorochrome labeled anti-rat IgG secondary antibody solution (1:50) was applied. The mixture was incubated at 2 - 8 °C for 30 min. Once again, the cell suspension was washed with Staining Buffer, filtered through a cell strainer and injected into FACS. As controls for each cell line, the cells were only labeled with the secondary antibody to account for any signal due to non-specific fluorescence. Higher mean fluorescence intensities from FACS correlate to a higher CD44 receptor expression on that cell type. FACS data was analyzed using FlowJo version 7.6.5 for at least 5,000 cells. Mean fluorescence intensity, without gating, was measured and a significant difference was determined as $p<0.05$.

6. CD44 receptor cell targeting and uptake of $HACA_{FA}$-SWCNTs

FACS, confocal microscopy and Raman microscopy were used to determine and measure cell uptake of HACA-SWCNTs. SCC7 and 3T3 cells were plated for over 24 hours and after reaching 60-80% confluency were incubated with 50 ug/mL of $HACA_{FA}$-SWCNT in serum free RPMI media.

a. Fluorescence activated cell sorting for uptake of $HACA_{FA}$-SWCNTs

FACS using an Accuir C6 flow cytometer (BD) was used to measure intracellular FA fluorescence from SCC7 and 3T3 cell lines, after cells were treated with 50 ug/mL $HACA_{FA}$-SWCNTs for 0, 30, 90 and 180 minutes. The SCC7 cell line serves as the CD44 positive cell group while 3T3 cells serve as the negative control for CD44 receptor uptake. After rinsing away excess SWCNTs, intracellular FA fluorescence intensity was measured. FACS data was analyzed using FlowJo version 7.6.5 for at least 5,000 cells. Mean fluorescence intensity, without gating, was measured and a significant difference was determined by $p<0.05$.

b. Fluorescence Confocal Microscopy of $HACA_{FA}$-SWCNTs uptake

In addition to FACS, $HACA_{FA}$-SWCNT uptake in SCC7 and 3T3 cells can be visualized using confocal microscopy. SCC7 and 3T3 cells were plated on LabTek II coverglass (Nalge Nunc International, Rochester, NY) for at least 24 hours at a density of 5×10^4 cells/mL and then incubated with $HACA_{FA}$-SWCNTs for 30 and 180 min. Additionally, CD44 receptors on SCC7 cells were blocked by excess concentrations (>5mg/mL) of high molecular weight HA during treatment with 50 μg/mL of $HACA_{FA}$-SWCNTs for 180 min. In this case, the high concentration of HA competitively binds onto the CD44 receptors and reduces the interaction between $HACA_{FA}$-SWCNTs and receptors. After incubation, the cells were washed with PBS three times and examined by an inverted Zeiss LSM 700 confocal microscope (Carl Zeiss MicroImaging, Ettlingen, Germany). Confocal imaging was carried out in 37 °C in 5% CO_2 and images were acquired using the same exposure time with the Zeiss Zen 2009 image software. Using Image J software (NIH, Bethesda, MD), the confocal images were analyzed by measuring fluorescence intensity across cell profiles.

c. Raman microspectroscopy

The robust G-band was monitored to detect the intrinsic optical signal of SWCNTs in the cell uptake studies by a confocal Raman microscope (Senterra, Bruker Optics, Billerica, MA) at 9-18 cm^{-1} resolution. The Raman microscope is equipped with a 40X/0.95 NA objective, 50 μm pinhole, 785 nm laser (35 mW at sample, 90-3200 cm^{-1} spectral range), 532 nm laser (14 mW, 40-4500 cm^{-1}) and a transmission/fluorescence microscope system. The G-band is also dependent on SWCNT concentration and can also serve as a relative measure of the amount of SWCNTs in the recorded cellular location (Chapter 2).

SCC7 and 3T3 cells were plated in 35 mm glass bottom petri dishes (MatTek, Ashland, MA) and incubated with $HACA_{FA}$-SWCNTs after reaching 50% confluency. The cells were treated with 50 μg/mL of $HACA_{FA}$-SWCNT in serum-free media for 3 hours, washed with HEPES buffer, and then fixed using a formalin solution, Z-fix (Anatech, Battle Creek, MI). To gain an understanding of the SWCNT location, cell structures such as actin and nuclei were stained with rhodamine-phalloidin (Invitrogen) and DAPI (Vectashield Mounting Media with DAPI, Vector Labs, Burlingame, CA), respectively. Next, Raman spectra were collected at various points within (nucleus, perinuclear region, cytoplasm) and outside of the fixed SCC7 and 3T3 cells using the Raman microscope 785 nm laser focused to a 2 μm diameter spot. Raman scattering was collected from about a 2x2x7 μm focal volume for 10 s per spot. The characteristic Raman CNT G-band was used to identify SWCNTs. The G-band was integrated, or the intensity was collected, in the 1550-1610 cm^{-1} wavenumber range for at least three spots per location and normalized to the background (non-cell area) AUC. Data was collected and analyzed by Opus Spectroscopy Software (Ettlingen, Germany). In this way, the relative

SWCNT uptake among the different locations in the cells was identified. Additionally, pseudo-Raman signal contrast, phase contrast, FA fluorescence, actin and nuclei staining images were overlaid by ImageJ.

Furthermore, to determine if uptake of SWCNTs was indeed intracellular and not due to attachment to the cell membrane or pinned underneath the cell, z-profile Raman signals through suspended SCC7 cells were collected. The plated cells were treated with excess 100 μg/mL of HACA-SWCNT for 3 h, trypsinized, and fixed in suspension with 4% paraformaldehyde. The fixed cells were then drop-cast onto a quartz slide of 1 mm thickness with a 0.16 mm quartz slide placed on top. Raman mapping with the 532 nm laser was performed first to identify large G-band signals at about 2x2x5 μm focal volumes, and then z-focusing was performed at those locations. Coarse z-focusing was performed to identify the upper and lower dimensions of the cell. Finally, Raman spectra using the 532 nm laser were collected along z-step sizes of approximately 1-3 μm (to collect about 10 z-steps across the approximate 20 μm cell depth) for 10 s per step. A z-profile of the G-band and a representative intracellular Raman CH_2 band was created using Origin (OriginLab, Northampton, MA). The stretching vibrations of CH-groups of all cell molecules are found at 2862-2912 cm^{-1}. The CH band was integrated at 2800-3100 cm^{-1} and represented the cell interior. Water and slide contributions were subtracted from spectra before analysis.

6. Statistical Analysis

At least three different rounds of $HACA_{dye}$-SWCNT dispersions were prepared and fluorescence readings were performed in triplicate. Student's t-test was used to compare fluorescence quenching capabilities between $HACA_{dye}$ and $HACA_{dye}$-SWCNTs and fluorescence recovery data of $HACA_{dye}$-SWCNTs with and without hyal. Cytotoxicity results were run in pentaplicate

and one-way ANOVA was used to analyze statistical significance. FACS data was analyzed based on 5,000 cell events per group and compared by Student's t-test of SCC7 and 3T3 cell lines and one-way ANOVA with Tukey's *post hoc* test among different treatment groups in each cell group. Raman G-band AUC was compared using Student's t-test between SCC7 and 3T3 cell lines and one-way ANOVA with Tukey's *post hoc* test among various locations in the cell for each SCC7 and 3T3 cell group. Z-profile between CH_2 and G band Raman signal AUCs was correlated by Pearson's product-moment correlation.

D. Results

The in vitro activity of HACA-SWCNTs was examined in this study by: 1) cell viability after treatment with HACA-SWCNTs, 2) CD44 targeting of HACA-SWCNTs, 3) cell uptake of HACA-SWCNTs in cells with high and low expression of CD44. Cell uptake of SWCNTs was detected indirectly by fluorescence intensity and microscopy, and directly by Raman spectroscopy. Furthermore, a fluorescence activation system of dye-labeled HACA-SWCNTs was developed, where the fluorescence of the dye conjugated on HACA was quenched when coated onto SWCNTs but recovered after intracellular uptake of HACA-SWCNTs. This system provides an understanding of the relationship between HACA and SWCNTs and is therefore a factor of an intact coating.

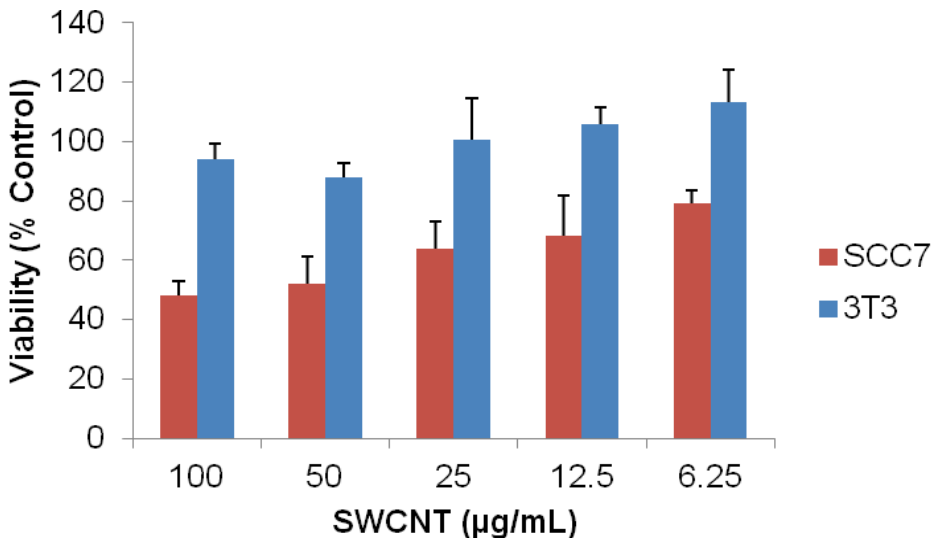

Figure 2: SCC7 and 3T3 Cell Viability after Incubation with Different Concentrations of HACA-SWCNTs.

As seen in Figure 2, squamous cell carcinoma cells (SCC7) at high HACA-SWCNT doses (100 and 50 ug/mL) exhibited low cell viability (48±4.8% and 52.2±9.0% viability, respectively), but no toxicity was observed by HACA-SWCNTs in 3T3 cells (100 ug/mL 98.2±5.2% viability). With lower doses of SWCNTs, cell viability increased.

Before determining the CD44 targeting by HACA-SWCNTs, CD44 expression was measured on two respective cell lines: CD44 receptors were labeled with fluorophore-labeled CD44 antibodies, and the labeled fluorescence intensity was detected for 5,000 cells by FACS. As a relative measure, higher fluorescence intensity signifies higher CD44 receptors. SCC7 cells expressed more CD44 receptors than 3T3 cells by approximately 3.8-fold greater ($p < 0.05$) (Figure 3A,B). Based on these results, SCC7 cells serve as CD44 over-expressing cells, while 3T3 cells serve as a negative control cell line with low CD44 receptor expression for HACA-SWCNT cell uptake studies.

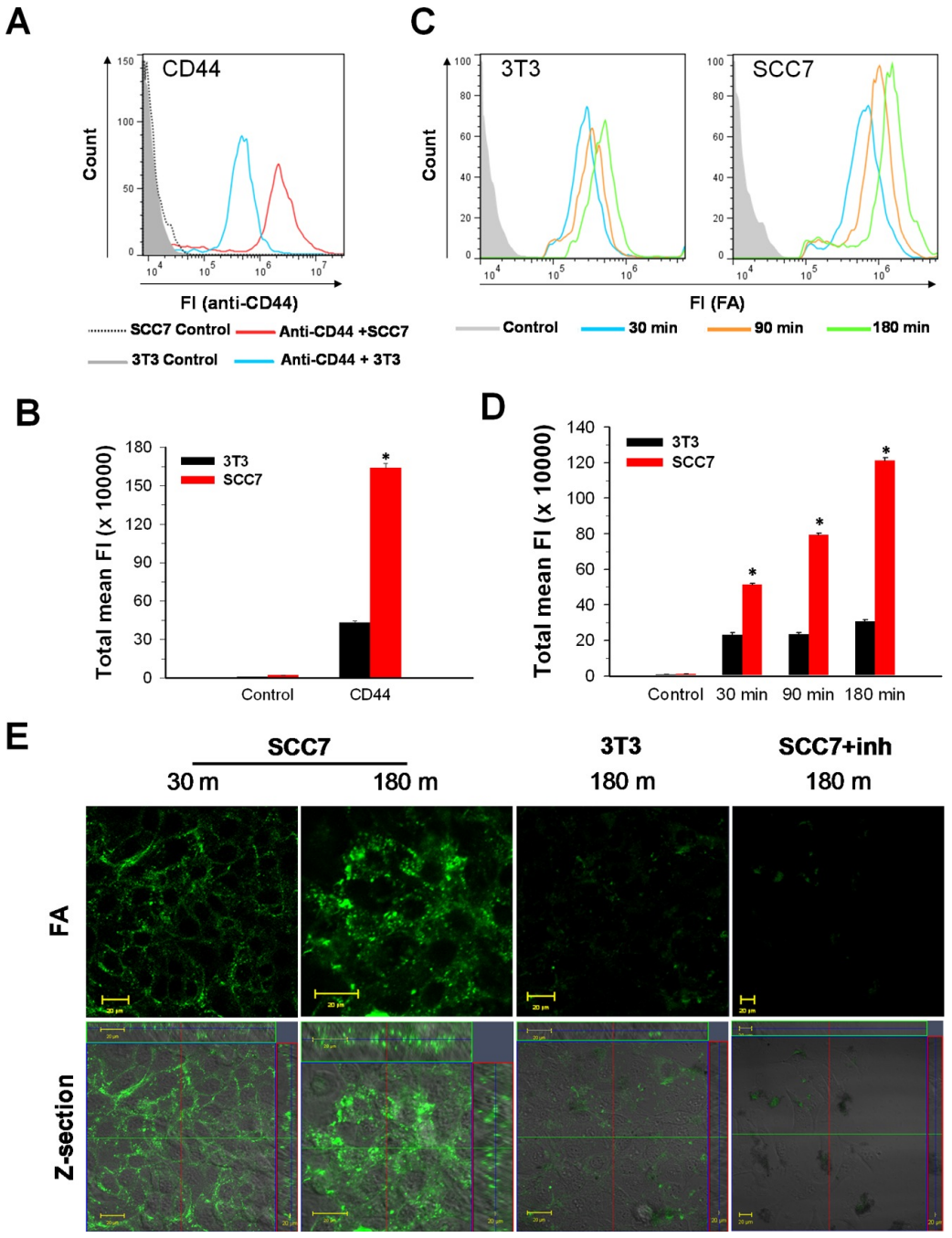

Figure 3: HACA-SWCNT uptake into CD44 overexpressing cells determined by fluorescence. A) CD44: CD44 receptor expression of SCC7 and 3T3 cells analyzed by FACS after CD44 antibody labeling. 3T3 and SCC7: FACS distribution of FA fluorescence in respective cell types after 30 min (blue), 90 min (orange), and 180 min (green) treatment with $HACA_{FA}$–SWCNT. B) Quantitative analysis of FACS total mean fluorescence (S.D., n = 5,000 cells) for data in (A). C) Confocal fluorescence images of SCC7 and 3T3 cells treated with $HACA_{FA}$–SWCNT for 30 and 180 min. SCC7 cells were inhibited by excess HA (SCC7 + inh.) before treatment with $HACA_{FA}$–SWCNT. * $p<0.05$

To study the potential of HACA-SWCNTs as fluorescence activatable probes, $HACA_{dye}$ and $HACA_{dye}$-SWCNT fluorescence intensity fold from 3.3 nM $HACA_{dye}$ was measured over the 3.3 - 213 nM concentration range of $HACA_{dye}$ (Figure 4A). Without SWCNTs, $HACA_{FA}$ and $HACA_{Cy5.5}$ fluorescence increased by 25 ± 0.1 and 38.9 ± 4.0-fold at 213 nM $HACA_{dye}$ from 3.3 nM, respectively. As the concentration of $HACA_{dye}$ increases, the amount of dyes per HA molecules increase, which in turn increases the fluorescence intensity. On the other hand, with SWCNTs, $HACA_{FA}$-SWCNT and $HACA_{Cy5.5}$-SWCNT fluorescence increased 1.4 ± 0.1 and 1.7 ± 0.2-fold at 213 nM $HACA_{dye}$. This low increase in fluorescence as compared to the non-SWCNT samples, indicate that SWCNTs quench the fluorescence of the dyes labeled on HA. Therefore, by comparing the native fluorescence of the $HACA_{dye}$ and the SWCNT quenched fluorescence, it was established that SWCNTs quenched $HACA_{FA}$ and $HACA_{Cy5.5}$ fluorescence at 213 nM by 17.8 ± 0.1 and 23.1 ± 2.7-fold, respectively.

To determine if the fluorescence can be recovered from the $HACA_{dye}$-SWCNT samples, hyaluronidase (hyal, Hyaluronidase from bovine testes, 750-3000 units/mg, Sigma Aldrich) was introduced to the solutions. Fluorescence activation of 213 nM $HACA_{FA}$-SWCNT (based on the concentration of $HACA_{FA}$) after addition of 400 units/mL of hyal lead to 10 ± 2.7-fold fluorescence recovery after 40 minutes (Figure 4B). An increase in the fluorescence recovery time after adding enzyme along with an increase in enzyme activity increased the recovered fluorescence intensity in a linear matter as measured by an optical imaging system (Figure 4C). A lower fluorescence activation effect was seen for $HACA_{Cy5.5}$-SWCNT with a 5-fold fluorescence recovery after 60 minutes (Figure 4D).

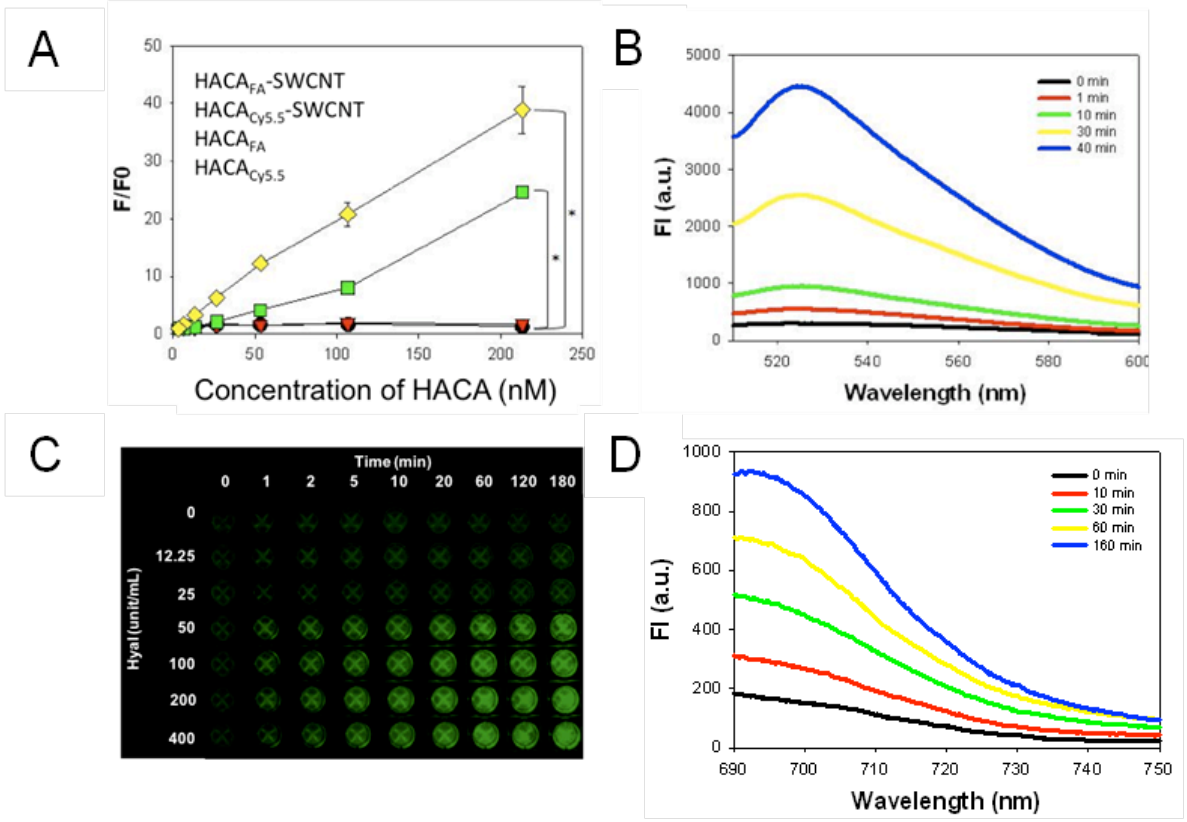

Figure 4: HACA Fluorescence Activation Properties. A) Fluorescence fold increase from 3.3 nM HACA$_{dye}$ as a measure of increasing HACA$_{dye}$ concentration with and without SWCNTs. HACA$_{FA}$ ex/em: 490 nm/525 nm; HA$_{Cy5.5}$ ex/em: 675 nm/695 nm. B) HACA$_{FA}$–SWCNT fluorescence recovery over time after 400 units of hyal was added to 50 µg/mL (in respect to HACA$_{FA}$) of HACA$_{FA}$–SWCNT. C) Fluorescence over time of HACA$_{FA}$-SWCNTs after being activated with different concentrations of hyal. D) HACA$_{Cy5.5}$-SWCNTs fluorescence (ex: 675 nm) after 400 units of hyaluronidase was added to 50 µg/mL of HACA$_{Cy5.5}$-SWCNTs over time.

Selective cancer cell uptake of HACA$_{FA}$-SWCNTs was investigated using the fluorescence activation. Cells treated with HACA$_{FA}$-SWCNTs (50 µg/mL) for 30, 60 and 180 min at 37 °C were measured for intracellular fluorescence (Figure 3C,D). FACS data exemplified a time dependent uptake of HACA$_{FA}$-SWCNTs in SCC7 cells, implying a CD44 receptor-mediated uptake of SWCNTs (Figure 3C,D). On the other hand, minimal fluorescence intensity and no time dependency was seen in 3T3 cell uptake. Interestingly, the cellular uptake ratio of

$HACA_{FA}$-SWCNTs between SCC7 and 3T3 cells was similar to their differences in CD44 receptor expression. Total mean fluorescence was 3.9 ± 1.6-fold greater in SCC7 than 3T3 cells, after 180 min of HA_{FA}-NTs uptake, similar to the 3.8 ± 0.40-fold greater CD44 labeling on SCC7 cells. In confocal microscopy, green fluorescence signals from activated $HACA_{FA}$ were more intense in SCC7 cells than in the 3T3 cells, as seen by confocal microscopy (Figure 3E). When the SCC7 cells were treated with excess HA to inhibit the CD44 receptors, no intracellular fluorescence signals were observed of a high dose of $HACA_{FA}$-SWCNTs. This indicates that CD44 receptors are responsible for the efficient cellular uptake of $HACA_{FA}$-SWCNTs.

As seen in Figure 5, Raman spectra were collected from various points (representative yellow points) of fixed SCC7 (Figure 5A) and 3T3 cells (Figure 5B) after uptake of 50 μg/mL of $HACA_{FA}$-SWCNT for 3 h. The accumulation of SWCNTs in SCC7 cells for the perinuclear region was emphasized by the ratio of G-band intensity in the perinculear region to the cytoplasmic region. SCC7 cells exhibited a 3.7 fold greater ratio than 3T3 cells for the preferential accumulation in the perinucleus. SWCNTs in 3T3 cells showed no preference for accumulation in any region of cell (Figure 5C). Z-profile Raman microscopy was performed across SCC7 cells treated with $HACA_{FA}$-SWCNTs for 3 h. As shown in Figure 5D, G-band AUC was identified inside the SCC7 cell, corresponding with the intracellular CH_2 signal. Repeated recordings at the same positions did not affect SWCNT displacement by the Raman laser.

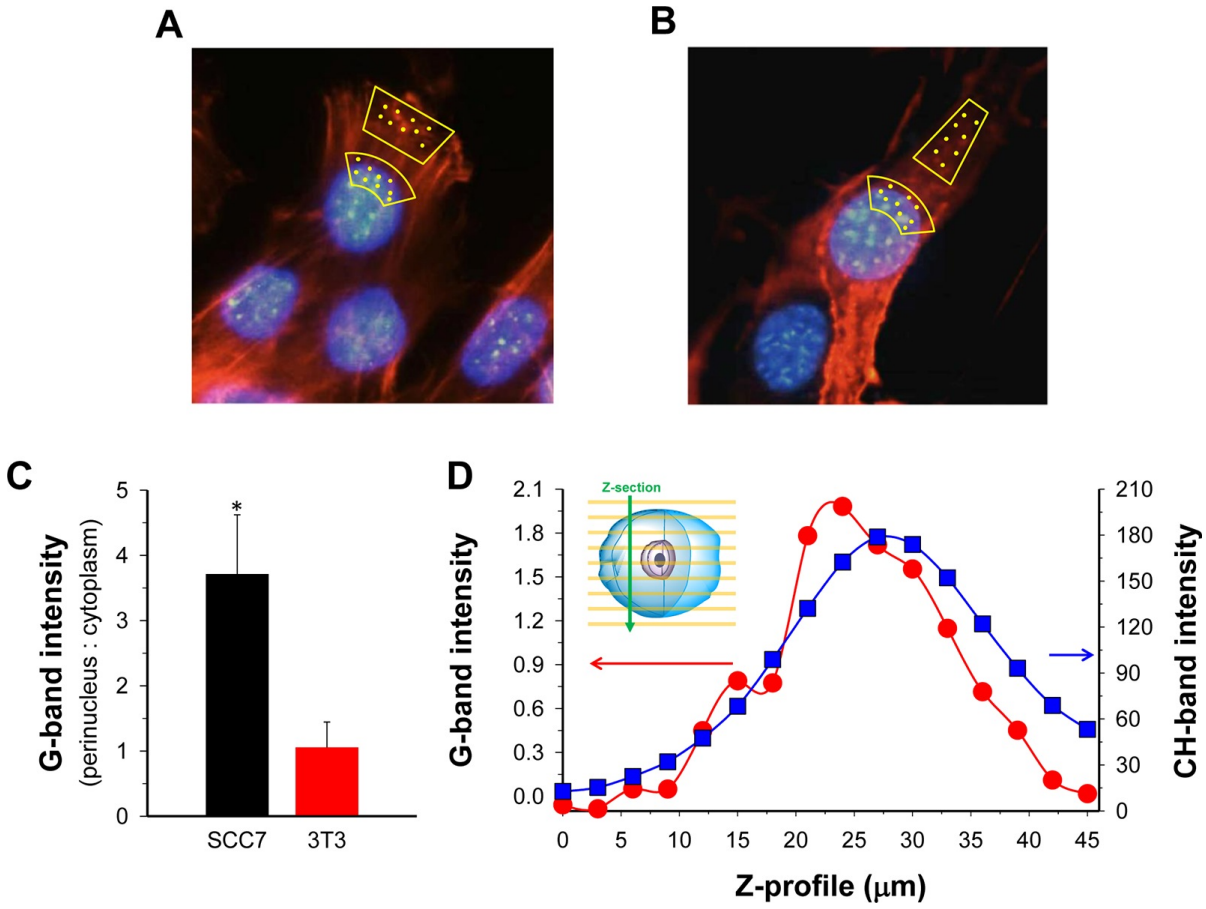

Figure 5: Raman spectroscopy of internalized HACA-SWCNTs. A, B) Representative cell images with actin and nuclei staining displaying where Raman spectra were collected in cell culture for SCC7 cells (A) and 3T3 cells (B). Yellow spots represent locations. C) Integral intensity of SWCNT G-band at 1550−1610 cm^{-1} at locations specified in A and B. Error bars display S.E. for three SCC7 and three 3T3 cells (6−30 points at each location). D) Integral intensity of G-band and stretching vibration band of CH groups across the z-axis of an SCC7 cell suspended between microscope slides. Integration range for CH: 2800−3100 cm^{-1}. Inset describes how z-sectioning was performed with Raman, where the green bar is the laser and the yellow stripes are the z-sections where data was collected.

E. Discussion

Analysis of fluorescence and Raman data confirms higher uptake of SWCNTs in CD44 receptor overexpressing cells (SCC7) than in low CD44 expressing cells (3T3). Based on the results and previous works involving HA nanoparticles,[1, 16] it is hypothesized that CD44-

mediated endocytosis is responsible for the HACA-SWCNT uptake. HACA-SWCNTs target CD44, a common receptor for numerous metastatic malignancies (Table 1). These properties may induce the increased cytotoxicity in SCC7 cells over 3T3 cells after incubation with HACA-SWCNTs (Figure 2). At high doses of HACA-SWCNTs, SCC7 cells see about a 50% cytotoxicity compared to control SCC7 cells. Importantly, 3T3 cells viability was not affected by the HACA-SWCNTs. Therefore, it can be hypothesized that the induced cytotoxicity occurs because of the high uptake of HACA-SWCNTs, encouraged by the multivalency effect of HA on the surface of SWCNTs and its hyaladherin, CD44. This cytotoxic effect should be further studied with other hyaladerin, HARE and LYVE-1, expressing cells to determine if it can be used as a specific cytotoxic drug.

The fluorescence activation system of $HACA_{dye}$-SWCNTs, graphically depicted in Figure 1, was able to provide fluorescence signal amplification to monitor and track SWCNT uptake in cells when in the presence of the intracellular enzyme, hyal. Firstly, fluorescence quenching by SWCNTs was confirmed (Figure 4). As the dye concentration increased 65 times (with 130 FA molecules/HA in $HACA_{FA}$ and 7 Cy5.5 molecules/HA in $HACA_{Cy5.5}$), fluorescence increased by no more than 1.7 fold in the presence of SWCNTs. To rule out a possibility of self-quenching, the $HACA_{dye}$ without SWCNTs was found to increase in a linear manner. A statistically significant difference ($p<0.05$) between $HACA_{dye}$ with and without SWCNTs in fluorescence fold increase from 3.3 nM to 213 nM was detected for both $HACA_{FA}$ and $HACA_{Cy5.5}$. The increase in fluorescence fold was greater for $HACA_{Cy5.5}$ than $HACA_{FA}$ with increasing HACA concentration. There is about 18 times more FA molecules per HA than Cy5.5 molecules per HA molecules in the $HACA_{dye}$ system, but the quantum yield of Cy5.5 is over 13 times higher than FA. These factors, like the degree of substitution, quantum yield and possibly self-quenching,

could affect the differences in fluorescence emission between $HACA_{Cy5.5}$ and $HACA_{FA}$. The role of the two dyes is for specific biological activity and not to compare between each other. FA is a fluorescent dye with emission in the visible light spectrum (525 nm). It is commonly used for in vitro biological assays and most microscopes include this filter. Therefore, all in vitro experiments in this study utilized $HACA_{FA}$. But a dye like Cy5.5 (emission 695 nm) that emits in the near-infrared region is required for in vivo optical imaging in order to pass through the biological transparency window without absorbance by tissue and blood. Therefore $HACA_{Cy5.5}$ will be utilized for in vivo experiments.

It was hypothesized that the fluorescence quenching could be recovered by degrading the HA_{dye} backbone, which would reduce interactions of the dye molecule and the quenching SWCNT. Hyaluronidases (hyal), such as Hyal-1, Hyal-2, and PH-20, can specifically degrade HA.[10] Therefore, hyal was added to the quenched $HACA_{dye}$-SWCNT system. Fluorescence recovery occurred in a time and enzyme activity dependent manner, indicating that the reaction is fully dependent on the enzymatic reaction (Figure 4 B,C,D). In vivo, hyal activity is estimated to be on the mIU scale of activity units, much lower than these in vitro studies.[45] Fluorescence recovery for 213 nM $HACA_{FA}$ system with addition of 400 I.U. hyal, lead to a 10 fold fluorescence recovery (Figure 4B) but the quenching ratio at this concentration was over 20 fold (Figure 4A). Full recovery of the fluorescence was not measured, because the experiments were performed in a closed system (cuvette) where there are still highly probable interactions between the SWCNT and dye. It is hypothesized that in a cellular model, the fluorophore could exit the endosome more freely than SWCNTs, which are shown to remain in endosomes for days,[46] and reduce those quenching interactions. Further catabolism studies of hyal with HA are required to understand the enzyme activity and fragmentation of HACA and HACA-SWCNTs. Although the

dynamics of the catabolic cascade of physiological HA are still not quite understood,[10] systematic chemical characterization methods, such as gel permeation chromatography, can be used to measure HACA fragments after enzyme degradation in a closed system.

For cellular studies, it is important to determine where the hyal activation will take place. Two hyals, Hyal-2 and PH20, are glycosylphosphatidylinositol-anchored proteins on the plasma membrane. PH20 is specifically located on sperm cells. But Hyal-2 is more prevalently and ubiquitously found on cells. It initiates cleavage of high molecular weight HA to smaller HA fragments of 50-100 saccharide units.[20] The location of this initial degradation is not fully characterized, and many reports hypothesize that the Hyal-2 degradation occurs in lysosomes[47] or during partial internalization by specialized cell surface compartments.[10] This is further supported by the fact that human Hyal-2 is active in pH 4 with no activity detected at pH 5.[47] Yet, it is the intracellular Hyal-1 that is responsible for systemic HA turnover in most cell types. It is highly acid active with an optimum pH around 3.8 and most active in lysosomes, eventhough the lysosomal pH is about 4.5.[10] It can degrade most sizes of HA[10] and is overexpressed in squamous cell carcinoma (SCC).[48] Therefore, it is hypothesized that the main degradation and subsequent fluorescence activation would occur inside SCC cells by Hyal-1 and possibly Hyal-2. Therefore, $HACA_{dye}$-SWCNTs provide fluorescence quenching and hyal activation properties to serve as sensors for SWCNT cellular uptake.

Using the $HACA_{dye}$-SWCNT activatable probe, fluorescence intensity inside the cell is correlated with $HACA_{dye}$-SWCNT uptake. The significantly higher mean fluorescence intensity in SCC7 cells over 3T3 cells measured by FACS, even at short treatment times, implies that SCC7 cells preferentially take up HACA-SWCNTs. In addition, when HACA-SWCNTs were treated to the cells over longer periods of time (30 min to 1.5 hrs), a steady increase in

fluorescence was detected in SCC7 cells, while no differences were detected in 3T3 cells (Figure 3D). The treatment time dependent uptake of $HACA_{FA}$-SWCNTs into CD44 positive cells signifies that HACA-SWCNTs are endocytosed in a controlled manner, probably by a CD44 receptor dependent manner. Further microscopy studies demonstrate that when CD44 receptors are inhibited by excess HA, no fluorescence is visualized inside cells (Figure 3E). Based on these fluorescence studies, it can be concluded that HACAFA-SWCNTs are taken up into cells by dependent on the CD44 receptor. Eventhough the fluorescence activation is dependent on the interaction between HACA and SWCNTs, it is possible that the $HACA_{FA}$ is degraded extracellularly, leaving SWCNTs either outside the cell or on the cell surface while the dye is taken up. Therefore, it is important to directly detect SWCNT uptake into cells.

Raman microscopy can directly detect the signature G-band for SWCNTs within cells. The intensity and area under the curve (AUC) of the G-band is directly related to the amount of SWCNTs. When a higher AUC or intensity of the G-band is measured within the cell, a higher SWCNT uptake can be confirmed. Based on Raman imaging of the G-band, SCC7 cells showed over a three time higher accumulation of SWCNTs in the perinuclear region than the cytoplasmic region, where 3T3 cells showed no preferential accumulation (Figure 5C). This type of subcellular accumulation implies that an active form of uptake was taken, such as: CD44 receptor mediated endocytosis, motor protein-driven delivery along microtubules through the cytoplasm, and then escape from endosomes closer to the cell nuclear region.[49] To further confirm that SWCNT uptake in SCC7 cells passed through the cell membrane, Raman z-profiles of SCC7 cells were analyzed. It was found that the G-band AUC z-profile within SCC7 cells correlates with the CH-band z-profile, the intracellular location marker. Taken together, it is

concluded that HACA-SWCNTs are taken up into CD44 overexpressing cells by CD44 receptor mediated endocytosis.

SWCNTs, just as many nanoparticles, can be taken up into cells based on numerous factors, such as their size, shape and surface properties.[50] Based on the fluorescence and Raman data in this study, it was confirmed that HACA-SWCNTs are endocytosed in a CD44 receptor mediated way. Based on previous HA-based systems discussed in the Introduction, HA on the surface of SWCNTs prefer to bind to cells with a high CD44 receptor density because of the increased probability of interacting with the CD44 receptor as well as the increased avidity once bound to multiple binding sites. Among the HA receptors discussed in the Introduction, CD44 is the only ubiquitous HA receptor that could mediate endocytosis in fibroblasts and squamous cell carcinoma (SCC) cells. Cells with normal CD44 expression and low expression, such as 3T3 cells, have lower binding potential to the HA sugars confined to the surface area of the nanotubes. In this way, HACA-SWCNTs will preferentially bind to metastatic cancer cells because of the overexpression of CD44 over healthy cells with normal expression of CD44. Once HACA-SWCNTs preferentially bind to metastatic cancer cells, the uptake of the HA molecule by CD44 receptor mediated endocytosis will aid in the uptake of the entire nanoplatform, as reported for HA liposomes. In conclusion, reasonable cell viability and cancer cell specific uptake of HACA-SWCNTs was confirmed in this study, building the potential of HACA-SWCNTs for in vivo tumor targeted imaging and/or therapy.

F. References

1. K. Y. Choi, G. Saravanakumar, J. H. Park and K. Park, *Colloids Surf., B*, 2012, **99**, 82-94.

2. A. J. Day and G. D. Prestwich, *J. Biol. Chem.*, 2002, **277**, 4585-4588.

3. B. P. Toole, *Nat. Rev. Cancer*, 2004, **4**, 528-539.

4. B. Zhou, J. A. Weigel, L. Fauss and P. H. Weigel, *J. Biol. Chem.*, 2000, **275**, 37733-37741.

5. E. N. Harris, S. V. Kyosseva, J. A. Weigel and P. H. Weigel, *J. Biol. Chem.*, 2007, **282**, 2785-2797.

6. E. N. Harris, J. A. Weigel and P. H. Weigel, *J. Biol. Chem.*, 2004, **279**, 36201-36209.

7. E. A. Turley, P. W. Noble and L. Y. W. Bourguignon, *J. Biol. Chem.*, 2002, **277**, 4589-4592.

8. R. Peach, D. Hollenbaugh, I. Stamenkovic and A. Aruffo, *J. Cell Biol.*, 1993, **122**, 257-264.

9. J. Lesley, V. C. Hascall, M. Tammi and R. Hyman, *J. Biol. Chem.*, 2000, **275**, 26967-26975.

10. R. Stern, *Glycobiology*, 2003, **13**, 105R-115R.

11. Q. Hua, C. B. Knudson and W. Knudson, *J. Cell Sci.*, 1993, **106**, 365-375.

12. D. J. Aguiar, W. Knudson and C. B. Knudson, *Exp. Cell Res.*, 1999, **252**, 292-302.

13. M. Culty, H. A. Nguyen and C. B. Underhill, *J. Cell Biol.*, 1992, **116**, 1055-1062.

14. H. Jiang, R. S. Peterson, W. Wang, E. Bartnik, C. B. Knudson and W. Knudson, *J. Biol. Chem.*, 2002, **277**, 10531-10538.

15. S. P. Thankamony and W. Knudson, *J. Biol. Chem.*, 2006, **281**, 34601-34609.

16. K. Y. Choi, H. Chung, K. H. Min, H. Y. Yoon, K. Kim, J. H. Park, I. C. Kwon and S. Y. Jeong, *Biomaterials*, 2010, **31**, 106-114.

17. V. M. Platt and F. C. Szoka, *Mol. Pharmaceutics*, 2008, **5**, 474-486.

18. L. Collis, C. Hall, L. Lange, M. Ziebell, R. Prestwich and E. A. Turley, *FEBS Lett.*, 1998, **440**, 444-449.

19. H. J. Greyner, T. Wiraszka, L.-S. Zhang, W. M. Petroll and M. E. Mummert, *Matrix Biol.*, 2010, **29**, 503-510.

20. R. Stern, *Sem. Cancer Bio.*, 2008, **18**, 275-280.

21. D. Naor, R. V. Sionov and D. Ish-Shalom, *Adv. Cancer Res.*, 1997, **71**, 241-319.

22. W. Knudson, *Frontiers in bioscience : a journal and virtual library*, 1998, **3**, d604-615.

23. M. Culty, M. Shizari, E. W. Thompson and C. B. Underhill, *J. Cell. Physiol.*, 1994, **160**, 275-286.

24. T. Reya, S. J. Morrison, M. F. Clarke and I. L. Weissman, *Nature*, 2001, **414**, 105-111.

25. M. Al-Hajj, M. S. Wicha, A. Benito-Hernandez, S. J. Morrison and M. F. Clarke, *Proc. Natl. Acad. Sci. U. S. A.*, 2003, **100**, 3983-3988.

26. D. M. Simeone, *Clin. Cancer Res.*, 2008, **14**, 5646-5648.

27. L. Du, H. Wang, L. He, J. Zhang, B. Ni, X. Wang, H. Jin, N. Cahuzac, M. Mehrpour, Y. Lu and Q. Chen, *Clin. Cancer Res.*, 2008, **14**, 6751-6760.

28. P. K. Borjesson, E. J. Postema, J. C. Roos, D. R. Colnot, H. A. Marres, M. H. van Schie, G. Stehle, R. de Bree, G. B. Snow, W. J. Oyen and G. A. van Dongen, *Clin. Cancer Res.*, 2003, **9**, 3961S-3972S.

29. U. Rupp, E. Schoendorf-Holland, M. Eichbaum, F. Schuetz, I. Lauschner, P. Schmidt, A. Staab, G. Hanft, J. Huober, H. P. Sinn, C. Sohn and A. Schneeweiss, *Anti-cancer drugs*, 2007, **18**, 477-485.

30. B. M. Tijink, J. Buter, R. de Bree, G. Giaccone, M. S. Lang, A. Staab, C. R. Leemans and G. A. M. S. van Dongen, *Clin. Cancer Res.*, 2006, **12**, 6064-6072.

31. D. Coradini, S. Zorzet, R. Rossin, I. Scarlata, C. Pellizzaro, C. Turrin, M. Bello, S. Cantoni, A. Speranza, G. Sava, U. Mazzi and A. Perbellini, *Clin. Cancer Res.*, 2004, **10**, 4822-4830.

32. Y. H. Yun, D. J. Goetz, P. Yellen and W. Chen, *Biomaterials*, 2004, **25**, 147-157.

33. S. Lee, K. Park, K. Kim, K. Choi and I. C. Kwon, *Chem. Commun.*, 2008, 4250-4260.

34. S. Lee, J. Xie and X. Chen, *Curr. Top. Med. Chem.*, 2010, **10**, 1135-1144.

35. M. Swierczewska, S. Lee and X. Chen, *Phys. Chem. Chem. Phys.*, 2011, **13**, 9929-9941.

36. X. Huang, M. Swierczewska, K. Y. Choi, L. Zhu, A. Bhirde, J. Park, K. Kim, J. Xie, G. Niu and K. C. Lee, *Angew. Chem., Int. Ed.*, 2012, **51**, 1625-1630.

37. L. Zhu, J. Xie, M. Swierczewska, F. Zhang, X. Lin, X. Fang, G. Niu, S. Lee and X. Chen, *Bioconjugate Chem.*, 2011, **22**, 1001-1005.

38. L. Zhu, J. Xie, M. Swierczewska, F. Zhang, Q. Quan, Y. Ma, X. Fang, K. Kim, S. Lee and X. Chen, *Theranostics*, 2011, **1**, 18.

39. M. S. Dresselhaus, G. Dresselhaus, R. Saito and A. Jorio, *Phys. Rep.*, 2005, **409**, 47-99.

40. J. H. Choi, F. T. Nguyen, P. W. Barone, D. A. Heller, A. E. Moll, D. Patel, S. A. Boppart and M. S. Strano, *Nano Lett.*, 2007, **7**, 861-867.

41. Z. Liu, C. Davis, W. Cai, L. He, X. Chen and H. Dai, *Proc. Natl. Acad. Sci. U. S. A.*, 2008, **105**, 1410-1415.

42. M. E. Prince, R. Sivanandan, A. Kaczorowski, G. T. Wolf, M. J. Kaplan, P. Dalerba, I. L. Weissman, M. F. Clarke and L. E. Ailles, *Proc. Natl. Acad. Sci. U. S. A.*, 2007, **104**, 973-978.

43. J. M. Wörle-Knirsch, K. Pulskamp and H. F. Krug, *Nano Lett.*, 2006, **6**, 1261-1268.

44. H. Ali-Boucetta, K. T. Al-Jamal and K. Kostarelos, *Methods in molecular biology (Clifton, N.J.)*, 2011, **726**, 299-312.

45. S. Nagaraju, K. S. Girish, Y. Pan, K. A. Easely and K. Kemparaju, *Clin. Lab. Sci.: J. of the Am. Soc. for Med. Tech.*, 2011, **24**, 172-177.

46. A. E. Porter, M. Gass, K. Muller, J. N. Skepper, P. A. Midgley and M. Welland, *Nat. Nanotechnol.*, 2007, **2**, 713-717.

47. G. Lepperdinger, J. Müllegger and G. Kreil, *Matrix Biol.*, 2001, **20**, 509-514.

48. E. J. Franzmann, G. L. Schroeder, W. J. Goodwin, D. T. Weed, P. Fisher and V. B. Lokeshwar, *Int. J. Cancer*, 2003, **106**, 438-445.

49. J. Suh, D. Wirtz and J. Hanes, *Proc. Natl. Acad. Sci. U. S. A.*, 2003, **100**, 3878-3882.

50. A. E. Nel, L. Madler, D. Velegol, T. Xia, E. M. Hoek, P. Somasundaran, F. Klaessig, V. Castranova and M. Thompson, *Nat. Mater.*, 2009, **8**, 543-557.

Chapter 4:

Application of Hyaluronic Acid Wrapped Single-Walled Carbon Nanotubes *In Vivo*

A. Abstract

The aim of this study is to monitor the activity of HACA-SWCNTs in vivo, and the hypothesis is that HACA-SWCNTs target cancer cells in vivo based on the enhanced permeability and retention (EPR) effect of tumors to nanoparticles and the exhibited CD44 receptor targeting. The accumulation in tumors and other organs will be measured over time after intravenous injection of HACA-SWCNTs to a squamous cell carcinoma (SCC) mice model. A multimodal imaging technique will be utilized to track all components of the nanoplatform in vivo with positron emission tomography, photoacoustic imaging and fluorescence imaging. Based on PET and PA imaging, HACA-SWCNTs exhibited tumor targeting within one hour after injection, most likely due to a passive EPR effect. Fluorescence emission was visualized at the tumor site only 24 hours post-injection by in vivo NIRF imaging. Based on the fluorescence activatable probe developed previously (Chapter 3), the activated fluorescence intensity implies that the HACA-SWCNTs were endocytosed into tumor cells through CD44 mediated endocytosis. Therefore, by utilizing different imaging modalities to track the HACA-SWCNT in vivo behavior, it was shown that HACA-SWCNT target the tumor region by passive means and enter tumor cells by actively targeting the CD44 receptor.

B. Introduction

This study relates to the in vivo tumor targeting capability of HACA-SWCNTs. HACA-SWCNTs are hypothesized to target cancer cells *in vivo* based on the enhanced permeability and retention (EPR) effect of tumor to nanoparticles and the exhibited CD44 receptor targeting (Chapter 3).

The EPR effect is a phenomenon that accounts for the accumulation of macromolecular agents in solid tumors (reviewed in ref [1]). Unlike normal tissues and organs, many solid tumors have hypervasculature with defective vascular architecture, known as leaky vasculature, along with impaired lymphatic drainage. This type of system is used to sustain the rapid growth of the tumor by allowing ample nutrients and oxygen to collect in the area. In addition, the tumor microenvironment generates vascular permeability factors, like bradykinin and nitric oxide, to enhance nourishment collection.[2] The EPR effect is also utilized for delivery of nano-sized imaging and therapeutic agents to solid tumors, as a passive targeting method.[3] For example, nanomedicine in the clinic, such as Doxil® or Abraxane®, utilize the passive targeting method to deliver high doses of anticancer drugs with decreased toxic side effects.[4, 5] Nanocarriers, instead of diffusing through the leaky vasculature, can escape into the tumor tissue from the circulation and accumulate in the tumor site because of the poor drainage. Extravasation is said to occur for particles with sizes at about 400 nm.[6] Although passive targeting is effective in cancer nanomedicine, active targeting can enhance tumor delivery.

In a seminal paper by Liu et al., phospholipid–polyethylene glycol (PL-PEG) coated SWCNTs were studied for their in vivo biodistribution and tumor targeting capability.[7] The PL-PEG-SWCNTs exhibited high stability *in vivo* and were subjected to chemical modification with arginine–glycine–aspartic acid (RGD) peptide to actively target the $\alpha_v\beta_3$ receptor, which is overexpressed during tumor angiogenesis and metastasis. The ligand targeted SWCNTs had an almost four fold increase in tumor accumulation over SWCNTs without targeting ligands.[7] Therefore, active targeting can significantly improve passive targeting to the tumor.

To examine the in vivo targeting ability, a murine squamous cell carcinoma tumor xenograft model was prepared and intravenously injected with HACA-SWCNTs. A multimodal

imaging approach, including positron emission tomography (PET), photoacoustic (PA) imaging and optical fluorescence imaging, was utilized to track specific qualities of HACA-SWCNTs *in vivo* during tumor uptake over time (Figure 1). Multimodal imaging offers a synergistic improvement to diagnostic and tracking ability in a research and increasingly more in a clinical setting. By combining the advantages of each imaging system, unique features of the HACA-SWCNT platform are detected.

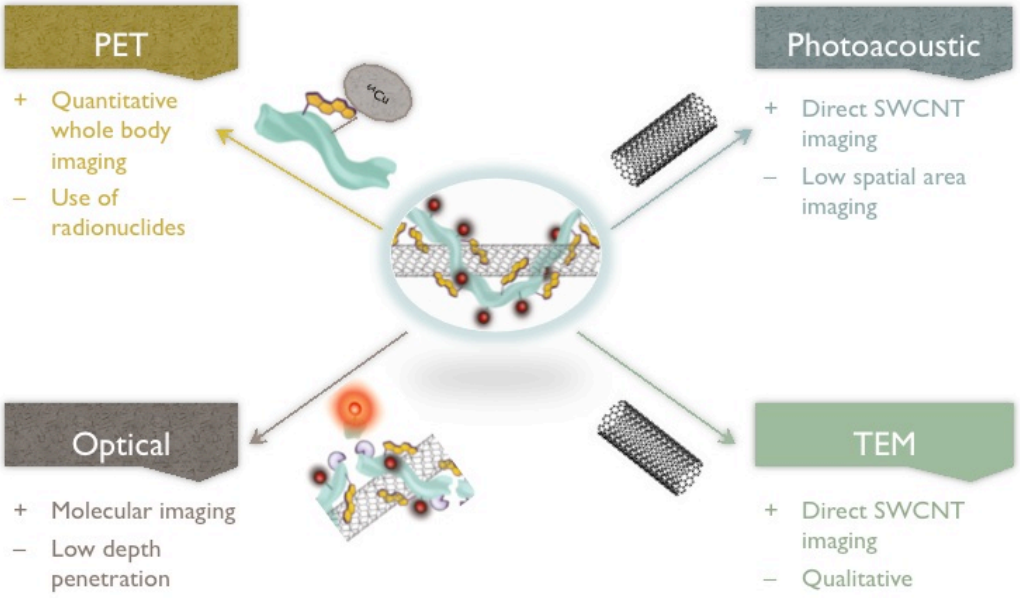

Figure 1: Multimodal imaging approach to track all aspects of the HACA-SWCNT platform. Advantages (+) and disadvantages (-) of the imaging modalities are listed.

PET is commonly utilized for anatomical imaging for quantitative, whole body data. This type of low-resolution imaging is especially useful for biodistribution and tumor targeting efficient studies. Yet this type of imaging requires the labeling of a radionuclide tracer onto a single molecule, and hence only one part of the HACA-SWCNT system. In this study, the carboxyl groups of HACA will be conjugated with a 1,4,7,10-tetraazacyclodecane-1,4,7,10-tetraacetic acid (DOTA) molecule, that is commonly used to complex metals for radiopharmaceuticals or MRI imaging, for chelation of the radionuclide ^{64}Cu into its central ring

structure. Therefore PET evaluation will provide good quantitative biodistribution data, but imaging data only follows HACA-SWCNTs indirectly by detecting the HACA coating only.

PA is needed to directly image SWCNTs in vivo. SWCNTs have a strong optical absorption in the NIR range of 6.2 x 10^6 $M^{-1}cm^{-1}$ (SWCNT 400 nm in length), as compared to most organic molecules; for example, green fluorescent protein has an optical absorption of ~ 2.1 x 10^6 $M^{-1}cm^{-1}$. The high optical absorption in the NIR range can be used to track SWCNTs by PA imaging over tissue and blood.[8] Based on the PA effect, PA contrast agents, like SWCNTs or blood, absorb and convert applied energy from non-ionizing laser pulses into heat.[9, 10] This heat causes thermoelastic expansion, which can be detected by ultrasonic emissions and converted into images by ultrasonic transducers. Although PA tomography is a newly developed technology, it is most commonly used to image and quantify levels of vascularization and oxygen saturation in tumors and other tissues, detecting feature such as tumor angiogenesis or hypoxia.[11, 12] Because the thermoelastic expansion is a result of a specific absorption by the SWCNTs, PA imaging provides high spatial resolution along with deep tissue penetration of SWCNTs above blood. For example, at a 1064 nm wavelength, SWCNTs exhibit a six-fold enhancement in photoacoustic signal over blood.[10] In vivo PA imaging of SWCNTs has also shown similar enhancement in a wide band optical absorption with excitation wavelengths between 690-820 nm.[13, 14] The ideal wavelength for photoacoustic imaging of SWCNTS in vivo is 690 nm, because the photoacoustic signal of SWCNTs and the contrast between SWCNTs and haemoglobin is the highest (Figure 1).[14] Yet, PA imaging is limited in spatial resolution, preventing whole body analysis. In this study, PA will be used to directly image SWCNT accumulation in tumors post-injection of HACA-SWCNTs to correlate SWCNT tumor accumulation with the radiolabeled HACA-SWCNTs as tracked by PET.

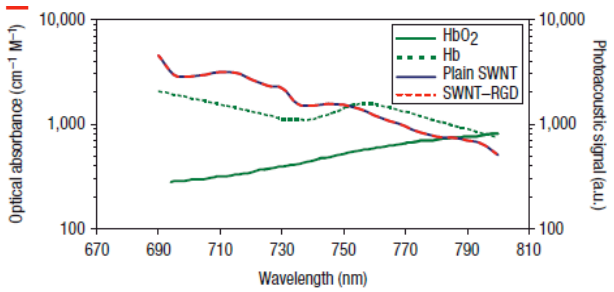

Figure 2: Optical absorbance within the NIR region of SWCNTs and hemoglobin[14]

In Chapter 3, the potential of $HACA_{Cy5.5}$-SWCNTs fluorescence activation was studied. With this type of NIR fluorescence (NIRF) activatable probe system, the low depth penetration of optical imaging can be overcome.[15] Based on cellular studies, it is hypothesized that $HACA_{Cy5.5}$-SWCNT *in vivo* imaging will be possible after the probe accumulates at the tumor site by the EPR effect and is then endocytosed into tumor cells. Fluorescence emission exemplify the unique quenching interaction between $HACA_{Cy5.5}$ and SWCNTs. Therefore optical tracking goes beyond recognizing the location of HACA (PET imaging) or SWCNTs (PA imaging) but instead signals the cellular uptake of the unified $HACA_{Cy5.5}$-SWCNT system. Ever since the first discovery of these in vivo fluorescent activatable probes,[16] it has served as an effective technique to study molecular events in the body when an appropriate delivery technique is used. However, in human clinical studies, NIRF imaging is still limited by its depth penetration and skin artifacts. Therefore, intravital microscopy (IVM) along with advanced endoscopes are utilized to image fluorescent signals for human clinical applications.[17] [18] Another relevant clinical application of fluorescence imaging is in image-guided surgery, where the fluorescence signal can be activated or visualized during surgical resection of tumor tissue. When a molecular activated fluorescent probe is utilized, the surgeon can differentiate the tumor margins during surgery to completely remove small tumor sections that could otherwise be missed and cause remission or metastasis.[19]

SWCNT biodistribution and excretion studies have conflicting data, mainly if SWCNTs are taken up the reticuloendothelial system (RES), such as the spleen, liver and lymph nodes. The RES system is the major defense system in the body, and in most sophisticated therapy and imaging delivery methods, fast RES uptake is avoided to allow circulation time to reach its intended target. PEG is commonly utilized to delay RES uptake. Generally, the injected particles are coated with various plasma proteins, collectively called opsonins, that aid to target antigens to that particle for an immune response, a process called opsonization. The RES, made up of phagocytic cells like Kupffer cells of the liver, target and remove the opsonized particles.[20] In general, nanomaterials tend to be taken up by the RES system.[21, 22] But two early studies involving covalently radiolabeled SWCNTs intravenously injected into non-tumor bearing mouse models exhibited low RES uptake and free excretion.[23, 24] Of note, SWCNT excretion through the urine was reported within 3 hours after injection, and 99% of SWCNTs were excreted from the body in 24 hours post-injection.[23] Yet these studies tracked SWCNTs by the radiolabel, rather than direct SWCNT detection or multiple imaging techniques. In contrast, PEGylated SWCNTs, measured directly by Raman spectroscopy, accumulated in the liver and spleen one hour after intravenous injection and were slowly excreted for 2 months in the feces, most likely through the biliary pathway from the liver.[25] PEGylation decreases the rat of RES uptake, allowing increased blood circulation time for increased tumor uptake as well as slow excretion. Nondegradable substances, like certain gold[26] and mesoporous silica nanoparticles[27], are known to be excreted through the biliary pathway from the liver to the bile duct, intestine and eventually feces.[25]

In this study, HACA-SWCNTs will be studied for their ability to target tumors in a murine xenograft tumor model based on passive and active-targeting strategies. Tracking the

nanoparticles in vivo over time will include each element of the nanoplatform: PET imaging to follow the radiolabeled HACA, NIRF imaging to following the intracellular uptake of $HACA_{Cy5.5}$-SWCNTs, and PA imaging to directly detect SWCNTs in the tumor region. Additional tissue analysis will be performed to gain an understanding of the tumor targeting abilities and biodistribution of HACA-SWCNTs.

C. Research Design and Methods

HACA-SWCNT accumulation in tumors and other organs will be measured over time after intravenous injection of HACA-SWCNTs to tumor bearing mice. PET, PA, and optical imaging will be used to track HACA-SWCNTs *in vivo*. The response measures for PET imaging will be percent injected dose per gram of tissue (% ID/g) in the tumor ROI as calculated by decay-corrected radioactivity. The response measure for PA imaging will be the total tumor PA signal normalized to the laser energy applied. For NIRF imaging, *in vivo* and *ex vivo* fluorescence intensity units of the tumor will be the response measure. Data will be analyzed by plotting tumor uptake signals (%ID/g, PA arbitrary units, and fluorescence arbitrary units) as a factor of post-injection time. The final outcome of this study will provide a picture of the tumor-targeting capability and in vivo biodistribution of HACA-SWCNTs. Based on the different imaging techniques, different interpretations of HACA-SWCNTs can be made. For example, correlation of tumor accumulation as measured by PET of the radiolabeled HACA and PA signal of the SWCNT implies that HACA-SWCNTs remain properly coated *in vivo*. The tissue distribution of $HACA_{Cy5.5}$-SWCNTs will be quantified by measuring NIR fluorescence intensity of the ROI in the images and of the excised organs.

1. Animal Studies

All animal studies were conducted in accordance with the principles and procedures outlined in the NRC Guide for the Care and Use of Laboratory Animals and with approval by the Institutional Animal Care and Use Committee of the NIH Clinical Center. Tumor-bearing mice were prepared by subcutaneously injecting a suspension of 1×10^6 SCC7 cells in physiological saline (100 μL) into the front flank or hind limb of athymic nude mice (seven weeks old, 20 – 25 g). When the tumor sizes reached 100 mm^3 (approximately fourteen days after inoculation) the mice were intravenously (tail-vein) injected with HACA-SWCNTs, labeled with either Cy5.5 or ^{64}Cu, based on the imaging technique. For all imaging procedures, mice were anesthetized with 3% to 4% isoflurane using a nose-cone manifold and restrained on the imaging stage. For PA and optical imaging, the same mice with two different tumor locations were utilized.

2. Radiolabeling of HACA coating

To radiolabel the HACA for *in vivo* PET biodistribution studies of HACA-coated SWCNTs, DOTA was conjugated onto HACA and chelated with a radionuclide, ^{64}Cu. DOTA-amine (Macrocyclics, Dallas, TX) was conjugated onto HACA ($HACA_{DOTA}$) through amide formation in the presence of EDC and HOBt. SWCNTs were dispersed with $HACA_{DOTA}$ as in Chapter 2, forming $HACA_{DOTA}$-SWCNTs in distilled water. After the SWCNT coating, DOTA was chelated with the PET tracer ^{64}Cu. $^{64}CuCl_2$ was converted to $Cu(OAc)_2$ by addition of 0.5 mL of 0.4 M ammonium acetate (NH4Ac, pH 5.5) to 20 μL $Cu^{64}Cl_2$. $Cu(OAc)_2$ (1 mCi) was then added into the $HACA_{DOTA}$-SWCNT solution with agitation for one hour. To remove excess Cu, the conjugated SWCNTs will be purified by PD-10 column (GE Healthcare). The labeling efficiency

will be calculated based on radioactivity dosimeter readings before and after purification. The radio-labeling yield was 70 to 80%.

3. PET Imaging

PET scans will be performed with a microPET R4 rodent scanner (Siemens Medical Solutions, Malvern, PA). Intravenous injection of 100 μL with about 100 - 200 μCi ^{64}Cu-labeled HACA-SWCNT were performed on SCC7 tumor-bearing mice. Based on previous HACA data,[28] PET scans were collected starting at 1 hour post-injection and studied at time points up to 48 h post-injection. For each scan, 3-dimensional ROIs were drawn over the tumor and organs on decay-corrected, whole-body, coronal images. Then, the average radioactivity concentration was obtained from the mean pixel values within the ROI volume and converted to counts per milliliter per minute by using a predetermined conversion factor, previously described.[29, 30] Given a tissue density of 1 g/mL, the counts per milliliter per minute were converted to counts per gram per minute. The values were then divided by the injected radioactivity dose of HACA-SWCNTs to obtain the ROI-derived percentage injected dose per gram of tissue (% ID/g). After sacrificing the mice, PET scans were acquired on excised organs and tumor.

4. Photoacoustic Imaging

Athymic nude mice with tumors in the front flank and hind limb were intravenously (tail-vein) injected with $HACA_{Cy5.5}$-SWCNTs at a dose of 5 mg/kg. Non-invasive ultrasound and PA images were collected of tumors at pre-injection and at 2 h and 20 h post-injection to monitor SWCNT accumulation at the hind limb tumor site. Based on previous reports using SWCNTs as PA contrast agents, the ideal absorbance, where there is a distinct difference between blood absorbance and SWCNTs, was found to be between 600-800 nm.[14] Using a commercially developed PA imaging instrument by VisualSonic (Vevo 2100, Toronto, Canada), images were

collected at laser excitation energy below ANSI standards for laser skin exposure and PA signals were plotted based on 680 nm absorbance wavelength. All photoacoustic intensities were compared after the laser energy was normalized.

5. In vivo/Ex vivo NIRF Imaging

NIRF imaging was performed on the same mice as the PA imaging experiments using a Maestro all-optical imaging system after intravenous injection of $HACA_{Cy5.5}$-SWCNTs at a dose of 5 mg/kg SWCNT. Considering that the $HACA_{Cy5.5}$-SWCNT endocytosis into tumor cells will take more time than tumor accumulation, NIRF imaging was performed for over 3 days. Biodistribution and tumor accumulation profiles were monitored on the front flank tumors of mice by NIRF imaging at 24, 48, 72 and 96 h post-injection. After 96 h, mice were sacrificed and major organs and both tumors were excised. NIRF imaging of the organs was performed. The tissue distribution of $HACA_{Cy5.5}$-SWCNTs was quantified by measuring NIRF intensity at the ROI.

6. Ex vivo Cryo-TEM Imaging

Excised tumors were fixed in 4% formaldehyde solution for 10 min at room temperature and embedded in optimal cutting temperature compound (OCT) medium (Miles Inc, Elkhart, IN, USA). The frozen tumors were sectioned at approximately 10 mm in thickness on a cryostat. SWCNT distribution was observed using a Tecnai TF30 electron microscope (FEI Company) equipped with a GIF Tridiem imaging filter (Gatan Inc.) and operated at an accelerating voltage of 300 kV.

7. Statistical Analysis

Based on previous nanoparticle biodistribution studies with mice, at least three mice (n=3) per group are needed for sufficient statistical power. The statistical significance of differences

among the groups tested was determined using one-way ANOVA. A p-value less than 0.05 was considered significant and is specified by an asterisk. All tumor accumulation values from different imaging techniques will be expressed as means ± S.D. at each time point.

D. Results

First, the *in vivo* tumor accumulation of HACA-SWCNTs were imaged by PET at multiple time points for up to 48 h following intravenous injection of HACA$_{^{64}Cu\text{-}DOTA}$-SWCNTs (100 - 200 μCi in 100 uL PBS) to a SCC7 xenograft mouse model. A series of typical images are illustrated in Figure 3. HACA$_{^{64}Cu\text{-}DOTA}$-SWCNTs demonstrated a high tumor uptake of 9.8 ± 1.6 % ID/g in a considerably short time, less than 1 h, and accumulation was maintained up to 11.7 ± 0.4 % ID/g for 24 h and gradually decreased to 7.0 ± 0.2 % ID/g at 48 h post-injection. At 48 h post-injection, HACA$_{^{64}Cu\text{-}DOTA}$-SWCNTs exhibited uptake of 24.4 ± 3.2, 8.9 ± 0.7 and 17.2 ± 5.6 % ID/g in the liver, kidney, and spleen, respectively (Figure 4).

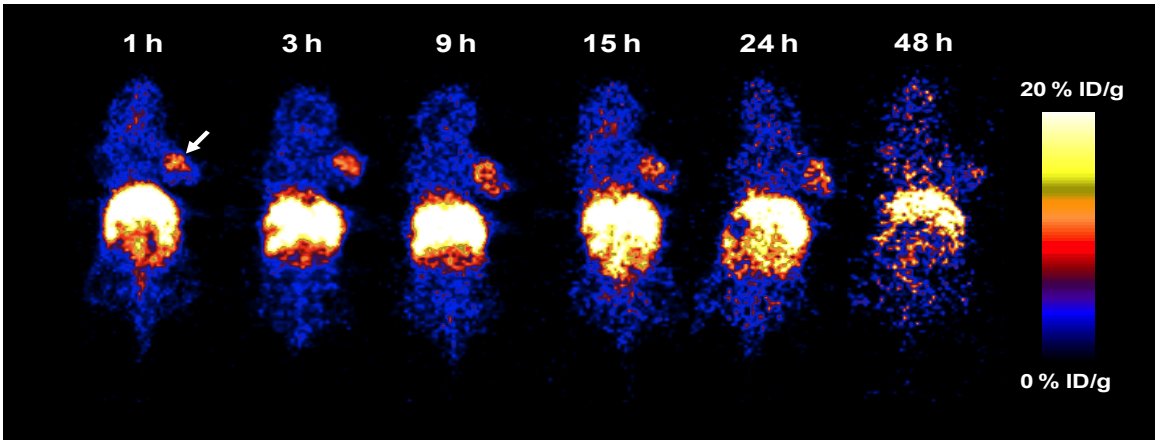

Figure 3: Positron emission tomography images of SCC7 tumor bearing mice at 1-48 h post-injection of 64Cu labeled HACA-SWCNTs.

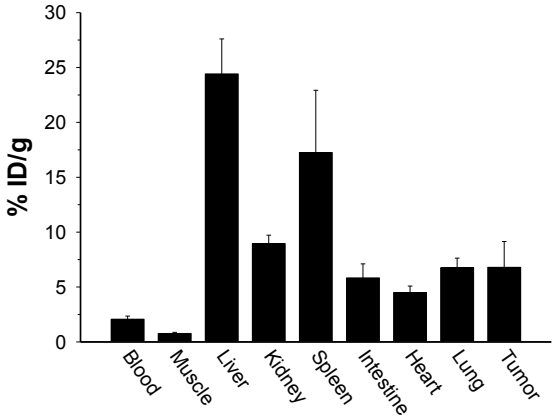

Figure 4: Injected dose per gram of PET data distributed over major organs after 48 hours. Error bars represent S.D., n=3.

Next, SCC7 tumors at the front flank and hind limb of the same mice were studied by NIRF and PA imaging, respectively. PA imaging discerned SWCNT absorbance at the tumor site 2 h post-injection, similarly to PET imaging. PA signal from the tumor was increased by 1.5 ± 0.1-fold at 2 h post-injection of HACA-SWCNTs compared to the pre-injection signal (Figure 5).

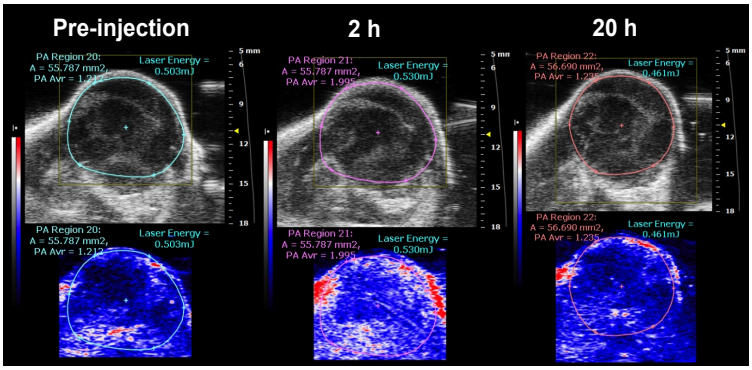

Figure 5: Ultrasound (top) and photoacoustic imaging (bottom) of the bottom hind limb SCC7 tumor of mice at preinjection and 2 and 20 h postinjection of $HACA_{Cy5.5}$-SWCNTs.

Unlike PET or PA imaging, fluorescence images exhibited strong NIRF signals at the tumor site only after 48 h post-injection (Figure 6). The radiant efficiency at the tumor reached 1.2 x 10^5. Although HACA-SWCNTs targeted the tumor site within one hour as demonstrated by PET and PA imaging, fluorescence activation is only visible after the hyal enzyme degrades the HACy5.5 on the HACy5.5-SWCNTs. Therefore, cellular uptake time and fluorescence quenching attributed to the later fluorescence emission. Major organs were carefully collected after sacrificing the mice at 96 h post-injection and the biodistribution was evaluated in terms of ex vivo fluorescence intensities (Figure 7). In accordance with *in vivo* fluorescence images, fluorescence was activated predominantly in both tumors. Tumor from the left hip (bottom) showed relatively low fluorescence signals compared to the tumor on the shoulder (top). The Cy5.5 in the bottom tumor was most likely photobleached by the continuous exposure to laser light during PA imaging.

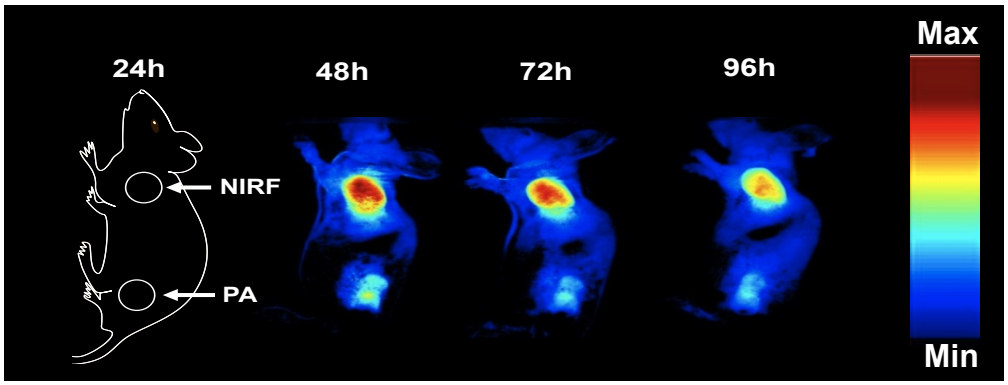

Figure 6: In vivo near infrared fluorescence imaging of SCC7 tumor-bearing mice at 24-96 h postinjection of $HACA_{Cy5.5}$-SWCNTs. Color bar represents the radiant efficiency (min: 0, max: 1.2 x 10^5).

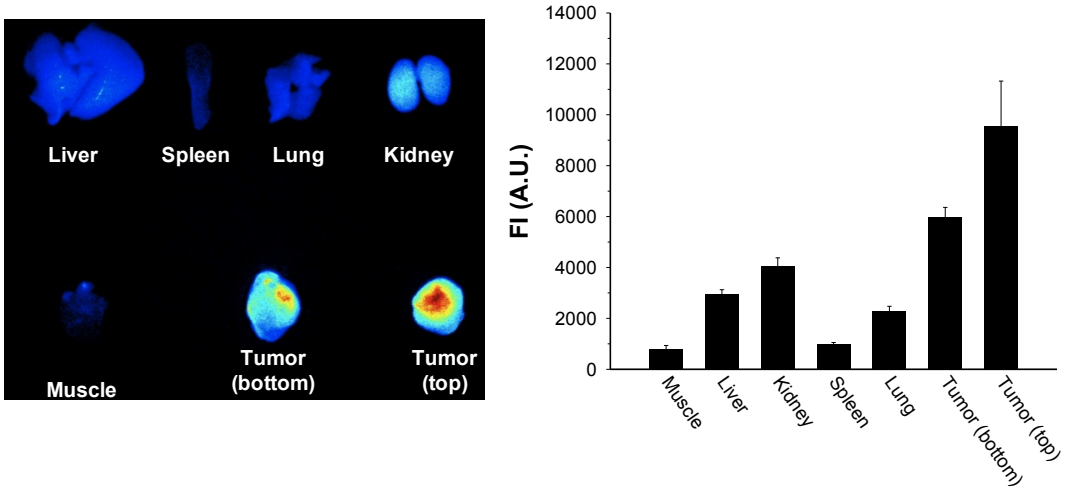

Figure 7. Quantitative analysis of NIRF of *ex vivo* biodistribution from Figure 6.

Finally, tumor uptake profiles for each modality over time were calculated. PA units were normalized to laser energy, PET radioactivity was calculated as the % injected dose per gram of the tumor, and fluorescence activation was reported as the fluorescence fold at the tumor over background regions (Figure 8). Tumor and liver sections were also analyzed by TEM. TEM images verified HA-NTs were successfully delivered into the tumor cells (Figure 9A) and mainly accumulated in lysosomes, while some liver uptake was also seen in the fenestrated vascular endothelium (Figure 9B).

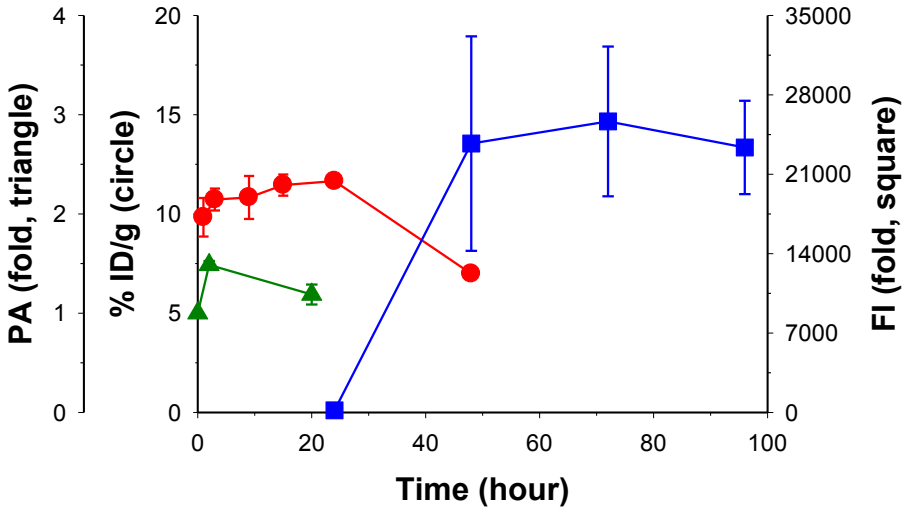

Figure 8: Quantitative analysis of all imaging modality intensities at the tumor site of mice treated with HACA-SWCNTs. Error bars represents SD, n=3 mice. Each modality is displayed on its respective y-axis (red circle: PET, % injected dose per gram; blue square: NIRG, tumor to background ration (TBR) of fluorescence intensity; PA, photoacoustic signal fold from preinjection time point).

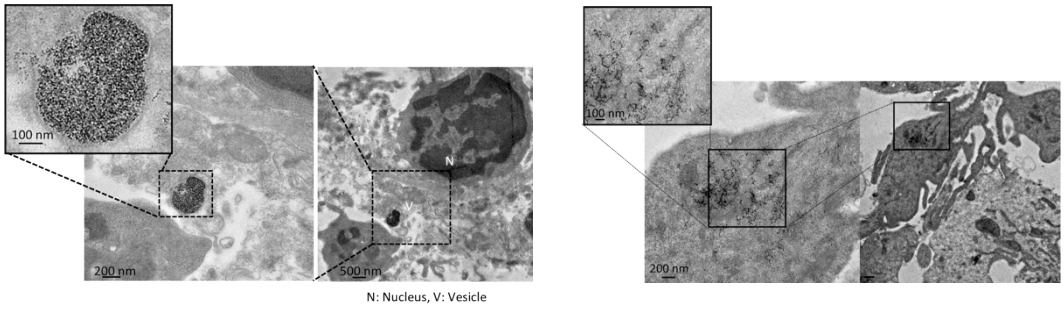

Figure 9: TEM images of tumor (left) and liver (right) tissue slices 96 h post-injection of HACA-SWCNTs.

E. Discussion

HACA-SWCNTs exhibited high tumor targeting *in vivo* after intravenous injection into an SCC7 tumor-bearing mice model. PET scans tracked the radionuclide-labeled HACA coating of the SWCNTs; while, PA imaging sensed the absorbance of SWCNTs directly. Tumor uptake profiles from PET and PA imaging showed tumor targeting within two hours, most likely due to the passive EPR effect as exhibited in other SWCNT biodistribution studies in tumor-bearing

mice (Figure 8).[7] Although HACA-SWCNTs exhibited similarly high tumor accumulation (11.7 ± 0.4 % ID/g) to PEGylated SWCNTs (10 – 15 % ID/g),[7] HACA-SWCNT tumor uptake occurred within 1 hour and remained at the site for 24 hours (9.8 ± 1.6 % ID/g). On the other hand, PEGyalted SWCNTs, designed for long circulation time, required more than 6 hours to reach a tumor accumulation plateau.[7] This rapid uptake and long-term accumulation of HACA-SWCNTs in tumor regions is an important feature for future biomedical applications. For example, HACA-SWCNTs can be used in tumor targeted drug delivery, where a long accumulation at the tumor site is required in order to properly deliver and release the drug in the tumor site and more important to the cancer cells. The simultaneous uptake of HACA, as seen in PET scans, and SWCNTs, as detected by PA imaging, confirm that HACA-SWCNTs were coated during passive targeting to the tumor. On the other hand, NIRF emission, which depends on the close interactions between of the $HACA_{Cy5.5}$ coating on SWCNTs (Chapter 3), was only detected 24 h post-injection. This delay in tumor accumulation signal compared to PET or PA imaging results may be attributed to the time needed for the HACA-SWCNTs to actively target CD44 receptors and be endocytosed to the SCC7 cells. Once endocytosed, the intracellular molecular interactions between HACA and hyal causes the fluorescence signal intensity to be recovered, acting as a sensor for cellular uptake developed in Chapter 3. However, this mechanism cannot be fully assessed without further long-term studies of $HACA_{Cy5.5}$ interactions and fluorescent recovery mechanisms with SWCNTs in physiological conditions. If there is no non-specific degradation, efficient quenching of HACA-SWCNTs up to 24 hr post-injection demonstrates that HACA is stably coated onto the SWCNT during its in vivo distribution. Taken together, the imaging results suggest HACA-SWCNTs accumulate at the tumor site within one hour (PET and PA imaging). Proper coating (low, non-specific fluorescence activation in NIRF

images) during its *in vivo* distribution must be further assessed. However, qualitative TEM images show accumulation of SWCNTs in vesicles, which may indicate that HACA-SWCNTs do enter tumor cells and, based on in vitro studies in Chapter 3, through CD44 mediated endocytosis.

The HACA-SWCNTs passively targeted the tumor site by the EPR effect and based on qualitative imaging and in vitro data enter tumor cells by CD44-HA interactions. The CD44 cell targeting and uptake by HACA-SWCNTs, as detected by NIRF imaging, plays a large role in tumor retention of the nanoplatform in vivo. Based on previous reports of PEG coated SWCNTs, the EPR effect accounts for an approximate SWCNT uptake of 3-4% ID/g.[7] The aspect ratio of SWCNTs can play an important role in increased extravasation from the blood stream to the tumor site via the leaky vasculature of the tumor, possibly because of a tumbling effect along the vessel wall, as modeling for silica disks.[31] However, although properly coated but non-targeted SWCNTs can still collect in the tumor regions in vivo, active targeting of the tumor greatly enhances the effect by at least 2.75 fold, as shown in the PEG coated SWCNT study.[7] The multivalency effect of HACA-SWCNTs to CD44 overexpressing cells increases active tumor targeting and binding. Just as discussed for HA-CD44 binding (Chapter 3), the increased probability of HA interacting with CD44 receptors on SCC7 cells can increase binding avidity and in turn cell uptake. HACA-SWCNTs with an aspect ratio over 1:400 can increase affinity to molecular targets due to the multivalency effect. CD44 is an important regulator between HA in the extracellular matrix and is therefore expressed in most vertebrate cells. However, elevated CD44 expression levels have been implicated in different malignancies compared to normal tissues, and that overexpression has been correlated with tumorigenesis and metastasis.[32-34] It is that significant overexpression of CD44 in most cancer cell types, including squamous cell

carcinoma (SCC) and cancer-initiating cells,[35] that is responsible for the tumor-targeting and cell uptake of HACA-SWCNTs in vivo. Additionally, an overexpression of hyal in the tumor region has been reported in similar head and neck tumor models,[28] which can further contribute to the high fluorescence activation at the tumor site over background (Figure 6,7).

Cryo-TEM images of excised tissue sections display that SWCNTs are indeed taken up into tumor cells and accumulate in endosomes/lysosomes. Moreover, SWCNTs are also present in liver tissue. A common limitation for many nanoparticles is the uptake by the RES, which leads to significant accumulation in the liver.[3] Although in vivo PET images display high liver accumulation of HACA-SWCNTs, NIRF imaging showed no fluorescence activation in the area. Without activation, it could be assumed that HACA-SWCNTs do not enter the liver cells. Yet, this low fluorescence signal in the liver can also be an artifact of the poor penetration of NIRF *in vivo*, unlike the low penetration needed for the subcutaneous tumor. Organs were excised after 96 hours and imaged with NIRF. Yet, the fluorescence activation most likely coincided with the quick and high liver uptake (24.4 ± 3.2 % ID/g) seen in PET scans during the first few hours post-injection. Therefore, the fluorescence signal may have cleared before ex vivo imaging was performed. Cryo-TEM of liver sections did exhibit carbon nanostructures in the fenestrated vascular endothelium. A specific HA receptor in the liver, HA receptor for endocytosis (HARE), is found on the liver sinusoidal endothelial cells of the endothelium[36] and is the main receptor responsible for HA turnover from the blood.[37-39] Therefore, HACA-SWCNTs are hypothesized to be taken up in the liver, and then endocytosed via HARE or phagocytosed by cells involved in the RES. The liver could then aid in the excretion of SWCNTs from the body. Since SWCNTs greater than 100 nm (~ 300,000 MW) exceed the renal excretion threshold of ~45,000 MW [40] or 5-6 nm nanoparticles[41] and the HACA-SWCNTs accumulated in the liver, the urinary excretion

pathway is ruled out. Based on previous excretion mechanisms of SWCNTs[7] and the detected liver uptake, HACA-SWCNTs are most likely excreted from the liver through the biliary duct and into the intestine, where SWCNTs are eventually excreted by the feces.[25] According to this pathway, the nanoparticles from the liver translocate through the fenestrated vascular endothelium into the Dissé spaces, as seen in the TEM images (Figure 9), to be processed into the biliary duct.[26] A more rapid clearance has been to shown to be dependent on highly positively charged moieties. HACA-SWCNTs have a zeta-potential that is negative and may cause sequestering within the liver and slower clearance rate. [27]

Previous biodistribution studies on SWCNTs non-tumor bearing mice, however, demonstrated low RES uptake and fast excretion through the urine.[23, 24] However, these studies involved only one imaging technique to track the SWCNTs: PET imaging of covalently radiolabeled SWCNTs. Therefore, SWCNTs were not directly accounted for in the body and only the radiolabel was tracked. If the radiolabel, such as ^{64}Cu, released from the SWCNT, the biodistribution data may only account for the free ^{64}Cu that has been shown to excrete through the urine in several hours.[42]

The HACA-SWCNT, with its proven tumor accumulation in vivo, can be utilized in cancer-targeted nanomedicine. For example, HACA-SWCNTs can be serve as optical probes for Raman microscopy or MRI or PARACEST imaging agents when the SWCNT undergoes endohederal filling with unique metals. The targeted SWCNTs can also be used as drug delivery vectors or prodrugs, where the conjugated anti-cancer drug on the HACA is released by the hyaluronidase degradation of the HA backbone during cellular uptake.[43] Additionally, the use of SWCNTs as activatable probes can open the door towards the design of SWCNTs as quenchers; additional fluorophore-substrate pairs can be designed for similar systems such as molecular

beacons. When tumor targeting is developed, studies on the sensing, drug delivery, and imaging capabilities of carbon nanomaterials can be pursued.

F. References

1. H. Maeda, J. Wu, T. Sawa, Y. Matsumura and K. Hori, *J. of Controlled Release*, 2000, 65, 271-84.
2. H. Maeda, J. Fang, T. Inutsuka and Y. Kitamoto, *Int. Immunopharmacol.*, 2003, 3, 319-28.
3. D. Peer, J. M. Karp, S. Hong, O. C. Farokhzad, R. Margalit and R. Langer, *Nat. Nanotechnol.*, 2007, 2, 751-60.
4. W. J. Gradishar, S. Tjulandin, N. Davidson, H. Shaw, N. Desai, P. Bhar, M. Hawkins and J. O'Shaughnessy, *J. Clin. Oncology*, 2005, 23, 7794-803.
5. A. Gabizon, H. Shmeeda and Y. Barenholz, *Clin. Pharmacokinetics*, 2003, 42, 419-36.
6. F. Yuan, M. Dellian, D. Fukumura, M. Leunig, D. A. Berk, V. P. Torchilin and R. K. Jain, *Cancer Res.*, 1995, 55, 3752-6.
7. Z. Liu, W. Cai, L. He, N. Nakayama, K. Chen, X. Sun, X. Chen and H. Dai, *Nat. Nanotechnol.*, 2007, 2, 47-52.
8. J.-W. Kim, E. I. Galanzha, E. V. Shashkov, H.-M. Moon and V. P. Zharov, *Nat. Nanotechnol.*, 2009, 4, 688-94.
9. N. W. S. Kam, M. O'Connell, J. A. Wisdom and H. Dai, *Proc. Natl. Acad. Sci. U. S. A.*, 2005, 102, 11600-5.
10. M. Pramanik, M. Swierczewska, D. Green, B. Sitharaman and L. V. Wang, *J. Biomed. Optics*, 2009, 14, 034018.
11. L. V. Wang, *Med. Phys.*, 2008, 35, 5758-67.
12. X. Wang, Y. Pang, G. Ku, X. Xie, G. Stoica and L. V. Wang, *Nat Biotech*, 2003, 21, 803-6.
13. M. Pramanik, K. H. Song, M. Swierczewska, D. Green, B. Sitharaman and L. V. Wang, *Phys. Med. Bio.*, 2009, 54, 3291.

14. A. De La Zerda, C. Zavaleta, S. Keren, S. Vaithilingam, S. Bodapati, Z. Liu, J. Levi, B. R. Smith, T.-J. Ma, O. Oralkan, Z. Cheng, X. Chen, H. Dai, B. T. Khuri-Yakub and S. S. Gambhir, *Nat. Nanotechnol.*, 2008, 3, 557-62.

15. R. Weissleder and V. Ntziachristos, *Nat. Med.*, 2003, 9, 123-8.

16. R. Weissleder, C. H. Tung, U. Mahmood and A. Bogdanov, Jr., *Nat. Biotechnol.*, 1999, 17, 375-8.

17. V. Ntziachristos, *Annu. Rev. Biomed. Eng.*, 2006, 8, 1-33.

18. R. K. Jain, L. L. Munn and D. Fukumura, *Nat. Rev. Cancer*, 2002, 2, 266-76.

19. Q. T. Nguyen, E. S. Olson, T. A. Aguilera, T. Jiang, M. Scadeng, L. G. Ellies and R. Y. Tsien, *Proc. Natl. Acad. Sci. U. S. A.*, 2010, 107, 4317-22.

20. C. C. Berry and A. S. G. Curtis, *Journal J. Phys. D: Appl. Phys.*, 2003, 36, R198.

21. S. M. Moghimi, A. C. Hunter and J. C. Murray, *Pharmacol. Rev.*, 2001, 53, 283-318.

22. S. M. Moghimi, A. C. Hunter and J. C. Murray, *FASEB J.*, 2005, 19, 311-30.

23. R. Singh, D. Pantarotto, L. Lacerda, G. Pastorin, C. d. Klumpp, M. Prato, A. Bianco and K. Kostarelos, *Proc. Natl. Acad. Sci. U. S. A.*, 2006, 103, 3357-62.

24. H. Wang, J. Wang, X. Deng, H. Sun, Z. Shi, Z. Gu, Y. Liu and Y. Zhao, *J. Nanosci. Nanotechnol.*, 2004, 4, 1019-24.

25. Z. Liu, C. Davis, W. Cai, L. He, X. Chen and H. Dai, *Proc. Natl. Acad. Sci. U. S. A.*, 2008, 105, 1410-5.

26. S. Hirn, M. Semmler-Behnke, C. Schleh, A. Wenk, J. Lipka, M. Schäffler, S. Takenaka, W. Möller, G. Schmid, U. Simon and W. G. Kreyling, *Eur. J. Pharm. Biopharm.*, 2011, 77, 407-16.

27. J. S. Souris, C.-H. Lee, S.-H. Cheng, C.-T. Chen, C.-S. Yang, J.-a. A. Ho, C.-Y. Mou and L.-W. Lo, *Biomaterials*, 2010, 31, 5564-74.

28. K. Y. Choi, H. Chung, K. H. Min, H. Y. Yoon, K. Kim, J. H. Park, I. C. Kwon and S. Y. Jeong, *Biomaterials*, 2010, 31, 106-14.

29. W. Cai, Y. Wu, K. Chen, Q. Cao, D. A. Tice and X. Chen, *Cancer Res.*, 2006, 66, 9673-81.

30. W. Cai, K. Chen, L. He, Q. Cao, A. Koong and X. Chen, *Eur. J. Nucl. Med. Mol. Imaging*, 2007, 34, 850-8.

31. G. Adriani, M. D. de Tullio, M. Ferrari, F. Hussain, G. Pascazio, X. Liu and P. Decuzzi, *Biomaterials*, 2012, 33, 5504-13.

32. M. Culty, H. A. Nguyen and C. B. Underhill, *J. Cell Biol.*, 1992, 116, 1055-62.

33. J. Lesley, V. C. Hascall, M. Tammi and R. Hyman, *J. Biol. Chem.*, 2000, 275, 26967-75.

34. R. Peach, D. Hollenbaugh, I. Stamenkovic and A. Aruffo, *J. Cell Biol.*, 1993, 122, 257-64.

35. M. E. Prince, R. Sivanandan, A. Kaczorowski, G. T. Wolf, M. J. Kaplan, P. Dalerba, I. L. Weissman, M. F. Clarke and L. E. Ailles, *Proc. Natl. Acad. Sci. U. S. A.*, 2007, 104, 973-8.

36. F. Braet and E. Wisse, *Comp. Hepatology*, 2002, 1, 1.

37. L. Fainboim, A. Cherñavsky, N. Paladino, A. C. Flores and L. Arruvito, *Cytokine Growth Fact. Rev.*, 2007, 18, 143-57.

38. B. Zhou, J. A. Weigel, L. Fauss and P. H. Weigel, *J. Biol. Chem.*, 2000, 275, 37733-41.

39. E. N. Harris, J. A. Weigel and P. H. Weigel, *J. Biol. Chem.*, 2004, 279, 36201-9.

40. L. W. Seymour, R. Duncan, J. Strohalm and J. Kopecek, *J. Biomed. Mater. Res.*, 1987, 21, 1341-58.

41. H. S. Choi, W. Liu, P. Misra, E. Tanaka, J. P. Zimmer, B. Itty Ipe, M. G. Bawendi and J. V. Frangioni, *Nat. Biotechnol.*, 2007, 25, 1165-70.

42. X. Chen, Y. Hou, M. Tohme, R. Park, V. Khankaldyyan, I. Gonzales-Gomez, J. R. Bading, W. E. Laug and P. S. Conti, *Journal Nucl. Med.*, 2004, 45, 1776-83.

43. K. Y. Choi, M. Swierczewska, S. Lee and X. Chen, *Theranostics*, 2012, 2, 156-178.

Chapter 5:

Utilizing Hyaluronic Acid Wrapped Single-Walled Carbon Nanotubes for Therapy *In Vivo* and Future Applications

A. Abstract

SWCNTs have been known to hold unique properties, but they can only be harnessed for biomedical applications when a suitable dispersing and targeting agent is found. In this study, biomedical theranostic applications for HACA-SWCNTs are demonstrated to inspire future capabilities. Specifically, by utilizing the unique absorbance properties and superior loading capacity of SWCNTs, HACA-SWCNTs are hypothesized to serve as effective photothermal therapy (PTT) and/or delivery agents. PTT uses an energy input to induce heating to the diseased region, where that heat will cause cellular damage and tissue ablation. In this case, HACA-SWCNTs will be taken up into cells and irradiated with a biological transparent NIR laser to induce cell death. In addition, HACA-SWCNT will also be functionalized with an additional treatment monitoring sensor to emphasize its ability to carry various molecules into the cell. Together, HACA-SWCNTs can serve as theranostics agents, where tumor regions are imaged, treated, and monitored after treatment.

B. Introduction

HACA-SWCNTs have shown to be dispersible (Chapter 2), tumor targetable (Chapter 3,4), and fluorescence activatable upon molecular signals (Chapter 3). Yet, because of HACA's ability to be further conjugated with other functional groups and the unique absorbance properties of SWCNTs, HACA-SWCNTs can also serve as cancer-targetable therapeutics. Many nanoplatforms have been utilized to deliver anticancer drugs or serve as therapeutics themselves, so called nanomedicine. Nanomedicine is an evolving field.[1] Early systems were made up of drug-loaded liposomes or micelles, while current systems involve specialized materials with precise targets based on the discovery of new biomarkers. Therapeutics combined with

diagnostic imaging make up the theranostics field and allow for treatment planning and monitoring. In this study, HACA-SWCNTs are exemplified as a theranostics platform.

With its established advantages in tumor targeting and imaging, HACA-SWCNTs can be utilized in tumor targeted ablation. In the clinic, image-guided tumor ablation is performed by interventional oncologists most commonly by radiofrequency and microwave means. Ablation is considered an effective local treatment for localized tumors and is most commonly accompanied by additional therapies like surgery, chemotherapy or radiation. One example is the use of radiofrequency ablation for the ablation of primary or metastatic liver cancers,[2] and kidney cancer.[3] In this system, needle-like electrodes are inserted into the tumor through the skin or during open surgery, upon which radiofrequency is applied, causing frictional heating to the region. Just as in radiofrequency ablation, photothermal ablation causes an increase in temperature that is responsible for the tumor ablation. Photothermal therapy (PTT) however utilizes either a continuous or pulsed wave laser as the energy source. A laser in the NIR region is usually required during a noncontact method in order to achieve depth penetration past body hair or skin.

To destroy the tumor region, temperatures above 50°C in the tissue must be reached.[4] Hyperthermia occurs at temperatures above 42°C. Between 42 and 45°C, cells are more susceptible to damage, such as to anticancer drugs or radiation therapy. Yet, at prolonged exposure to these temperatures, some cells can still remain unaffected. On the other hand, at 46°C for 60 minutes, cells will undergo irreversible cellular damage. At temperatures between 50–52°C, cytotoxicity can be induced much more rapidly in 4–6 minutes. Temperatures at 60°–100°C destroy nucleic acid-histone complexes and key enzymes, and the cells will undergo

instant irreversibly damage to cells. Therefore, the necessary temperature for tumor ablation, by so-called coagulation necrosis, is above 50°C.[4, 5]

Because PTT efficiency can be greatly enhanced under a laser in the NIR region, materials with high absorbances in the NIR have been utilized as thermal sensitizers in the tumor region. For example, gold nanorods have been thoroughly studied for their ability in PTT.[6-8] Because gold nanorod NIR absorbance can vary based on the adjustable length of the rod, their absorbance can be fine-tuned to the laser energy for efficient uptake and conversion to heat.[9] Yet, even though gold nanorods have a much higher NIR absorption at $\sim 1 \times 10^9 M^{-1} cm^{-1}$ than SWCNTs at 6.2×10^6 M^{-1} cm^{-1},[10] gold nanoparticles are quickly deformed by the laser irradiation. It was theoretically found that their absorption band is permanently bleached, decreasing the ability to induce thermal ablation.[11] Because SWCNTs have a higher NIR absorption coefficient compared with NIR fluorescenct dyes (Cy5.5 (Amersham Biosciences): 1.0×10^5 M^{-1} cm^{-1}; IRDye 800CW (Li-COR Biosciences): 2.4×10^5 M^{-1} cm^{-1}), they have been extensively utilized in PTT studies. Based on a side-by-side comparison of SWCNTs and gold nanorods, SWCNTs required a lower dose of nanoparticle (3.6 mg/kg vs. ~35 mg/kg) and lower laser power (0.6 W/cm^2 vs. 2 W/cm^2) for tumor elimination by PTT.[12] Therefore, SWCNTs can more efficiently transform absorbed energy into photothermal energy.[10] SWCNTs serve as PTT sensitizers, so lower laser irradiance can be used to achieve cytotoxic heating to the tumor region. For example, SWCNTs labeled with various targeting groups have shown to be effective under continuous wave laser irradiation and recent examples are included in Table 1. However, it is also important to notice that only one study used a power during laser irradiation that was within the maximum skin exposure limits set by the American National Standard for the Safe Use of Lasers for a continuous wave 808 nm[12] laser and 980 nm[13], ~ 0.33 W/cm^2 and 0.73

W/cm^2, respectively. One study of note showed that when PEGylated SWCNTs were intratumorally injected at at dose of about 0.4 mg/kg into the solid tumor and irradiated with an 808 nm laser, the tumor was completely eradicated without recurrence of the tumor over 6 months.[14] However, the study utilized a power density of 76 W/cm^3. Yet, there is still potential for SWCNTs as PTT agents for tumor eradication. Therefore, the feasibility of HACA-SWCNTs in PTT will be studied.

SWCNT Platform	Injection	Dose (mg/kg)	Laser Wavelength (nm)	Irradiance (W/cm^2)	Duration (min)	Reference
Monoclonal Antibody-SWCNT			805-811	5	7	[15]
Folic Acid-SWCNT			808	1.4	2	[16]
PEG-Phospholipid-SWCNT	i.v, i.t	3.6, 0.4	808	0.6, 76 cm^{-1}	5, 3	[12, 14]
Glycated Chitosan-SWCNT	**i.t**	**1-25**	**980**	**0.5-1**	**2**	**[17]**

Table 1: Recent examples of SWCNT platforms in PTT using a continuous wave laser. If studies were in vivo, their injected dose is noted as well as if the injection was intratumoral (i.t.) or intravenous (i.v.).

Additionally, HACA-SWCNTs can also be used as delivery agents to the targeted tumor site. As seen by the fluorescence activatable system described in Chapter 3, the SWCNTs delivered dye molecules into the cell. HACA-SWCNTs can similarly be used to deliver and release other molecules into the cell, for example anticancer drugs or activatable probes. To further recognize the ability of HACA-SWCNTs as a delivery agent, a caspase-3 activatable probe was conjugated to the HACA and the activity of the probe was studied. Caspases are intracellular cysteine proteases that are essential in apoptosis, and therefore cancer cells suppress caspase expression to continue proliferation.[18] Yet, when an effective therapy is applied,

caspases are expressed. Importantly, caspase-3 is a direct biomarker of late stage apoptosis. Therefore, the imaging probe directly measures when the HACA-SWCNTs are delivered into the cell and when the probe detects caspase-3. This design of this caspase-3 probe was previously established in the lab.[19] In brief, the nanosensor is comprised of a specific caspase-3 substrate, DEVD, with a quencher and a Cy5.5 dye on each end of the substrate. The quencher is able to absorb the fluorescence of the dye molecules by Forster resonance energy transfer (FRET). However, the substrate is cleaved in the presence of caspase-3, in turn disrupting the energy transfer and allowing fluorescence to be detected.

By utilizing the unique absorbance properties ($6.2 \times 10^6\ M^{-1}cm^{-1}$)[10] and superior loading capacity (~2600 m^2/g)[20] of SWCNTs along with the unique capabilities of biomaterial-coated SWCNTs (Chapter 2,3,4), HACA-SWCNTs are hypothesized to serve as effective PTT or delivery agents. SWCNTs have been known to hold unique properties, but they can only be harnessed for biomedical applications when a suitable dispersing and targeting agent is found. In this study, biomedical theranostic applications for HACA-SWCNTs are demonstrated to inspire future capabilities.

C. Research Design and Methods

In this study the feasibility of HACA-SWCNTs in therapy and therapy monitoring is studied. Therapy will be performed by 808 nm laser irradiation of HACA-SWCNTs, which in turn will produce high temperatures to induce cytotoxicity. Furthermore, HACA-SWCNTs will be studied for their ability to deliver a treatment monitoring sensor, a caspase-3 probe that detects apoptosis.

1. Photothermal Therapy

Based on previous PTT studies, the requirements for tumor ablation are matched with the laser setup available in the lab in Table 2. As seen in this table, it is emphasized that for a suitable PTT agent, the laser irradiation should not be below the human skin exposure limit. However in the HACA-SWCNT system, it is observed that 50 ug/mL SWCNTs reach the tumor site when intravenously injected (Chapter 3 PET results, ~12% ID/g in tumor region). Therefore, this concentration is maintained in all experiments to account for a realistic tumor accumulation. Phantom studies of HACA-SWCNTs in vials or subcutaneously injected into mouse were performed to determine the necessary laser power and distance from the laser to achieve relevant conditions for PTT in vivo. Cells treated with HACA-SWCNTs compared with PEG-SWCNTs and irradiated with an 808 nm laser were studied for viability.

Thermal Ablation Requirements for Therapy	**Laser Set-Up**
Within human skin exposure limit for 808 nm: ~0.33 W/cm^2	Laser irradiance: 0.2 W/cm^2 50 ug/mL SWCNTs*
Temperature: > 45°C	Reach 50°C at 7 min
Heating area for tumor: ≥ 1cm^2	Distance from laser to cell/tumor: ~2.5 cm

Table 2: Requirements for effective PTT with the corresponding conditions for the 800 nm continuous wave laser. In addition, the limitation of the laser setup is using no more than 50 ug/ml HACA-SWCNT, which is the approximated amount of SWCNTs that reach the tumor region from PET data (Chapter 3).

a. Laser Setup

An 808 nm continuous wave, collimated diode laser system (LaserGlow Technologies, Toronto, Canada) was used in all experiments. Power was determined using an air-cooled thermopile

sensor (Coherent, Santa Clara, CA) and the laser beam diameter was monitored with an IR viewing card (ThorLabs, Newton, NJ).

b. Phantom Laser Irradiation Studies

Samples of 50 ug/ml HACA-SWCNTs were irradiated with an 808 nm laser at varying powers. Temperature was monitored by a FLIR Infrared Camera (Model SC305, Portland, OR) along with the corresponding ExaminIR Max software. Temperatures about 45 °C are required for thermal ablation of cells and tissue. Phantom studies were performed with HACA-SWCNTs enclosed in PCR plastic tube as well as subcutaneously injected in Matrigel to athymic nude mice (eight weeks old, 20-25 g).

c. Cell Irradiation Studies

SCC7 (murine squamous cell carcinoma) cells were cultured in RPMI 1640 medium containing 10% fetal bovine serum (FBS) in 100 mm dishes. Cells were seeded into 96 well plates at least 24 hours prior to studies at a density of about 8,000 cells/well. Experimental groups were incubated with 25 ug/mL HACA-SWCNTs and PEG-SWCNTs in serum free RPMI 1640 media with 15 mM HEPES buffer for 1.5 hrs. The laser experimental groups were irradiated with the 808 nm laser for 15 minutes. The focused beam diameter was approximately 0.6 cm and the power was set to 2.67 Watts/cm^2 to induce a temperature of ~65°C. It took approximately 6 minutes to reach the 65°C temperature during the 15 minute irradiation. The experimental groups included HACA-SWCNT and PEG-SWCNT treated cells with and without laser irradiation (4 groups). As well as cells heated in a 65°C incubator and an un-treated SCC7 control group (2 groups). All groups underwent the same conditions, including the time the samples were outside

of the incubator during laser treatment. After irradiation, all cells were washed with PBS, replaced with RPMI media, and placed back into standard cell culture conditions.

d. Cytotoxicity Assay

Lactate dehydrogenase (LDH) assay was performed five hours after irradiation to measure percent cytotoxicity in each cell group. LDH is a stable cytosolic enzyme that is released upon increased membrane permeability, which is associated with cyototoxicity. The LDH colorimetric LDH assay correlates the amount of cell death by the amount of LDH spillage into the media. Media was collected from each well and centrifuged at 16,000 x g for 25 minutes to remove any excess SWCNTs in the sample. After centrifugation, 50 µL of the supernatant from each tube was collected and transferred into a new 96 well plate, and the rest of the assay followed the manufacturer's protocol (CytoTox 96 Non-Radioactive Cytotoxicity Assay, Promega). The maximum LDH release was determined by lysing a row of control cells and assaying the cell lysate, and spontaneous LDH release was controlled for by assaying the media of untreated cells. The percent cytotoxicity was calculated as:

$\%\ Cytotoxicity = \frac{(Exptl\ LDH\ Release\ 490)}{Max\ LDH\ Release\ 490}$. Studies were performed in pentaplicate.

2. Probe Delivery

In another embodiment of this study, fluorescein-labeled HACA-SWCNTs were conjugated with a nanosensor comprised of a caspase 3 substrate, with a dark quencher (BHQ3) and a Cy5.5 dye on each side. This nanosensor was previously investigated.[19] The quencher is a molecule that absorbs fluorescence at a certain wavelength of a fluorophore by FRET. Since Cy5.5 dye has an emission at 695 nm, black hole quencher 3 (BHQ-3) was used to absorb

fluorescence in the 620-730 nm wavelength range. The caspase-3 substrate, DEVD, served as the linker between the dye and quencher. This sensor was conjugated onto the HA backbone ($HA_{apo}CA$) with a crosslinker between the carboxyl groups of the disaccharides of HA and an incorporated cysteine residue (thiol) in the caspase-3 substrate. Once incorporated, $HA_{apo}CA$ was wrapped onto SWCNTs, making $HA_{apo}CA$-SWCNTs. Then the activity of the $HA_{apo}CA$-SWCNTs was examined for its detection and specificity ability for apoptosis and more specifically, caspase-3. In addition, the $HA_{apo}CA$-SWCNT probe was tested in cells before and after apoptosis was induced with tumor necrosis factor-related apoptosis-inducing ligand (TRAIL). TRAIL causes tumor cell-specific toxicity by activating apoptosis and upregulating caspase3 in SCC tumor models.[21-23]

a. Synthesizing Caspase-3 Probe with $HACA_{FA}$

The caspase-3 substrate, DEVD, with an incorporated cysteine group was labeled with activated Cy5.5 dye as described and characterized previously.[19] A crosslinker was needed to bind the cysteine (thiol group) from the caspase probe onto the carboxylates of HACA. Just as fluorescein was bound to the HA backbone, EDC and NHS chemistry was utilized to bind the NHS-PEG_{12}-maleimide (Thermo, IL) to the HA backbone. Then the cysteine on the probe was reacted with the maleimide group of the crosslinker on the HA. The crosslinker was mixed into HACA at pH 7 with gentle shaking for 1 h. Then, the caspase probe was added to the HACA-crosslinker solution and stirred for 1 h. Finally, $HA_{apo}CA$ was dialyzed against distilled water. The UV-Vis spectrum of particles was recorded on a Genesys 10s UV-Vis spectrophotometer.

b. In Vitro Caspase-3 Fluorescence Activation

About 50 ug/mL of $HA_{apo}CA$-SWCNT was incubated with 6.6 nM of caspase-3 in a reaction buffer at pH 7.5, 37 °C, and fluorescence was collected at specified time points. To study the

selectivity of the caspase-3 probe, fluorescence was collected after 90 min incubation with caspase-3, caspase-3 with inhibitor, caspase 8 and caspase-9 in a reaction buffer at pH 7.5, 37°C at 90 minutes. For the inhibitor study, 100 uM of caspase-3 inhibitor, Z-DEVD-FMK (Z: benzyloxycarbondyl group, FMK: fluoromethyl ketone), was added to the solution of HA_{apo}CA-SWCNT and caspase-3. The Z group enhances cellular permeability to deliver the FMK group, which inhibits the induction of apoptosis. The enzyme reaction buffer consists of: 50 mM HEPES ((4-(2-hydroxyethyl)-1-piperazineethanesulfonic acid), 100 mM NaCl, 0.1% CHAPS (3-[(3-cholamidopropyl)dimethylammonio]-1-propane sulfonate), 10 mM DTT (dithiothreitol) and 1 mM EDTA (ethylenediaminetetraacetic acid). All fluorescence measurements were collected on a F-7000 Fluorescence Spectrophotometer (Hitachi, Tokyo, Japan) at scan speed of 240 nm/min, with the PMT voltage set at 950 V. Fluorescence intensity measurements were collected with excitation at 675 nm and emission at 695 nm wavelengths. The maximum activation ability at 90 min as a factor of caspase-3 concentration (0-6.6 nM) was imaged using an Maestro all-optical imaging system (Caliper Life Sciences, Hopkinton, MA).

c. Imaging of Fluorescence Activation in Cells

SCC7 cells were seeded in 35 mm petri dish at ~1 x 10^5 cells. After incubation with ~50 ug/mL HA_{apo}CA-SWCNT for 2 h, the cells were washed twice with PBS and treated with 0.1 ug/mL TRAIL at 37°C. Cells were imaged over time using an Olympus IX81 microscope with respective filters for FA and Cy5.5.

D. Results

1. Photothermal Therapy

To examine if HACA-SWCNTs can be used for PTT applications, temperature changes after laser irradiation of HACA-SWCNTs were studied. Based on the average amount of HACA-SWCNTs that targeted the tumor in the biodistribution studies from Chapter 3, about 50 ug/mL concentrations of SWCNTs were used in all phantoms. Based on 3 separate readings, HACA-SWCNTs required a power density greater than 0.2 W/cm^2 to achieve a temperature above 45°C (Figure 1). Thermal images of HACA-SWCNTs during laser irradiation showed that it took eight minutes to reach the maximum temperature and did not increase any further. The in vivo phantom study also demonstrated that the region of HACA-SWCNT injection reached temperatures of 45°C with a laser irradiation at 0.2 W/cm^2. Importantly, temperatures had a greater increase in the shoulder region where little adipose tissue exists as compared to the hip region, a superficial adipose depot.

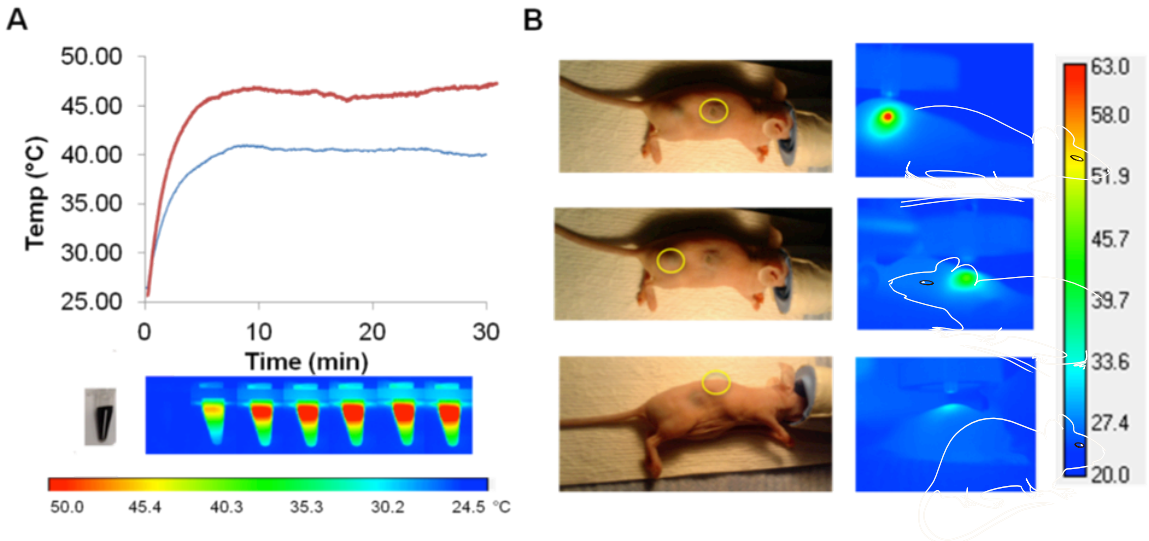

Figure 1: Phantom laser irradiation of 50 ug/mL HACA-SWCNTs in A) Eppendorf tubes (red 0.2 W/cm^2, blue 0.15 W/cm^2) B) subcutaneously injected in mice at 0. 2 W/cm^2. Scale bar represents temperature in °C.

In vitro studies of HACA-SWCNTs and PEG-SWCNTs showed an increase in cytotoxicity for SWCNT-treated cells over laser-treated cells alone (HACA-SWCNTs with and without laser: 62.40±6.2%, 16.83±2.0%, PEG-SWCNTs with and without laser: 52.59±8.7%, 12.48±0.8%, all $p<0.05$), indicating that laser irradiation and temperature increase caused cytotoxicity (Figure 2). Laser irradiation on cells without SWCNTs showed only 16.07±2.4% cytotoxicity. In addition, HACA-SWCNTs after laser irradiation showed a slight increase in cytotoxicity over PEG-SWCNTs (62.40±6.2% vs. 52.59±8.7%, $p<0.05$), possibly due to the targeted intracellular uptake of HACA-SWCNTs. SCC7 cells heated in an incubator at ~50°C, rather than being laser irradiated, showed only 19.06±1.9% cytotoxicity.

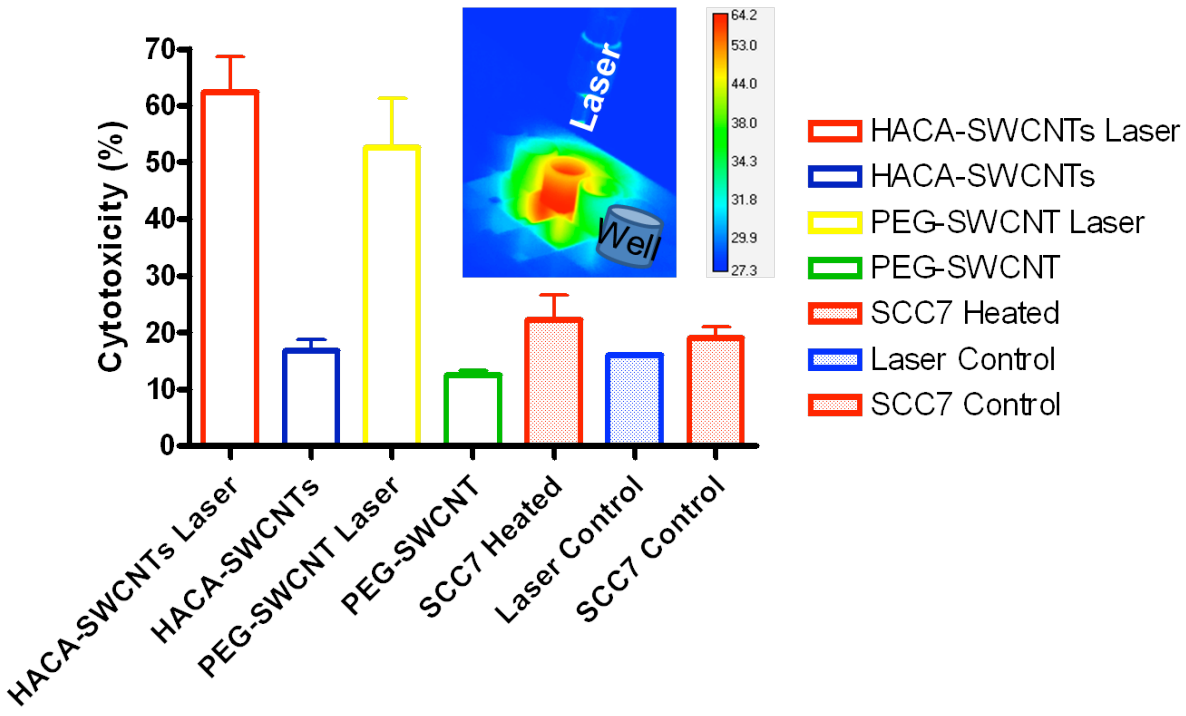

Figure 2: Laser irradiation of SCC7 cells. Groups are statistically significant from HACA-SWCNTs Laser ($p<0.05$, $n=5$). Inset is a thermal image of a well undergoing laser irradiation in a 96 well plate.

2. Probe Delivery

To study if HACA-SWCNTs can be used as delivery agents, a caspase-3 probe was conjugated onto $HACA_{FA}$ and then coated onto SWCNTs. As seen in the UV-absorbance in Figure 3a, both FA and Cy5.5, from the caspase-3 probe, dye peaks are seen with a generally high absorbance background from the SWCNTs. Caspase-3 detection was evaluated by incubating the fluorescein-labeled $HA_{apo}CA$-SWCNT in an enzyme reaction buffer along with caspase 3. As shown in Figure 3b, the fluorescence signal for Cy5.5 was quenched before caspase-3 was added to the solution (0 min). The signal began to recover within 5 minutes of adding the caspase and continued to increase up to 90 minutes. Fluorescence activation at 5 minutes was 5.0±0.8 fold greater than initial and reached a total of 10.0±1.1 fold greater at 90 minutes. No difference in activation was seen over 90 minutes. Fluorometry and fluorescence optical images demonstrate that the intensity of the recovered fluorescence signal is proportional to the concentration of caspase-3 (0-6.6 nM, r^2=0.97) (Figure 3c).

Selectivity for caspase-3 was also demonstrated by evaluating the $HA_{apo}CA$-SWCNT fluorescence after incubation with caspase-3 with an inhibitor (Cas + inh), caspase-9 (Cas-9), and caspase-8 (Cas-8). As shown in Figure 3d, fluorescence signals are only recovered for caspase 3 in a time dependent manner. $HA_{apo}CA$-SWCNT fluorescence signals during incubation with the other caspase remained quenched with minor fluorescence activation. At 90 minutes the fluorescence activation fold from the intial amount for caspase with inhibitor, caspase-8, and caspase 9 was 0.19 ±0.05, 0.26 ±0.05, 0.22 ±0.03-fold, respectively.

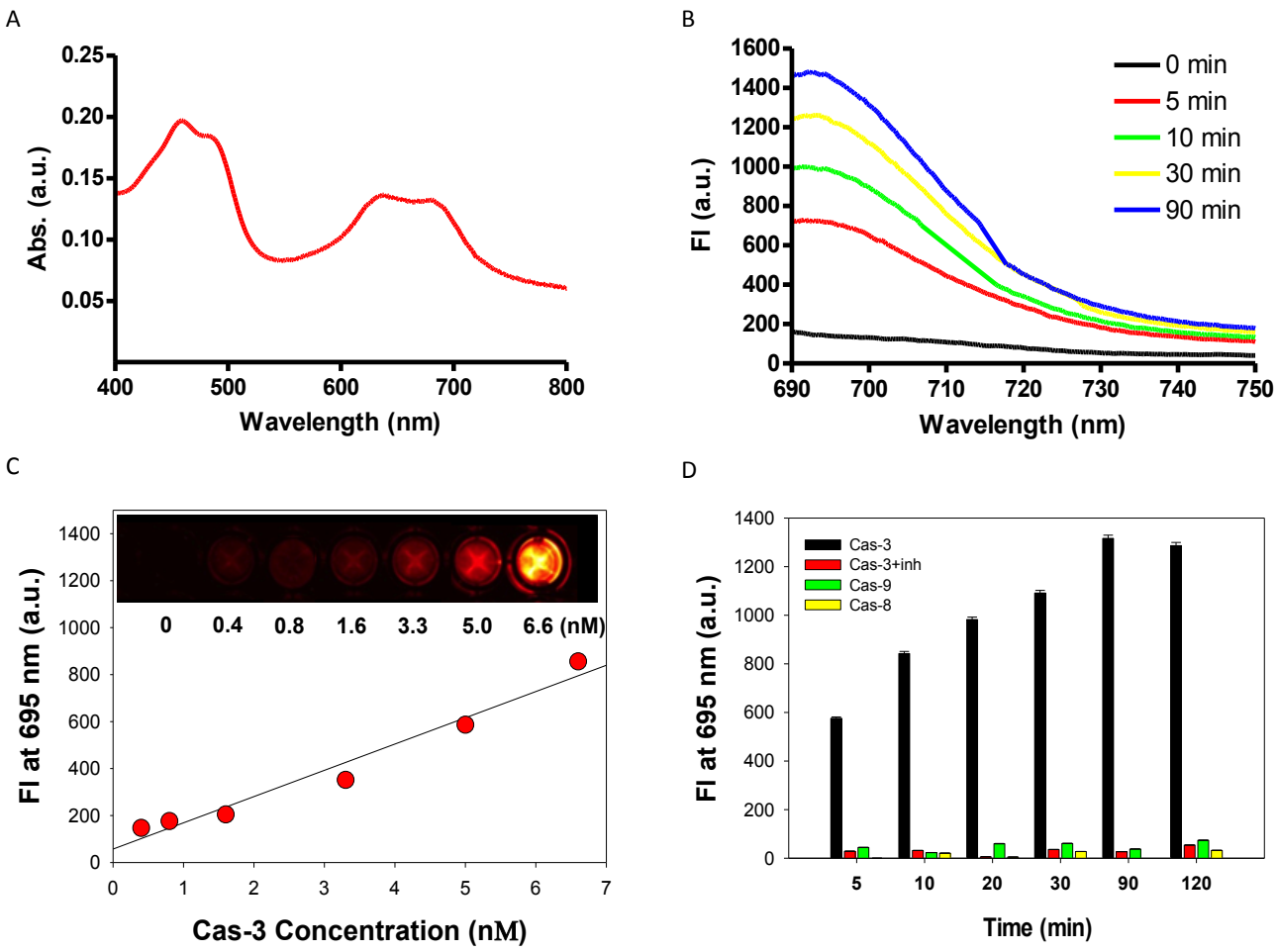

Figure 3: Caspase-3 Cy5.5 fluorescence activation and specificity when caspase-3 apoptosis probe is conjugated onto HACA-SWCNTs (HA_{apo}CA-SWCNT). a) UV-vis spectra of FA labeled HA_{apo}CA-SWCNT b) Cy5.5 fluorescence emission spectra of HA_{apo}CA-SWCNT when incubated in enzyme reaction buffer with caspase-3 for 0-90 minutes. C) Fluorescence optical images and fluorescence values of HA_{apo}CA-SWCNT when incubated with different concentrations of caspase-3 (0-6.6 nM). D) Specificity of fluorescence activation of HA_{apo}CA-SWCNT for caspase-3 when incubated with caspase-3 (Cas-3), caspase-3 with an inhibitor (Cas + inh), caspase-9 (Cas-9), and caspase-8 (Cas-8). Data points represent the means of triplicate experiments and standard deviation.

Once the activity of the caspase-3 apoptosis probe was demonstrated when conjugated onto HA_{apo}CA-SWCNT, its activity in cells with induced apoptosis was evaluated based on fluorescence microscopy (Figure 4). When cells were incubated with HA_{apo}CA-SWCNT, the FA signal was seen as previously demonstrated during cell uptake (Chapter 3). Once cells were treated with a high dose of an apoptosis-inducing ligand, TRAIL, cells began to emit a stronger

Cy5.5 image, indicating the probe was activated. In addition, cells began to visually undergo apoptosis, as seen by the appearance of apoptotic bodies.

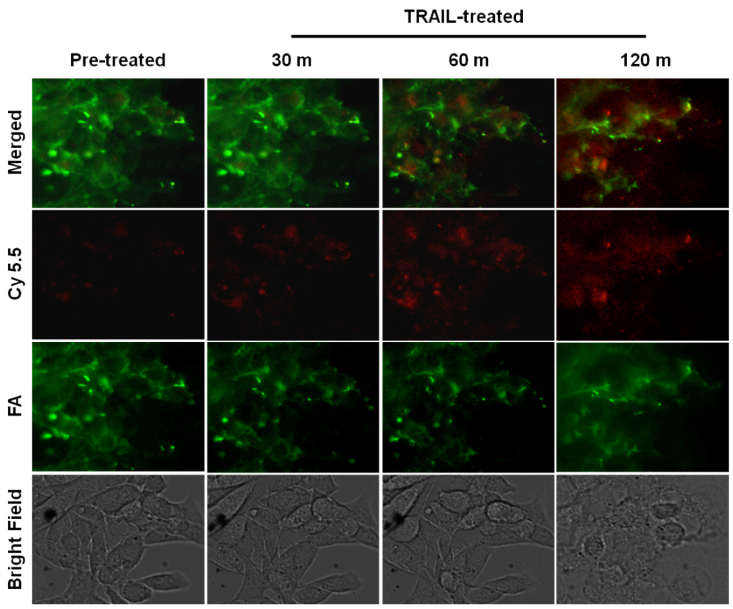

Figure 4: Imaging of cell uptake and caspase-3 activation in SCC7 cells. Red (Cy5.5)=caspase-3; Green (fluoresceinamine)=cell uptake.

E. Discussion

Based on their established properties, HACA-SWCNTs can be utilized to target, image and potentially treat tumors. During PTT studies, HACA-SWCNT concentration was restricted to 50 ug/mL, based on the percent of injected dose of HACA-SWCNTs that targeted the tumor region as calculated from PET scan images (Chapter 4). HACA-SWCNTs were examined for their ability to induce cytotoxic heating to cells after NIR laser irradiation. Based on in vivo phantom studies of HACA-SWCNTs injected subcutaneously in a non-tumor bearing mice, a laser power of 0.2 W/cm^2 could be used to induce heating above 45°C.[4, 5] This is the minimum temperature shown to induce cell ablation during radiofrequency and microwave ablation therapies. Importantly, the laser power of 0.2 W/cm^2 was within the skin exposure limits set by the American National Standard for the Safe Use of Lasers for continuous wave 808 nm lasers,

unlike other published studies (Table 1). Still, the tissue areas that reached temperatures above 45°C in the in vivo phantom study showed necrosis 10 hours post-irradiation, and mouse skin was burned at this power setting. In this study, it was qualitatively seen that the temperature increase after laser irradiation to HACA-SWCNT subcutaneously injected sites varied over 5 C between the shoulder region and hip region. Laser irradiation at 808 nm occurs well within the biological optical window where there is a low effect on the effective attenuation coefficient, dependent on the tissue absorption and scattering factors of the NIR light. But temperature measurements using an infrared camera are not effective in measuring tissue depths above microns. Yet, this demonstrates the importance to study how HACA-SWCNTs conduct heat in tissue, especially addressing perfusion-mediated tissue cooling due to removal of heat by blood flow.[4, 24] In an in vivo tumor model many additional factors in terms of heat transfer and biological inflammatory response must also be considered for effective ablation therapy. These issues will be raised in the following section outlining future studies.

During the in vitro cytotoxicity studies, treatments with both HACA-SWCNTs and PEG-SWCNTs were able to induce toxicity (62.40 ± 6.2% and 52.59 ± 8.7% cytotoxicity, respectively) to SCC7 cells after laser irradiation. Cytotoxicity was measured as the percentage of LDH released of the maximum LDH release of SCC7 cells. Yet, a laser power of 2.67 W/cm^2 was required to induce toxic effects in cells after 6 hours. A laser power below 2 W/cm^2 did not show cytotoxicity above 50%. This is a ten-time higher laser power than the one found to induce hyperthermia-required temperatures of HACA-SWCNTs in vials alone or subcutaneously injected in nude mice (Figure 1). Other studies involving the development of PTT agents use a higher power of NIR lasers during in vitro studies than studies of the material alone or in vivo. For example in the seminal study by Hirsch, et al. of gold nanoshells for PTT, an 820 nm laser

was utilized for both in vitro and in vivo studies but the laser power for the in vitro study was 35 W/cm^2, but was greatly reduced to 4 W/cm^2 for in vivo studies with effective ablation.[25] Similarly, Melancon, et al. demonstrated that hollow gold nanoshells can induce temperatures up to 45°C using an 808 nm laser at powers of 8 W/cm^2 but for in vitro ablation studies a power of 40 W/cm^2 was used.[26] The requirement for a higher power during in vitro ablation studies in this and other studies is not understood, but a monolayer of cells is not an accurate model for direct laser irradiation. Future photothermal ablation studies should focus on more realistic models, specifically a tumor mouse model.

In addition, cell viability studies are required to determine the cell death mechanisms during laser irradiation with and without SWCNTs. Cytotoxicity assays from Chapter 3 and this chapter involve correlating lactate dehydrogenase (LDH) with cell viability and cytotoxicity. LDH is an endogenous enzyme found in the cytosol of all cell types. After lysing all cells remaining after HACA-SWCNT treatment, the total LDH can be measured and correlated with the total viable cell population. When cell membranes become permeabilized, a mark of toxicitiy, LDH is released into the culture supernatant. By measuring LDH only released into the culture media, the released LDH can be correlated with the extent of cytotoxicity to the region. This type of assay was performed in this chapter to study the toxicity effects 6 hours after laser irradiation on samples with and without SWCNTs. Four hours after necrosis is induced, cells exhibit a permeabilized membrane leading to a significant release of LDH. Yet, apoptosis similarly can induce LDH release in a similar time frame with overexpression of caspases and ATP. The cell death mechanism can by deduced by additional assays, such as a combination of propidium iodide (PI) assay and Annexin V labeling. PI is a cell impermeable dye, while Annexin V is an apoptosis marker for cell membrane exposed phosphatidylserine. If PI is able to

enter cells and no Annexin V is detected, then necrosis is the cause of cell death. On the other hand, if Annexin V is highly labeled on the membrane of laser irradiated cells, then apoptosis is inferred to occur. Additional in-depth studies may also aid in the determination of the cell death mechanism. Such assays, along with additional cell types and tumor models are laid out in Section F: Future Work.

Furthermore, in vivo studies of intravenously injected HACA-SWCNTs can help determine the true advantage of these targeted PTT agents. As seen in previous chapters, HACA-SWCNTs can distribute at the tumor site with over 10% ID/g. After extravasating into the tumor region and directly entering cancer cells, HACA-SWCNTs after laser irradiation can cause local heating at regions that are molecularly relevant to the disease by possibly delineating the tumor margin, otherwise missed by direct radiofrequency or microwave ablation. Since HACA may target cancer-initiating cells, or so-called cancer stem cells, through CD44 receptors,[27-29] tumor ablation with targeted nanoparticles may reduce the use of adjuvant therapies and more importantly reduce tumor metastasis. The experimental layout for future in vivo targeting and PTT studies is included in Section F: Future Work.

In this chapter, HACA-SWCNTs were also exemplified to deliver an apoptosis sensor into cells (Figure 4). As demonstrated in Chapter 3, $HACA_{dye}$-SWCNTs are able to endocytose into CD44 overexpressing SCC7 cells, where they interact with hyaluronidase 1, causing dye molecules labeled onto HACA to release from the SWCNT platform. Using a similar approach, HACA-SWCNTs can deliver probes or therapeutic molecules. In this example, a caspase-3 activatable probe was labeled onto the HA backbone and delivered into cells after HACA-SWCNT uptake (Figure 4). Importantly, the probe maintained its fluorescence activity and specificity when conjugated onto HACA-SWCNTs (Figure 3). This type of sensor, when

delivered into the cancer cells, can be utilized to monitor treatment. In vivo apoptosis probes are especially useful for in vivo high-throughput screening of different types of anticancer molecules and to recognize drug resistance. Future work can take advantage of the high surface area of SWCNTs and its ability to bind a variety of molecules to deliver therapeutics to the site of malignancy. For example, HACA-SWNCTs can be used to target and intracellularly deliver anticancer pro-drugs to tumors.[18] Yet, the carbon nanomaterials field is moving towards utilizing unique properties of SWCNTs, such as its high thermal conductivity, electron conductivity, mechanical strength, and its intrinsic optical signals for various biomedical applications over its high surface area for drug delivery.

F. Future Work

In this chapter, two therapy applications of HACA-SWCNTs were introduced. The first being its use as a PTT agent and the second a delivery agent. As seen in Chapter 4, HACA-SWCNTs can target the tumor region and be used as an imaging agent. Together, HACA-SWCNTs show potential to target, image and treat tumors, while monitoring treatment - a true theranostic agent. Yet, before HACA wrapped carbon nanomaterials can be translated into clinical applications, future studies must be performed to study toxicity, biodistribution, and in vivo PTT applications in additional cell types and tumor models.

1. Biodistribution and Long-Term In Vivo Fate of HACA-SWCNTs

In addition to the tumor targeting efficiency studies of HACA-SWCNTs from Chapter 4, long-term studies of HACA-SWCNTs activity are necessary to understand their overall accumulation. Such studies must be performed in non-tumor bearing mice models, such as Balb/c mice, to prevent early mortality due to tumor growth. Important questions need to be addressed to understand the HACA-SWCNT distribution and clearance *in vivo*. How long

HACA-SWCNTs remain in the body and their accumulation in different organs can indicate its safety for in vivo applications. What is the long-term in vivo fate of HACA-SWCNTs? What is the blood circulation half-life of SWCNTs? What is the clearance pathway of HACA-SWCNTs?

Studies performed in Chapter 4, utilized PET, NIRF, and PA imaging to track HACA-SWCNTs for their tumor accumulation. For future long-term distribution studies lasting over 3 months, PET imaging would require isotopes with longer half-lives than ^{64}Cu ($t_{1/2}$: 12.7 h), such as ^{89}Zr (78.4 h) or ^{111}In (2.8 d), that require expensive precautions during animal handling. Optical imaging, which is utilized to monitor fluorescence activation after HA degradation in vivo (Chapter 4), is not a viable imaging option for a 3 month long study, because non-specific HA degradation may occur. Based on previous long-term distribution studies of SWCNTs, HACA-SWCNTs can be monitored by Raman spectroscopy and imaged by PA in excised organs of a mouse.[30] These imaging techniques directly detect the intrinsic optical signals of SWCNTs (as discussed in Chapter 2 Introduction), rather than using labels (radiolabels or fluorescent dyes) that can fall-off or degrade over time in physiological conditions. In addition, the Raman G-band peak, unaffected when measured in tissue lysate or serum conditions, can be quantitatively correlated with the SWCNT concentration (Chapter 2, Figure 4).[30] Similarly, Raman spectra can be collected on both feces or urine, when properly prepared for measurements under lysis buffer, to monitor the excretion of SWCNTs over time.

To address the high liver uptake seen from PET scans in tumor-bearing nude mice (24.4 ± 3.2 % ID/g at 48 h post-injection, Chapter 4, Figure 3), similar long-term studies can be performed after blocking the HA receptor for endocytosis (HARE, introduced in Chapter 3 Introduction) HARE is found to be a specific receptor for HA and chondroitin sulfate that enables its turnover after being endocytosed, predominantly in liver sinusoidal endothelial cells.

By blocking this receptor, HA is not endocytosed into the liver endothelial cells,[31] possibly initiating different pathways of clearance that are SWCNT driven over HA. For example, previous long-term distribution studies of PEGylated SWCNTs exhibited high uptake in the liver but with near-complete clearance from all major organs 2 months post-injection.[30] This previous biodistribution study is an important comparison to HACA-SWCNTs. It can help elucidate the influence that HACA, specifically HA interactions with its receptors, has on the biodistribution of HACA-SWCNTs over non-targeted PEG-SWCNTs. However, currently, the only monoclonal antibody for HARE that prevents HA endocytosis has only been studied in rats. The antibody, mAb-174 (designated for the 174 kDa HARE target it blocks), shows specificity for sinusoidal endothelial cells in the liver, spleen and lymph nodes of rats.[31] To use this antibody to block HA uptake in this proposed Balb/c model, a preliminary study must be performed to measure the specificity for mAb-174 in mice liver sinusoidal endothelial cells.

Finally, this proposed 5 month study will also monitor potential systemic toxicity of HACA-SWCNTs compared to control mice by monitoring mouse mortality rates, mouse body weights as well as a serum chemistry panel on collected blood samples. After sacrificing the mice for ex vivo analysis, blood will be collected and then separated for respective blood chemistry studies. Standard serum proteins will be monitored for any metabolic changes of the SWCNT treated mice from the non-treated mice. Of note, proteins monitoring liver function will be closely monitored. Serum chemistry will include a standard panel of markers, such as glucose, cholesterol and albumin. A hepatic function screen should include: aspartate aminotransferase (AST), alanine aminotransferase (ALT), alkaline phosphates (ALP), gamma-glutamyl transpeptidase (GGT). These are the most common markers to evaluate liver enzyme abnormalities in the blood. Hepatocytes express ALT and AST enzymes intracellularly.

However, under hepatocellular injury, the cell membranes become compromised causing these enzymes to release in to the blood. ALT is specific to hepatocytes, while AST is also expressed in cardiac and red blood cells. Therefore increased levels of both ALT and AST in the blood indicate toxicity, but ALT is specific to hepatic toxicity. On the other hand, ALP and GGT are proteins released by hepatocytes in the biliary ducts after physical damage, such as blockage, in the ducts. Cholestatic damage, the damage caused by decreased or obstructed flow of bile from the liver to the intestine, is especially relevant to monitor if the hypothesized biliary excretion pathway of SWCNTs causes toxicity in hepatocytes.

Experimental Variables and Response Measures. PA imaging signal and Raman spectra of excised organs and blood of mice treated with and without HACA-SWCNTs will be collected. PA signal intensity and Raman G-band will be correlated with SWCNT concentration and monitored over time. The response measure is the SWCNT %ID/g of all major organs over post-injection, and the average rate of accumulation for each organ will be calculated. The blood collected at these time points will be utilized to measure serum levels and compared with non-treated mice for toxicity. Urine and feces samples before and after HACA-SWCNT will be collected at the same time points with biodistribution studies and then analyzed to measure the SWCNT concentration changes over time in urine and feces to determine excretion rates. To determine the circulation half-life of HACA-SWCNTs, blood samples will be collected at much earlier and more frequent time points. The SWCNT concentration and its conversion to %ID/g of blood will be plotted against post-injection time in minutes. From the fitted exponential curve, the circulation half-life can be calculated and eventually compared to previous reports of PEGylated SWCNT half-lives. Finally, mortality rates and body weight changes will be monitored for the treated and untreated group and compared over the 5 month period. If

preliminary studies on HARE antibody block HA uptake in mice, all studies above will be compared with a blocking group along with a control, untreated group.

Experimental Design. SWCNT biodistribution studies will be performed on six-week old Balb/c mice for 5 months after injection of HACA-SWCNTs. Based on previous biodistribution studies,[30] approximately 5 mice per time point per group totaling 40 mice per group will be used. Biodistribution studies will involve sacrificing the animal at each time points (0, 1, 15, 30, 60, 90, 120, 150 days) and excising and weighing all major organs as well as blood samples (~100 uL). PA imaging of excised organs will be obtained and then the organs will be prepared for Raman spectroscopy measurements. First, the organs will be solubilized in a lysis buffer consisting of SDS, Triton and DTT. Next, the tissue is homogenized with cup horn sonication. Finally, the lysate is heated at temperature above 70 C for 2 hours to obtain a clear homogenate. These methods are reported elsewhere.[30] A calibration curve of PA signal intensity and Raman G-band intensity and AUC versus SWCNT concentration will be collected, using the same imaging conditions (laser wavelength, laser power, laser spot size, collection time). Similarly to the experimental design of Raman measurements in Chapter 3, Raman G-band peak will be a characteristic signal of SWCNTs. Once the concentration of SWCNTs is correlated with the calibration curve, the percent injected dose of SWCNTs per gram of tissue (%ID/g) is calculated for each organ at each time point. The blood collected will be utilized for serum chemistry to compare metabolism and liver toxicity with the control mice. A standard panel of markers, such as glucose, cholesterol and albumin will be collected. The following levels are necessary to measure hepatic function: aspartate aminotransferase (AST), alanine aminotransferase (ALT), alkaline phosphates (ALP), gamma-glutamyl transpeptidase (GGT). To determine the circulation half-life of HACA-SWCNTs, blood samples will be collected at much earlier and more frequent

time points (0, 1, 3, 5, 10 mins). Blood (<8 uL) will be collected from the orbital sinus under anesthesia. The blood will be mixed with lysis buffer and analyzed by Raman spectroscopy and the % ID/g of SWCNTs in the blood will be calculated. The % ID/g will be calculated as previous described in reference #30. Finally, urine and feces will be collected at respective long-term time points and measured for SWCNT using similar methods to the excised organs. Urine and feces will not be collected continuously. Instead, on the day of the sacrifice, mice will be divided into separate compartments covered with plastic wrap. Any urine or feces that is void, will be collected. If contamination between the feces and urine occur, more advanced methods in excretion collection must be utilized. Body weights for treated and untreated mice at each time point along with any deaths will be recorded. If preliminary studies below exhibit effective blocking of HA in mice after antibody treatment, a HARE blocking group will also be included in all the above studies.

Blocking HARE: To determine the biodistribution of HACA-SWCNTs after liver uptake is blocked, the specificity for the HARE antibody, mAb-174, to mouse liver cells must be studied. Firstly, liver endothelial cells need to be isolated and cultured from mice, as described in previous studies of rat liver cells.[31] Next, the mAb-174 will be tested for its ability to target HARE in mouse liver cells. Liver endothelial cells along with isolated mouse fibroblasts as a negative control will be incubated with mAb-174 for ~ 1 hour and FACS analysis will performed to determine the binding extent of the antibody to the cell types. The experimental design would be similar to the CD44 labeling and FACS analysis from Chapter 3. If the antibody binds to mouse HARE as measured by a significant difference in mean fluorescent intensity of liver endothelial cells and fibroblasts, then blocking ability for HA cellular uptake must be examined. Radiolabeled HA and HACA (described in Chapter 4 Methods) would be treated to the plated

live endothelial cells at a constant concentration with varying amounts of mAb-174 (~1-15 ug/mL) for 60 minutes alongside a control value with no antibody treatment. After rinsing away excess HA and antibodies, cells would be measured for their radioactivity as a percent of the control radiolabeled HA or HACA treated cells. This would provide a graph of the amount of endocytosis of HA in the antibody treated cells. If the antibody blocks endocytosis below 25% of the control, then the antibody can be utilized for future in vivo blocking studies. The antibody can be administered systemically before HACA-SWCNT injection of the biodistribution studies. If the antibody is not active in mice, significant studies will be required to first detect HA-binding proteins in hepatocytes and sinusoidal endothelial cells using an established method for rat cells[32] and using the models set forth by Weigel et al.[31, 33]

Data Interpretation. The key data collected in this study is the long-term monitoring of SWCNTs in all major organs. Where HACA-SWCNT accumulate in vivo will be compared with previously published PEG-SWCNTs,[30] and with HARE blocking, providing clues on the HA effect of SWCNT accumulation in vivo. In addition, a steady decrease in SWNCT concentration from major organs and the SWCNT concentration in urine and feces will be utilized to hypothesize the excretion pathway. The hypothesized excretion pathway of HACA-SWCNTs is through the biliary ducts of the liver and into the intestine, where SWCNTs are finally excreted through the feces. In this study, SWCNT measurements in the feces, along with the liver and intestine, will confirm this pathway. Renal excretion of SWCNTs has also been reported.[30] The accumulation of SWCNT signals in the kidneys, bladder and urine will indicate what is the prevalent clearance mechanism at different time points. A common path for nanoparticles is the accumulation in the RES, mainly the liver and spleen, where particles are slowly excreted via both urine and feces.[34] If slow clearance rates with high uptake in the liver and spleen exist,

SWCNT uptake in the RES can be derived. If HACA-SWCNTs do not clear from major organs over a three month period, a serve limitation in the SWCNT platform translation to clinical applications exists, and toxicity is most likely detected. Body weight loss, increased mortality rates and significantly different serum chemistry in the HACA-SWCNT group over the control group indicate toxicity by the platform. Significant increases in AST, ALT, ALP and GGT level over control mice indicate sever liver toxicity. A high concentration of AST may also indicate toxicity in other organs, especially cardiac cells. A high ratio (>2) of ATL to AST indicate specific toxicity to the liver. Statistically significant increases over control for AST and ALT levels indicate general toxicity to liver cells once their membranes are permeabilized, while high levels of ALP and GGT indicate biliary duct damage or obstruction. HACA-SWCNTs are hypothesized to travel through the biliary ducts for excretion. Obstruction would reduce excretion in the feces and cause further toxicity to the liver. This possible mechanism can be analyzed by the timeline of ALP/GGT and ATL/AST increases, respectively.

Limitations. A major limitation is the sensitivity of Raman spectroscopy and PA imaging to the concentration of SWCNTs. SWCNT accumulation at later time points may still exist but may not be detected by either detection method. The limit of detection must be established during calibration curves of Raman G-band and PA intensities versus SWCNT concentration to understand the possible SWCNT concentration at non-detectable signals. To provide a pattern of organ accumulation and clearance of SWCNTs, a large concentration (> 0.5 mg/mL) of SWCNTs will be injected to make sure that SWCNTs can be detected at early time points. But such a high concentration can induce toxicity that would not otherwise occur at lower concentrations that still exhibit tumor targeting ability. Therefore, if SWCNTs show over 90% clearance from all major organs after 3 months but toxicity is detected, lower HACA-SWCNT

concentrations can be studied without significant toxicity as measured by serum markers. Toxicity in this study is limited to serum markers. Eventhough these disease markers are well-established methods, additional animals for each time point in each group can also be added in order to collect organs for histology analysis. Histological analysis can provide a direct manner to specifically determine liver toxicity when comparing groups with and without HARE blocking. In addition to future in vitro cytotoxicity studies, histology on paraffin embedded tissue sections can indicate if unblocked HARE induced higher damage to the liver over blocked samples. Histological examination can be performed with hematoxylin and eosin staining and with terminal deoxynucleotidy trasnferase biotin-dUTP nick-end labeling (TUNEL) to image DNA damage due to apoptosis or necrosis.

2. In Vivo Photothermal Therapy Studies

In this chapter, HACA-SWCNTs were shown to induce hyperthermia necessary for cell death. However, the goal of a tumor-targeted SWCNT platform, like HACA-SWCNTs, is to treat the tumor region. Therefore, an in vivo study utilizing HACA-SWCNTs to target and then treat the tumor region after laser irradiation by PTT is needed. In an in vivo tumor model many additional factors in terms of heat transfer and biological inflammatory response must also be considered for effective ablation therapy. For example, how PTT agents conduct heat in tissue may change due to the so-called heat sink effect, where the increased heat is dissipated and removed by increased blood flow.[4] As discussed previously, in vitro studies of PTT require higher laser powers than in vivo studies to induce cell death and tumor ablation. This may possibly be due to the activation and enhancement of immune response to tumor cells by the increase temperatures.[35-36] With additional biodistribution studies of HACA-SWCNTs in Balb/c mice (above) as well as SCC7 tumor bearing Balb/c mice, future PTT studies should include animal

models with normal immune systems, rather than nude mice which were currently studied. Balb/c mice, for example, may allow an immune response to the remaining tumor cells at the ablation site and aid in cancer cell death to prevent metastasis. Therefore, in future PTT studies, a mouse model with a normal immune system will be used. Below is an outline of the experimental in vivo PTT design. Although in vitro studies of PTT may not be an accurate model for tumor ablation, the SCC7 cell toxicity effect studied in this chapter require further characterization of its cell death mechanism using additional cell death assays and temporal studies.

Experimental Variables and Response Measures. The effect of the laser irradiation, existence of SWCNTs, and HACA-SWCNT injection type will be examined on the tumor bearing mice. The tumor size and mouse survival rate will be measured.

Experimental Design. Six-week old Balb/c mice will be subcutaneously injected in the left flank with SCC7 cells and used in these in vivo studies. Five groups with five mice per group will be examined: I) negative control with no SWCNT nor laser, II) laser only group, III) SWCNT only group, IV) treatment group with intravenous injection, V) treatment group with intratumoral injection. Based on Figure 1, 50 ug/mL HACA-SWCNTs could be used to induce heating above 45°C with a laser (continuous wave 808 nm) power of 0.2 W/cm^2. Eventhough a ten time higher laser power was required to induce cytotoxicity in vitro (Figure 2), previous reports indicate that lower laser power is needed for in vivo tumor ablation by SWCNTs. In this in vivo study, two laser powers (0.2 and 3 W/cm^2) will be examined for PTT while using a high SWNCT concentration of about 0.5 mg/mL. Laser irradiation to the intratumoral injection group will be applied at 5 min post injection but at least 2 h after intravenous injection. Surface temperatures of the subcutaneous tumor will be monitored in real-time during laser irradiation using an

infrared camera. Tumor volume will be monitored approximately every 2 days for up to 2 months. According to animal care and use regulations, mice with tumor diameters larger than 15 mm or if sick will be sacrificed. Mice survival data will be collected. One-way ANOVA analysis will be performed to compare tumor volume response for each experimental group and survival data will be compared using the Kaplan-Meier method.

Data Analysis and Interpretation. In vivo experiments will determine if SCC7 tumor ablation is possible using NIR lasers and HACA-SWCNTs. The effects on tumor size will be examined with laser only, SWCNT only and SWCNT+laser injected either intravenously or intratumorally groups. Effective PTT therapy can only be confirmed if the laser irradiated group with SWCNTs had a statistically significant change in tumor size over the other groups. If the SWCNT only group had an effect on tumor size without significant decreases in mouse survival rates, then the SWCNTs may exhibit a targeted cytotoxic effect to the tumor without the need for laser irradiation. This type of treatment is possible as cells may endocytose a large concentration of SWCNTs. Differences in injection route of HACA-SWCNTs further the understanding of tumor targeting ability. Most PTT studies use tumor injection to achieve high concentrations of PTT agents directly at the tumor site and to reduce heating to healthy tissue. However, if the targeting efficacy of HACA-SWCNTs is high, then intravenous injection could have similar tumor ablation effects with more advantages. Intravenous injections of nanoparticles allow for a more evenly distributed concentration of particles throughout the entire tumor including the delineation between cancerous and healthy cells.

Limitations. A major limitation in this study is the inability to monitor molecular effects after laser irradiation. This reduces the study to focus on tumor size and survival rate outcomes. However, skin burning and scarring would greatly affect non-invasive tumor monitoring, such as

by fluorescence. Therefore, if tumor ablation is significant and no metastasis is detected after one month, histological analysis at various time-points after irradiation should be performed. Another limitation faced in this study, may be the variation in temperature increases due to the irregular distribution of HACA-SWCNTs within the tumor. To address this possible limitation, temperature during treatment must be monitored, and samples with large variations in temperatures should be excluded from further analysis. Larger sample sizes may be required for each group. To reduce large animal numbers, computational heat transport modeling[37] can help eliminate additional PTT experimental parameters, such as laser power.

3. Future Tumor Models

To extend the in vivo applications of HACA-SWCNTs additional cell types and tumor models (Chapter 3, Table 3) should be examined using similar protocols discussed in this work. Importantly, to address the large liver uptake of HACA-SWCNTs in vivo, liver cells should tested for their uptake of HACA-SWCNTs and viability after HACA-SWCNT treatment. Table 3 below includes a list of additional adherent cell types, along with their designations, that are available through ATCC to study. An additional primary cell line of interest is the rat liver endothelial cells that exhibit HARE, discussed in F.1. The tumor cells listed in Table 1 can be utilized to induce subcutaneous tumor growth in mice and further studied for their tumor targeting efficiency, as demonstrated in Chapter 4. In addition, imaging experiments performed in Chapter 4 should also be extended to spontaneous metastatic tumor models to examine HACA-SWCNT ability to identify and target smaller tumors and metastatic cells expressing CD44 for locomotion. Most importantly, CD44 blocking studies of tumors must be performed as an additional control to compare tumor targeting efficiency of HACA-SWCNTs. Such studies would include an intratumor injection of excess concentrations of HA.

Tumor Cells		Liver Cells		Macrophages	
Human prostatic adenocarcinoma	LnCAP	Mouse Hepatocytes	AML12	Mouse	RAW 264.7, J774
Human ovary adenocarcinoma	OVCAR-3	Human hepatocellular carcinoma cells	HepG2	Human/Mouse	WBC264-9C
Mouse melanoma	B16-F10				
Human breast adenocarcinoma	MDA-MD-231				
Human colorectal cancer	HCT 116				

Table 3: Cell types to examine for future tumor targeting efficiency studies of HACA-SWCNTs.

4. The Future of Carbon Nanotubes

To utilize the unique properties of carbon nanotubes, such as its high thermal conductivity, electron conductivity, mechanical strength, and its intrinsic optical signals, isolation of specific species of SWCNTs is required. The separation of SWCNTs based on their electronic and physical properties is the current focus of SWCNTs, and importantly an important task taken up by the National Institute of Standards and Technology (NIST). Separation techniques, such as density gradient ultracentrifugation or column purification, are currently lab-developed and are just facing commercialization. As these systems continue to be optimized specifically for its ease-of-use, the SWCNT field will be greatly enhanced. Firstly, researchers will be able to purchase SWCNTs with more confidence on its purity, and standards will form on SWCNT quality, similar to the ones set for chemical reagents. Secondly, with this increase in purity confidence by researchers, SWCNT applications will be fine-tuned and enhanced. For example, if a material scientist is currently spending months to isolate semiconducting SWCNTs with low yields for biosensor applications, the option to purchase already-isolated SWCNTs allows greater effort to be placed on that biosensor. Finally, biomedical applications can be greatly enhanced when specific lengths and chirality of SWCNTs are studied in vivo. Comparing such properties in vivo are important to develop understandings of the biological interaction with carbon

nanomaterials. HACA provides a simple technique to disperse carbon nanomaterials. In this way, various lengths and chirality of SWCNTs and shapes of carbon nanomaterials (MWCNTs, fullerenes, graphene) can be compared in their biodistribution and biological activity using this universal coating technique. Comparing organ accumulation and toxicity effects of carbon nanomaterials is an important step in defining and/or optimizing a specific carbon-based material for in vivo biomedical applications. Currently, data exists for many types of nanomaterials, but are not comparable because of the non-uniform nature of studies from different groups, such as the concentration, surface functionalization techniques and animal model. By using one coating material with the above protocol, the only differences among the groups are the shape, length, or chirality effects. In addition, HACA provides cancer-targeting capabilities to the SWCNTs, opening the door for the unique and fine-tuned properties of SWCNTs to be directly delivered and utilized at the site of most need.

G. References

1. D. Peer, J. M. Karp, S. Hong, O. C. FaroKhzad, R. Margalit and R. Langer, *Nat. Nanotechnol.*, 2007, **2**, 751-760.
2. L. R. Jiao, P. D. Hansen, R. Havlik, R. R. Mitry, M. Pignatelli and N. Habib, *Am. J. Surg.*, 1999, **177**, 303-306.
3. D. A. Gervais, F. J. McGovern, B. J. Wood, S. N. Goldberg, W. S. McDougal and P. R. Mueller, *Radiology*, 2000, **217**, 665-672.
4. S. N. Goldberg, G. S. Gazelle and P. R. Mueller, *Am. J. Roentgenology*, 2000, **174**, 323-331.
5. S. N. Goldberg, G. S. Gazelle, E. F. Halpern, W. J. Rittman, P. R. Mueller and D. I. Rosenthal, *Acad. Radiology*, 1996, **3**, 212-218.
6. L. Tong, Q. Wei, A. Wei and J. X. Cheng, *Photochem. Photobio.*, 2009, **85**, 21-32.
7. E. B. Dickerson, E. C. Dreaden, X. Huang, I. H. El-Sayed, H. Chu, S. Pushpanketh, J. F. McDonald and M. A. El-Sayed, *Cancer Lett.*, 2008, **269**, 57-66.
8. X. Huang, I. H. El-Sayed, W. Qian and M. A. El-Sayed, *J. Am. Chem. Soc.*, 2006, **128**, 2115-2120.
9. E. C. Dreaden, M. A. Mackey, X. Huang, B. Kang and M. A. El-Sayed, *Chem. Soc. Rev.*, 2011, **40**, 3391-3404.
10. J.-W. Kim, E. I. Galanzha, E. V. Shashkov, H.-M. Moon and V. P. Zharov, *Nat. Nanotechnol.*, 2009, **4**, 688-694.
11. F. Rudnitzki, M. Bever, R. Rahmanzadeh, K. Brieger, E. Endl, J. Groll and G. Huttmann, *J. Biomed. Optics*, 2012, **17**, 058003.

12. J. Robinson, K. Welsher, S. Tabakman, S. Sherlock, H. Wang, R. Luong and H. Dai, *Nano Res.*, 2010, **3**, 779-793.

13. C. Salthouse, S. Hilderbrand, R. Weissleder and U. Mahmood, *Opt. Express*, 2008, **16**, 21731-21737.

14. H. K. Moon, S. H. Lee and H. C. Choi, *ACS Nano*, 2009, **3**, 3707-3713.

15. P. Chakravarty, R. Marches, N. S. Zimmerman, A. D.-E. Swafford, P. Bajaj, I. H. Musselman, P. Pantano, R. K. Draper and E. S. Vitetta, *Proc. Natl. Acad. Sci. U. S. A.*, 2008.

16. N. W. S. Kam, M. O'Connell, J. A. Wisdom and H. Dai, *Proc. Natl. Acad. Sci. U. S. A.*, 2005, **102**, 11600-11605.

17. F. Zhou, S. Wu, S. Song, W. R. Chen, D. E. Resasco and D. Xing, *Biomaterials*, 2012, **33**, 3235-3242.

18. K. Y. Choi, M. Swierczewska, S. Lee and X. Chen, *Theranostics*, 2012, **2**, 156.

19. X. Huang, M. Swierczewska, K. Y. Choi, L. Zhu, A. Bhirde, J. Park, K. Kim, J. Xie, G. Niu and K. C. Lee, *Angew. Chem., Int. Ed.*, 2012, **51**, 1625-1630.

20. Z. Liu, X. Sun, N. Nakayama-Ratchford and H. Dai, *ACS Nano*, 2007, **1**, 50-56.

21. S. Y. Chae, T. H. Kim, K. Park, C.-H. Jin, S. Son, S. Lee, Y. S. Youn, K. Kim, D.-G. Jo, I. C. Kwon, X. Chen and K. C. Lee, *Mol. Cancer Ther.*, 2010, **9**, 1719-1729.

22. L. P. Chan, T. H. Chou, H. Y. Ding, P. R. Chen, F. Y. Chiang, P. L. Kuo and C. H. Liang, *Biochimica et Biophysica Acta*, 2012, **1820**, 1081-1091.

23. B. J. Nickoloff, J. Z. Qin, V. Chaturvedi, P. Bacon, J. Panella and M. F. Denning, *J. Investig. Dermatol. Symp. Proc.*, 2002, **7**, 27-35.

24. S. N. Goldberg, G. S. Gazelle and P. R. Mueller, *J. Vasc. Interv. Radiology*, 2009, **20**, S377-90.

25. L. R. Hirsch, R. J. Stafford, J. A. Bankson, S. R. Sershen, B. Rivera, R. E. Price, J. D. Hazle, N. J. Halas and J. L. West, *Proc. Natl. Acad. Sci. U. S. A.*, 2003, **100**, 13549-54.

26. M. P. Melancon, W. Lu, Z. Yang, R. Zhang, Z. Cheng, A. M. Elliot, J. Stafford, T. Olson, J. Z. Zhang and C. Li, *Mol. Cancer Ther.*, 2008, **7**, 1730-9.

27. M. Al-Hajj, M. S. Wicha, A. Benito-Hernandez, S. J. Morrison and M. F. Clarke, *Proc. Natl. Acad. Sci. U. S. A.*, 2003, **100**, 3983-3988.

28. D. M. Simeone, *Clin. Cancer Res.*, 2008, **14**, 5646-5648.

29. L. Du, H. Wang, L. He, J. Zhang, B. Ni, X. Wang, H. Jin, N. Cahuzac, M. Mehrpour, Y. Lu and Q. Chen, *Clin. Cancer Res.*, 2008, **14**, 6751-6760.

30. Z. Liu, C. Davis, W. Cai, L. He, X. Chen and H. Dai, *Proc. Natl. Acad. Sci. U. S. A.*, 2008, **105**, 1410-1415.

31. J. A. Weigel, R. C. Raymond, C. McGary, A. Singh and P. H. Weigel, *J. Biol. Chem.*, 2003, **278**, 9808-12.

32. J. Yannariello-Brown, B. Zhou, D. Ritchie, J. A. Oka, P. H. Weigel, *Biochem. Biophys. Res. Commun.*, 1996, **218**, 314-9.

33. B. Zhou, J. A. Weigel, A. Sazena, P. H. Weigel, *Mol. Biol. Cell,* 2002, **13**, 2853-2868.

34. A. Chrastina, K. A. Massey, J. E. Schnitzer, *Wiley Interdisciplinary Reviews: Nanomedicine and Nanobiotechnology*, 2011, **3**, 421-437.

35. Y. Chen, S. C. Gnyawali, F. Wu, H. Liu, Y. A. Tesiram, A. Abboutt, R. A. Towner, W. R. Chen . *J. Biomed. Opt*., 2008, **13** 044033.

36. W. R. Chen, H. Liu, J. W. Ritchey, K. E. Barttels, M. D. Lucroy, R. Nordquist, *Cancer Res.,* 2002, **62**, 4295-4299.

37. G. v. Maltzahn, J. H. Park, A. Agrawal, N. K. Bandaru, S. K. Das, M. J. Sailor, S. N. Bhatia *Cancer Res.,* 2009, **69**, 3892-3900.